REVIEWS OF GEOPHYSICS, VOL. 23, NO. 4, PAGES 313–356, NOVEMBER 1985

The Inference of North Atlantic Circulation Patterns From Climatological Hydrographic Data

D. J. OLBERS

Max-Planck-Institut für Meteorologie, Hamburg, Federal Republic of Germany

M. WENZEL AND J. WILLEBRAND

Institut für Meereskunde an der Universität Kiel, Kiel, Federal Republic of Germany

We present a review of β spiral techniques which have recently been developed for the determination of absolute velocity profiles from hydrographic observations. A specific technique is then designed and applied to the North Atlantic part of Levitus' (1982) climatological hydrographic atlas with the aim of estimating reference velocities and diffusivities for heat, salt, and potential vorticity. These quantities are determined on a 1° grid from the local gradients of temperature and salinity under the constraints of the thermal wind relations and the conservation of the respective tracers including diapycnic and isopycnic mixing terms. The estimation procedure includes the statistical framework of inverse modeling in the weighting of the constraints by the data noise variances and the determination of the covariances of the model parameters. The resulting circulation pattern bears strong resemblance to the classical view of the North Atlantic circulation as put foreward by Wüst (1935) and Defant (1941). The upper layers are dominated by the Gulf Stream/North Atlantic current system with a broad subtropical gyre recirculation. In the lower layer a western boundary current is fed from Norwegian Sea overflow penetrating the Gibbs fracture zone and partly circulating around the Labrador Sea. As a consequence of the climatological averaging the currents appear in broad shape with much reduced velocities, in particular in the upper layer. The vertical structure reveals an almost horizontal level of no motion pattern much along the concepts of Defant (1941). Diffusion coefficients were determined for an upper layer (depth of mixed layer to 800 m depth) and a lower layer (800 m to 2000 m). The spatial pattern of these coefficients correlates with maps of eddy activity, showing higher values in the strong current regimes and low values within the subtropical and subpolar gyre. Average values in the lower layer of the quiet regions are 10^{-5} m^2/s and 10^2 m^2/s for the diapycnal and isopycnal diffusivity, respectively, and 10^{-1} m^2/s for the vertical diffusivity of vorticity (which yields 10^2 m^2/s for the lateral diffusivity of potential vorticity). Toward the regions of strong currents and in the upper layer these values roughly increase by an order of magnitude.

CONTENTS

1. INTRODUCTION

The main body of knowledge about the general circulation of the oceans has been drawn from observations of temperature and salinity. These quantities are relatively easy to measure, and in contrast to velocity observations, the climatological signal in the T, S fields is less contaminated by energetic smaller-scale motions induced by eddies and waves. Inference of flow characteristics from temperature and salinity data has gone along two almost distinct paths: the water mass analysis techniques, with the core layer method [*Wüst*, 1935] and the isentropic analysis [*Montgomery*, 1938; *Parr*, 1938] as most prominent representatives, and the methods depending on the dynamical balance of the large-scale flow, such as the dynamic method [*Helland-Hansen and Nansen*, 1909] and the various extensions which partly are the subject of this paper.

The water mass analysis attempts to determine the broad-scale movement of the water bodies by identifying the location of their sources and sinks which roughly define a pathway along which the water has to move somehow and gradually lose its characteristics by mixing with surrounding water masses. The power of these methods resides in the fact that large-scale connections in the flow field can be inferred directly from the observed large-scale pattern of the properties. However, since local balances are not considered, an attempt to understand in detail how the fluid establishes these connections is not made. The water mass analysis therefore uses the terminus spreading, thus avoiding the termini advection and mixing or diffusion which have a designated physical meaning in the local and large-scale balance of a fluid property.

The basic dynamical constraint of the large-scale flow in the ocean is the geostrophic balance between the pressure and Coriolis forces. However, temperature and salinity determine only the baroclinic part of the pressure arising from density stratification, whereas the barotropic part associated with the inclination of the sea surface remains unknown (and is essentially unobservable by standard oceanographic instrumentation). Consequently, the classical dynamical method depends heavily on subjective assumptions about the local barotropic

Paper number 5R0560.
8755-1209/85/005R-0560$15.00

pressure force or, equivalently, the level of no motion. A discussion of early speculations about the level of no motion [e.g., *Defant*, 1941] can be found in the work by *Reid* [1981].

With the use of the geostrophic balance, or more precisely the thermal wind equations which relate the vertical shear of the horizontal current to the local density gradient, not all information contained in the temperature and salinity observations has been exploited. Each property is subject to advection by the local absolute velocity which constrains the velocity component along the local property gradient. In the case of an adiabatic flow, for instance, the absolute velocity vector must lie in the isopycnal surface (or isohaline surfaces and surfaces of constant potential temperature). A water body which is bounded by such surfaces and vertical sections on the sides is thus only affected by the horizontal inflow into these sides. The local inflow of volume can be expressed in terms of the local relative velocity, which is determined by the known baroclinic pressure gradient and the unknown local reference velocity, i.e., the velocity at a specified reference level. Considering larger bodies of water enclosed by hydrographic sections (or even partly by coastlines) one obtains as generalization of Knudsen's hydrographic theorem [e.g., *Proudman*, 1953] an underdetermined set of equations for the reference velocities between the stations. Out of the infinity of solutions one may choose the one which suits a subjective judgment of the large-scale circulation, such as smoothness or minimum or maximum volume transport through the region considered. The subjective choice of a (local) level of no motion is thus replaced by (still subjective) assumptions about large-scale patterns of the flow. However, conservation of properties derived from temperature and salinity is guaranteed. In essence, this is the inverse method investigated by Carl Wunsch in various papers [*Wunsch*, 1977, 1978; *Wunsch and Grant*, 1982].

The alternative scheme for the determination of the reference velocities has been put forward by *Stommel and Schott* [1977] (for further references see section 3). Likewise, it is based on the thermal wind relations and on tracer conservation, but in contrast to Wunsch's method it emphasizes more the local aspect of these balances (the only large-scale element in the data handling arises from the necessity to smooth away eddies in the hydrographic fields in order to obtain reliable estimates of large-scale gradients). The method involves a linearized vorticity balance which, for planetary scale motions, relates the vortex stretching to the advection of planetary vorticity.

The essence of the method can again readily be explained for an adiabatic flow. Since density and potential vorticity are conserved by the system, the intersections of isopycnals with surfaces of constant potential vorticity (the geostrophic contours) must be streamlines, and thus the direction of the velocity vector is known at each level. So, when considering the horizontal components at two levels, it appears obvious that their absolute values are locked by the thermal wind relations, since these determine the relative velocity vector in terms of the known density gradients. Apparently, the method fails if isopycnals and surfaces of constant potential vorticity coincide so that velocity directions cannot be identified. Another case of failure arises when the absolute horizontal velocity vector does not turn with depth and so incompatibility with the relative velocity profiles can occur. A more subtle analysis of the dynamics, however, reveals [e.g., *Bryden*, 1980] that the planetary vorticity balance constrains the horizontal vorticity to spiral with depth. In fact, the presence of the gradient β of the planetary vorticity guarantees a spiraling hodograph giving the name β spiral to Stommel's concept. In practice, when applied to real, noisy hydrographic data the reference velocity is determined from a least squares principle, i.e., by considering the spiral between many vertical levels. The method can easily be extended to diabatic conditions. *Schott and Zantopp* [1980] have included vertical diffusion of density, and the main body of this paper descibes the attempt to additionally determine horizontal diffusion coefficients of the temperature and salinity and vertical diffusion coefficients of vorticity (or, equivalently, horizontal diffusion coefficients of potential vorticity). Homogeneity of potential vorticity on isopycnals has been observed in a wide layer beneath the wind-driven gyres in the ocean [*McDowell et al.*, 1982; *Holland et al.*, 1984]. Inclusion of data from this layer has very likely caused the breakdown of the β spiral method in some earlier applications [e.g., *Schott and Stommel*, 1978; *Behringer*, 1979] where no unique reference velocity could be identified. The basic problem has been known since the early work on the thermocline problem: *Needler* [1972] has shown that the thermocline equations (without proper boundary conditions) contain an arbitrary barotropic part if potential vorticity is a function of density. Fortunately, however, this relation is broken in the real ocean at deeper levels (say, roughly below 800 m in the North Atlantic), and the β spiral can be used to determine the barotropic velocity.

The application of the β spiral method reported in this paper differs in various respects from earlier work. At first, we use the climatological analysis of hydrographic data prepared by *Levitus* [1982] instead of single hydrographic sections which may be more synoptic. The climatological mean has the advantage of providing data on a $1° \times 1°$ grid for the entire ocean, so one should be able to deduce large-scale circulation patterns instead of estimating current profiles at single crossing points of sections. Further, the analyzed data are necessarily smoothed, and there is no need for elimination of eddy noise (at least away from boundaries and in regions where the original data coverage is good). On the other hand, as a disadvantage, the climatological analysis definitely filteres more than the instantaneous eddy field. The main hydrographic features commonly associated with the mean ocean circulation (as, for example, the Mediterranean water tongue or the Gulf Stream front) appear in a highly smoothed form, and the resulting circulation patterns are a rather broad brush image of reality. There is no way that it could possibly represent an actual state of the circulatioan (with the eddies removed).

Moreover, temporal as well as spatial averaging may introduce a bias in the diffusion parameters we try to estimate. Consider, for instance, a current system changing its position in the annual cycle. Averaging yields Reynolds stress terms, and the least squares fit yields diffusion coefficients even if mixing may be entirely absent in the actual state. With this restriction one should think of the resulting diffusion coefficients as representing an upper bound of the actual mixing in the ocean. Fortunately, our result will reveal that these bounds are rather small in large regions.

In contrast to other β spiral applications we attempted to include the consequences of data noise in the estimation procedure. Data noise leads to errors in the estimated parameters that can be computed by standard methods. The statistical set-up of a least squares estimation procedure is generally derived from a maximum likelihood principle. Given the data covariances, the method yields the parameter covariances, i.e., standard deviations and correlations. It also yields a test of

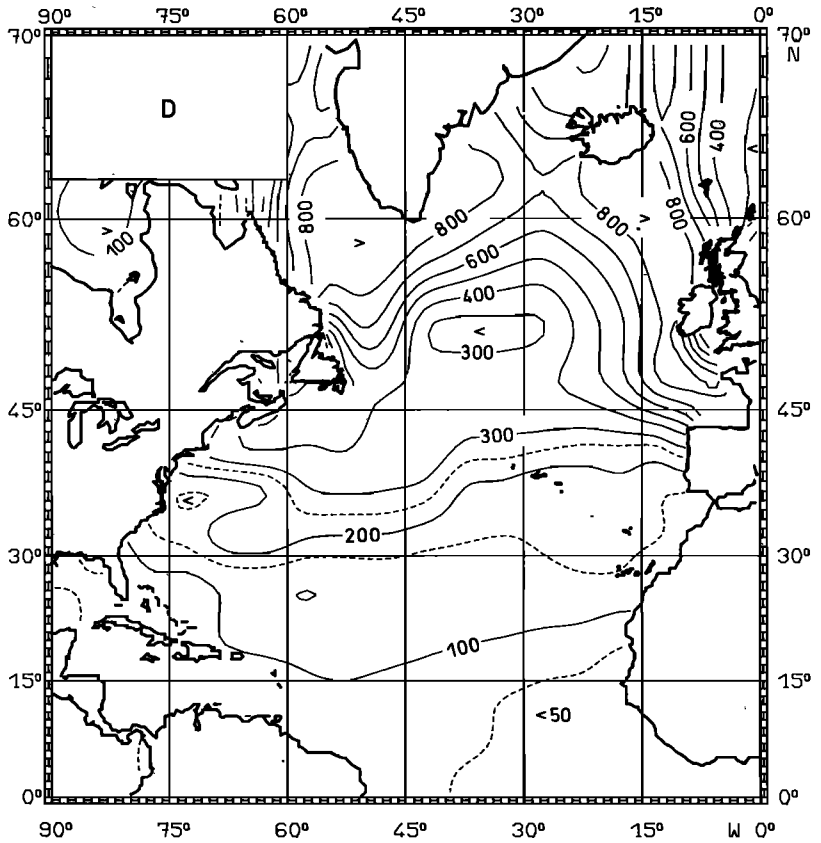

Fig. 1. Maximum depth D of the oceanic surface mixed layer. Smoothed version of the map given by *Robinson et al.* [1979].

the model validity, i.e., a statistical answer to the question of whether or not the β spiral dynamics represents an adequate description of the hydrographic data set. This last and obviously very important step, however, could not be pursued rigorously, since all our effort failed to get a meaningful estimate of the complete covariance matrix of the analyzed hydrographic data set. The only way of judging the model validity is by a comparison of the resulting velocity field and mixing parameters with our a priori knowledge thereof.

We have applied the β spiral method to the North Atlantic part of *Levitus'* [1982] analysis, since here the coverage by original data was by and large greatest, so that parameter estimation should be most promising. We would like to emphasize, however, that our approach should not be viewed as an attempt to get a complete picture of the circulation in the North Atlantic. Obviously, much more knowledge has been accumulated about the circulation from hydrographic data as well as from other complementary data than the information that could possibly be drawn from a local analysis of a highly smoothed temperature and salinity field. We would, rather, like to view our work as a test of the applicability of the β spiral method and its associated dynamics. As discussed above, such a test could be performed at single stations if firm statistical information were known. Lack of this knowledge, however, leaves us with some subjective judgment of the parameter patterns obtained from application of the method in a large domain.

2. DATA

The hydrographic data set used in this analysis is an updated version of the analysis by *Levitus and Oort* [1977] and represents an earlier version of the climatological hydrographic atlas prepared by *Levitus* [1982]. A detailed description of data sources, quality control, and representativeness as well as the objective scheme for constructing the temperature and salinity field is given by *Levitus* [1982]. Here we give a

TABLE 1. Number of Observations in 10° Squares Between 30°N and 40°N

Longitude, °W	D, m	H, m	Temperature			Salinity		
			$0-D$	$D-2000$	$2000-H$	$0-D$	$D-2000$	$2000-H$
10–20	160	5000	52,760	25,092	474	6,944	8,448	430
20–30	161	5000	48,107	18,993	330	4,961	6,001	323
30–40	168	4500	27,678	11,063	160	2,046	3,020	156
40–50	223	5000	215,645	46,961	1321	23,475	27,952	1248
50–60	237	5000	82,834	21,464	870	5,497	6,757	824
60–70	207	5000	451,617	121,339	4150	36,263	43,373	3918
70–80	150	5000	612,322	187,310	1612	51,615	39,046	1464

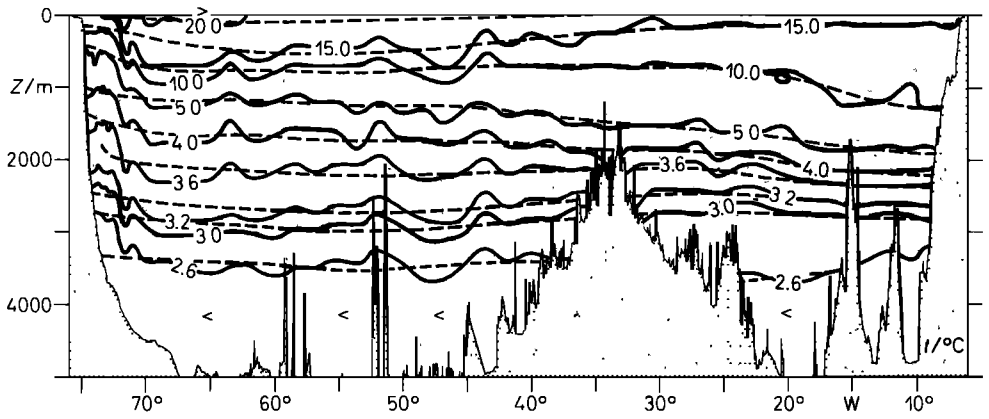

Fig. 2*a*

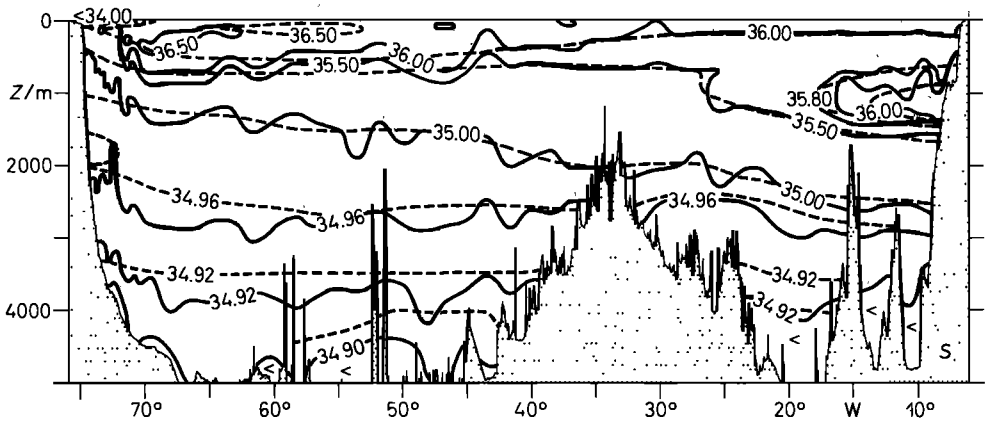

Fig. 2*b*

Fig. 2. Section of (*a*) in situ temperature and (*b*) salinity at 36°N together with the corresponding IGY section as taken from *Fuglister* [1960]. Dashed lines represent the Levitus analysis, and solid lines the IGY data.

brief qualitative description of the resulting temperature and salinity fields and the associated geostrophic currents relative to 2000 m. Further, we estimate the accuracy of the analyzed fields and of their gradients.

2.1. *The Analyzed Temperature and Salinity Fields*

Global temperature and salinity fields were compiled by *Levitus and Oort* [1977] from hydrographic stations as well as mechanical and expendable bathythermograph surveys. We will restrict our investigations to the North Atlantic portion shown in Figure 1. This figure displays the maximum depth $D(x, y)$ of the oceanic surface mixed layer, according to *Robinson et al.* [1979]. The relevance of this depth for our analysis will be discussed later in section 3.1. To exemplify the number of original data which entered the analysis of *Levitus and Oort* [1977], we list in Table 1 the total number of temperature and salinity observations in some 10° × 10° squares. For reasons that will become apparent later, those numbers are given separately for three depth ranges:

upper convective layer	$z > -D(x, y)$
main thermocline layer	$-D(x, y) \geq z \geq -2000$ m
deep layer	$z < -2000$ m

Further information on the regional distribution of data can be found in the work by *Levitus* [1982]. The raw data of temperature and salinity were reduced to mean values for each 1° square within each of the 33 standard levels from the surface to the bottom, with a 10-m increment in the upper 30 m, increasing to a 100-m increment between 300 m and 1500 m and a 500-m increment below 2000 m. From these 1° square values the analyzed fields have been derived by an objective method (see Appendix A for details). In this paper we consider only annual averages of all fields.

To demonstrate the smoothness of the analyzed fields in comparison to raw data, we display in Figure 2 a section of in situ temperature and salinity along 36°N together with the corresponding International Geophysical Year (IGY) section taken from *Fuglister* [1960]. Evidently, the analyzed fields do not contain the small-scale wiggliness with scales of 1°–2° attributed to eddies that is apparent in Fuglister's section. However, the large-scale features, e.g., the tongue of the Mediterranean water, have remained. The horizontal scales resolved by the analyzed fields are about 5°–10° except close to boundaries, where they shrink to about 2°–3°. In this respect the analyzed fields are directly apt for β spiral calculations, since the eddy noise has essentially disappeared. Explicit filtering techniques as applied, for example, by *Schott and Stommel* [1978] to synoptic sections obviously are redundant in our case.

Maps of potential temperature and salinity can be found in the work by *Levitus* [1982], where there is also some discussion of the major oceanographic features represented by the analyzed data set. In the later stage of this paper we will show and discuss some quantities derived from potential temperature and salinity. The main impression that should be mediated by these maps (and by the sections above as well) is

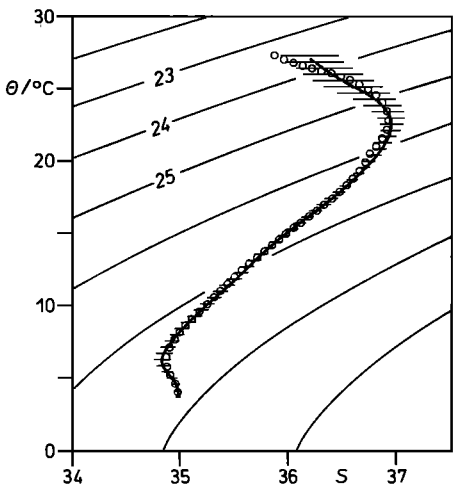

Fig. 3a

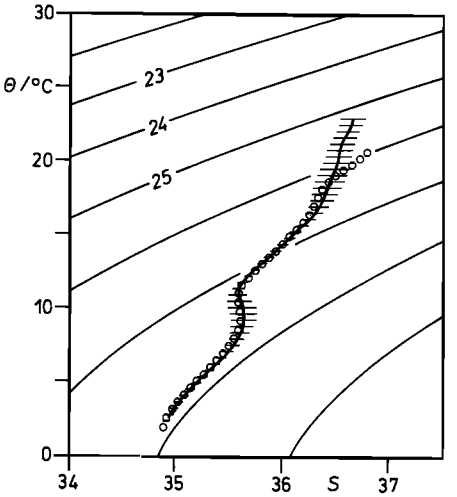

Fig. 3b

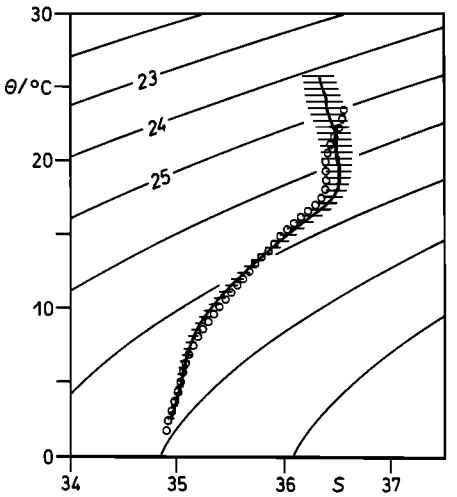

Fig. 3c

Fig. 3. Average θ-S curves for three areas of the *Emery and Dewar* [1982] analysis (solid lines) compared to the Levitus [1982] analysis (circles): (*a*) 15°–20°N, 35°–80°W, (*b*) 30°–40°N, 15°–25°W, and (*c*) 30°–40°N, 45°–70°W. Horizontal lines indicate standard deviation of Emery and Dewar.

that the large-scale water mass structure is reproduced but that gradients in the fields, in particular in boundary layers, have been substantially blurred by the climatological averaging procedure. This becomes apparent by comparing, for example, the gradient in potential temperature across the Gulf Stream in Figure 13 of *Levitus* [1982] with Fuglister's 200-m synoptic map from the Gulf Stream '60 experiment [*Fuglister*, 1963] or the entire fields north of 40°N with Dietrich's IGY atlas [*Dietrich*, 1969].

A further useful comparison of Levitus' analysis with an independent climatological mean of North Atlantic hydrographic data is given in Figure 3, which displays the average θ-S curves for three areas of the Levitus analysis with another recent analysis by *Emery and Dewar* [1982] based essentially upon the same National Ocean Data Center (NODC) data files. Whereas *Levitus* [1982] oriented his averaging procedure according to the data density and correlation scales on horizontal levels starting with a zonal mean, *Emery and Dewar* [1982] obtained their climatological mean by averaging over regionally connected bodies of water defined by an a priori water mass census. In this respect the latter analysis more closely follows traditional oceanographic concepts.

Generally, the Levitus curve lies well within one standard deviation of Emery and Dewar's values except at the uppermost levels. The curvature in Levitus' curve is slightly lower, conforming to the notion that the horizontal averaging is equivalent to somewhat stronger mixing.

The β spiral requires as input gradient fields of temperature and salinity and derived variables. Unfortunately, the data set does not provide direct information on the accuracy of the analyzed fields and their gradients. As discussed in Appendix A, the variance of the analyzed temperature and salinity field can roughly be estimated as

$$\hat{\sigma}^2 = \frac{2}{M}\sigma^2 \qquad (1)$$

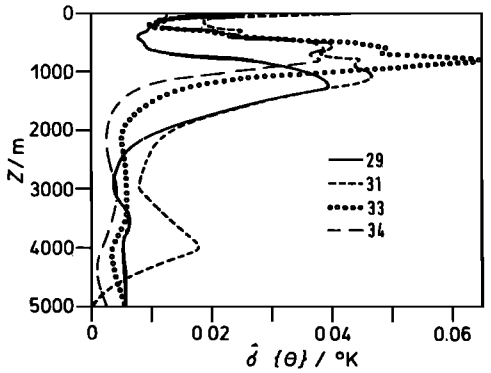

Fig. 4*a*

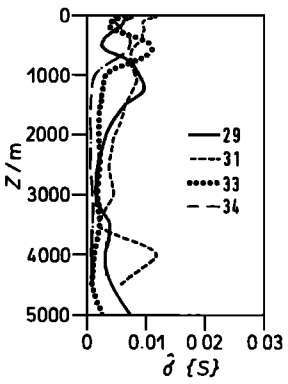

Fig. 4*b*

Fig. 4. Estimated accuracy of (*a*) temperature and (*b*) salinity for several 10° squares in the zonal band 30°–40°N. (29: 10°–20°W; 31: 30°–40°W; 33: 50°–60°W; 34: 60°–70°W).

where σ^2 is the variance of the observations and M is the number of independent observations which have contributed to the construction of the analyzed data point. Similarly, the variance of gradients of the analyzed fields is

$$\hat{\sigma}_\nabla{}^2 = \frac{8}{MR_e{}^2}\sigma^2 \tag{2}$$

where R_e is the effective radius of influence containing M observations (see Appendix A for details).

Figure 4 shows, as an example, profiles of the estimated accuracy of the temperature and salinity field for several 10° squares in the zonal band 30°N to 40°N across the Atlantic. The salient feature of the rms profiles is the maximum in the depth range 500–1300 m, particularly conspicuous in the rms temperatures, with typical values of 0.05 K (Figure 4*a*). It can be understood from the definition (1) of $\hat{\sigma}$ as a quotient of two quantities (σ^2 and M), both of which are generally (though for different reasons) decreasing with depth. The maximum reflects the large decrease of the number of observations in that depth range. At larger depths, that number decreases much more slowly because many of the hydrocasts cover the full water column. Here the decrease of $\hat{\sigma}$ corresponds to a decrease of the natural variability as measured by σ. At larger depths the computed accuracies are of the order of 0.005 K for temperature and 0.002‰ for salinity. These values, especially the value for salinity, seem unrealistically small considering a widespread prejudice among oceanographers regarding the accuracy of climatological data. As discussed in Appendix A, only the statistical part of the error is given by (1) and (2). The nonstatistical part (formally the contribution of the first-guess field) is expected to dominate in areas of low data density, i.e., especially in the deep ocean. After various other attempts we have decided to summarize that unknown nonstatistical error by a single number σ_0 that was added to the statistical error according to

$$\hat{\sigma}^2 = \frac{2}{M}\sigma^2 + \sigma_0{}^2 \tag{1'}$$

and similarly

$$\hat{\sigma}_\nabla{}^2 = \frac{4}{R_e{}^2}\left(\frac{2}{M}\sigma^2 + \sigma_0{}^2\right) \tag{2'}$$

The value of σ_0 was chosen as 0.02 K for temperature and 0.02‰ for salinity. This choice reflects our judgment on the

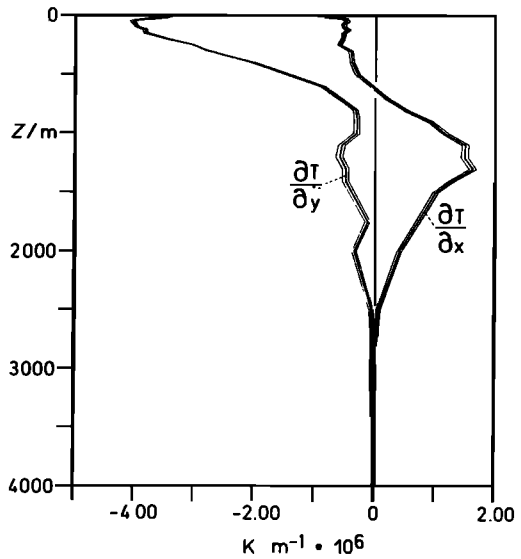

Fig. 5*a*

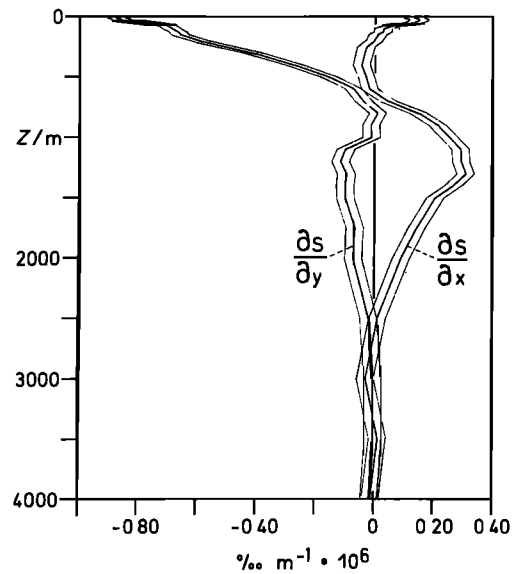

Fig. 5*b*

Fig. 5. Gradients of (*a*) temperature and (*b*) salinity at 35°N, 25°W. Strip indicates accuracy (±1 standard deviation).

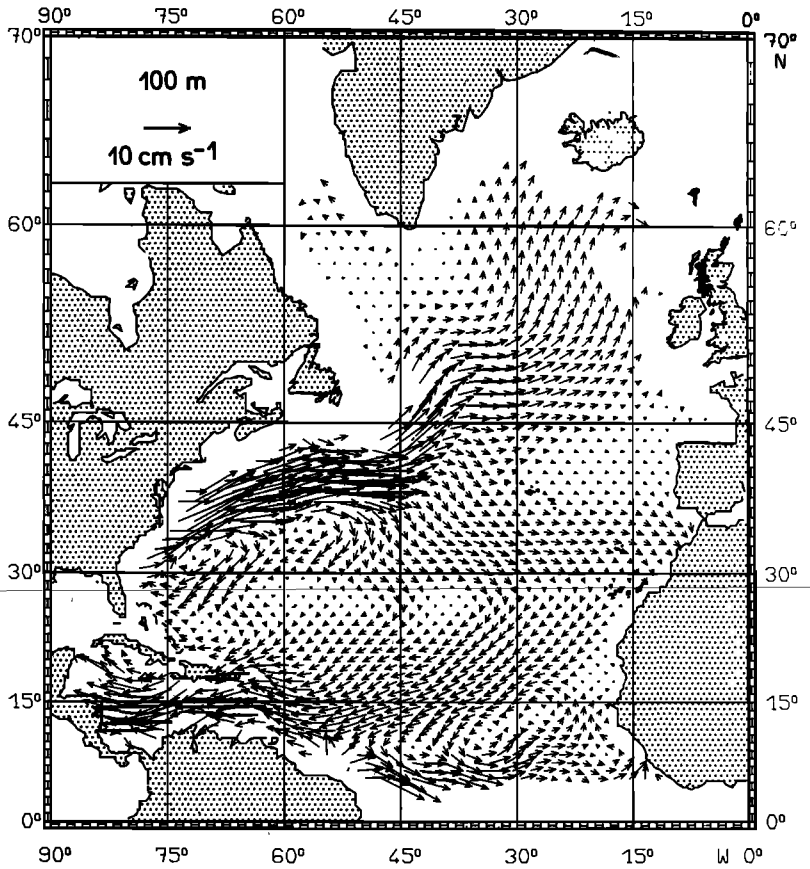

Fig. 6a

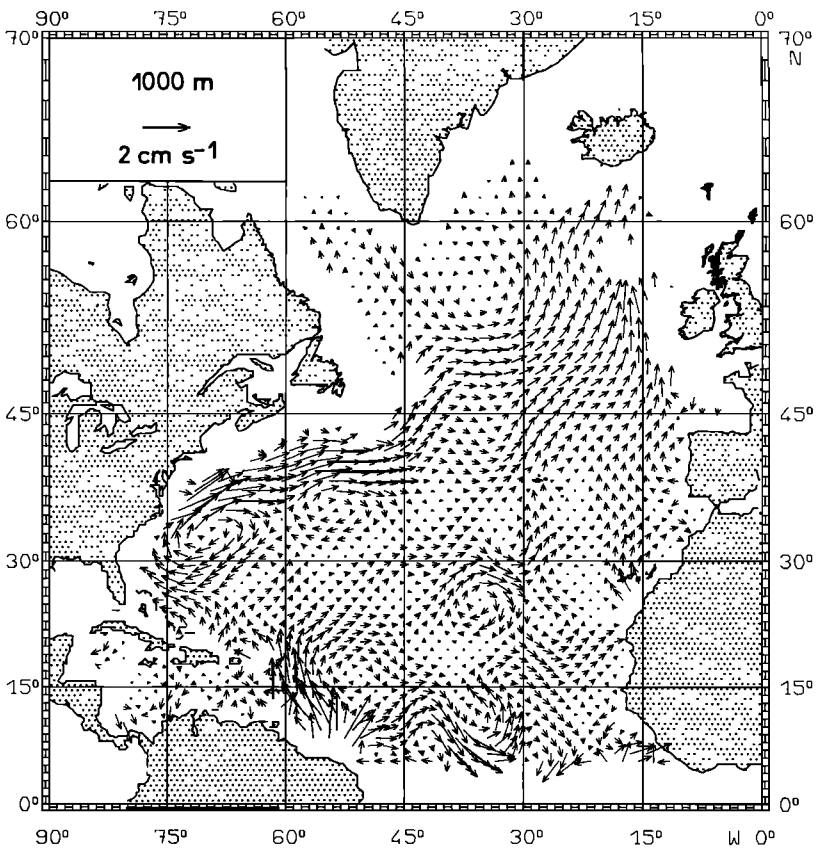

Fig. 6b

Fig. 6. Maps of horizontal geostrophic circulation relative to 2000 m at (*a*) 100 m depth and (*b*) 1000 m depth.

accuracy of the deep (e.g., 4000 m) temperatures and salinities (cf. Figures 21 and 31 of *Levitus* [1982]). At higher levels, where the statistical error is larger, the term $\sigma_0{}^2$ becomes irrelevant.

Figure 5 shows vertical profiles of horizontal temperature and salinity gradients from a position in the eastern Atlantic at 35°N. The profiles of both gradients are rather similar. The southward component has a maximum at the surface, whereas the eastward component has a maximum near 1200 m. Toward greater depths the gradients decrease to very small values. Also indicated in Figure 5 is the accuracy of the gradient as calculated according to (2'). It is evident that the local gradients are well defined above a certain depth level but are indistinguishable from zero below. In Figure 5 that level is close to 2500 m.

We have looked at corresponding profiles for many other positions. While the actual gradient profiles show a large amount of variation, all tend to zero within the error bounds at larger depths, usually below 1500–3000 m. As the accurate computation of field gradients is a necessary prerequisite of the following β spiral analysis, data at those levels are practically useless for that purpose. For that reason we have not used data below 2000 m for the β spiral fit, thereby significantly reducing noise in the calculations presented below.

2.2. *The Geostrophic Circulation Relative to 2000 m*

One step of our analysis is the calculation of the profiles of the geostrophic velocity from temperature and salinity data. Using the thermal wind relations, the density field ρ determines the horizontal velocities relative to the motion at a given level $z = z_0$.

$$\begin{pmatrix} u_r \\ v_r \end{pmatrix} = \frac{g}{f} \int_{z_0}^{z} dz' \begin{pmatrix} \rho_y \\ -\rho_x \end{pmatrix} \tag{3}$$

Further, the linearized vorticity balance enables one to calculate the contribution

$$w_r = \frac{\beta}{f} \int_{z_0}^{z} v_r \, dz' = \frac{g\beta}{f^2} \int_{z_0}^{z} dz' \, (z' - z)\rho_x \tag{4}$$

to the profile of the vertical velocity. Here we briefly discuss these fields for $z_0 = -2000$ m. Very roughly, this depth corresponds to a classical level of no motion [e.g., *Defant*, 1941], so that u_r and v_r should more or less reflect the classical picture of the geostrophic circulation. The reference velocities at 2000 m depth, $u_0 = u - u_r$ and $v_0 = v - v_r$, and the deviation from the vertical profile w_r will later be determined by the β spiral technique. Maps of the horizontal geostrophic circulation (u_r, v_r) according to (3) at two levels (100 m and 1000 m) are shown in Figure 6. A broad Gulf Stream region is seen at all levels with two recirculation regions at its southern flank, at 55°W and 70°W. Near 40°N and 40°W the circulation clearly splits into two different branches, a broad North Atlantic current and the Azores current between 30°N and 40°N, separated by a quiet region in the Iberian basin. The North Equatorial current is seen at the 100-m level, and there is also an indication of the Equatorial countercurrent between 5°N and 10°N. The lower levels exhibit a certain amount of variability on scales of 500–1000 km, e.g., around 10°N and around 25°N, 35°W. On the same scale there are areas with significantly smaller velocities. Those features are not in accordance with classical views of the climatological circulation and presumably reflect the variability in the data density.

Figure 7 shows the corresponding vertical velocity fields as computed from (4). The gross structure at the 100-m level is characterized by upwelling over the areas occupied by the Gulf Stream and North Atlantic current and by downwelling over the subtropical gyre. Very roughly, those regions agree with positive and negative values of the Ekman pumping velocity $w_E = \nabla \times (\tau/f)$ [*Leetma and Bunker*, 1978]. The values reach a few 10^{-4} cm/s and are of the order of (though somewhat larger than) the pumping velocity. At the 1000-m level, magnitudes are reduced by one order of magnitude. Here upwelling prevails except in a narrow strip between 30°W and 40°W. The strong increase toward the equator reflects the fact that $w \sim f^{-2}$ according to (4).

The relative circulation (u_r, v_r, w_r) displayed in Figures 6 and 7 is by construction locally mass conserving, i.e.,

$$(u_r)_x + (v_r)_y + (w_r)_z = 0 \tag{5}$$

However, the normal velocity component does not necessarily vanish at boundaries, and therefore the computation of integrated mass and heat fluxes would be meaningless.

In Figure 8 we compare geostrophic spirals obtained from historical sections with the climatological spiral calculations at the same location. The historical spirals in Figures 8*a* and 8*b* are those used by *Schott and Stommel* [1978] (points A and C), and the four spirals in Figure 8*c* are from the four cruises of the β triangle [*Behringer and Stommel*, 1980; *Armi and Stommel*, 1983]. The historical and climatological spiral have similarities; for example, the range of velocities are equal, and in general the turning tendencies with depth agree. It is, however, immediately evident that the differences are larger than can be accounted for by differences in the gradient calculations. Figure 8*c* shows that the differences between the climatological spiral and each individual spiral from the four cruises are of the same magnitude as the differences among these four spirals. We thus believe that the differences come about through different smoothing techniques of spatial and temporal variability.

2.3. *Potential Density and "Veronicity"*

The β spiral approach is based on the conservation of heat and salt, and in most applications the observed variables are taken to be potential temperature θ, salinity S, potential density $\sigma = \sigma(\theta, S)$ referred to surface pressure, or any pair of these. However, in the case of an advective-diffusive regime, another pair of variables is more convenient to use: potential density $\sigma(\theta, S)$ and a variable $\nu(\theta, S)$. The latter is defined as that functional of θ, S which, with given scaling of the axes, is orthogonal to the curves $\sigma(\theta, S) = \text{const}$ in the θ-S diagram, so that locally,

$$\begin{aligned} \sigma &= -\alpha\theta + \beta S \\ \nu &= \{\beta(\Delta S)^2\theta + \alpha(\Delta\theta^2)S\}/(\Delta\theta\Delta S) \end{aligned} \tag{6}$$

where $\Delta\theta$ and ΔS are the scales of the axes. Among others [*Stommel*, 1962; *Mamayev*, 1962; *Munk*, 1981], *Veronis* [1972] has most extensively discussed this tracer, which hence may appropriately be termed "potential veronicity." The tracer $\nu(\theta, S)$ is not uniquely defined because of its dependence on the (arbitrary) scaling of the θ and S axis. Presumably for that reason this tracer has not generally been accepted by the oceanographic community, and normally, temperature (or salinity) on isopycnal surfaces is preferred as a variable containing the information in θ and S that is not contained in $\sigma(\theta, S)$.

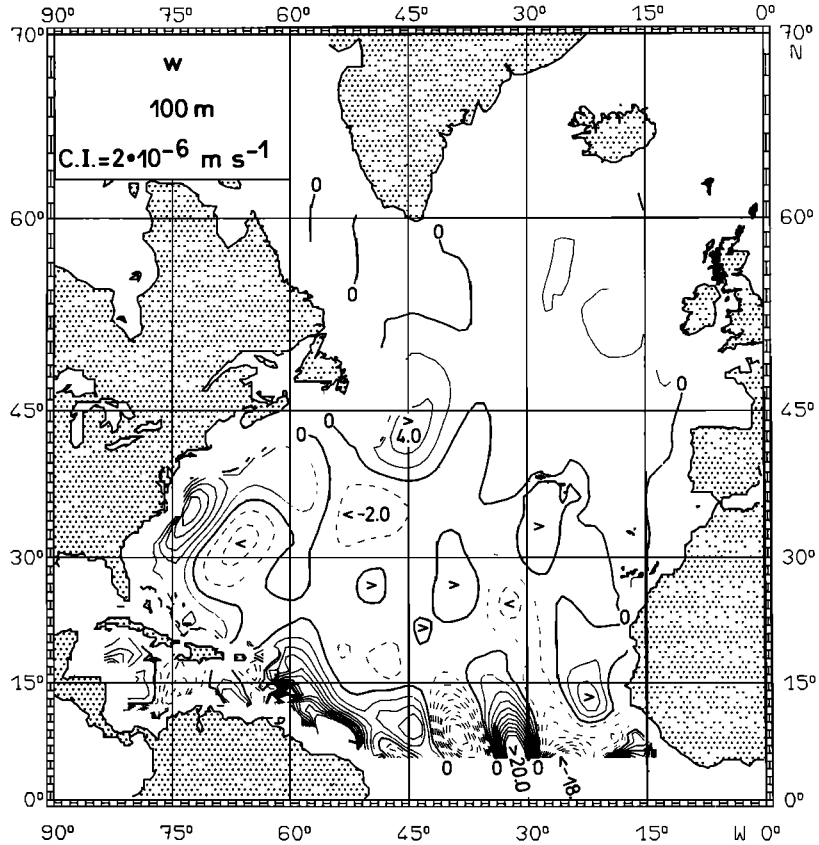

Fig. 7*a*

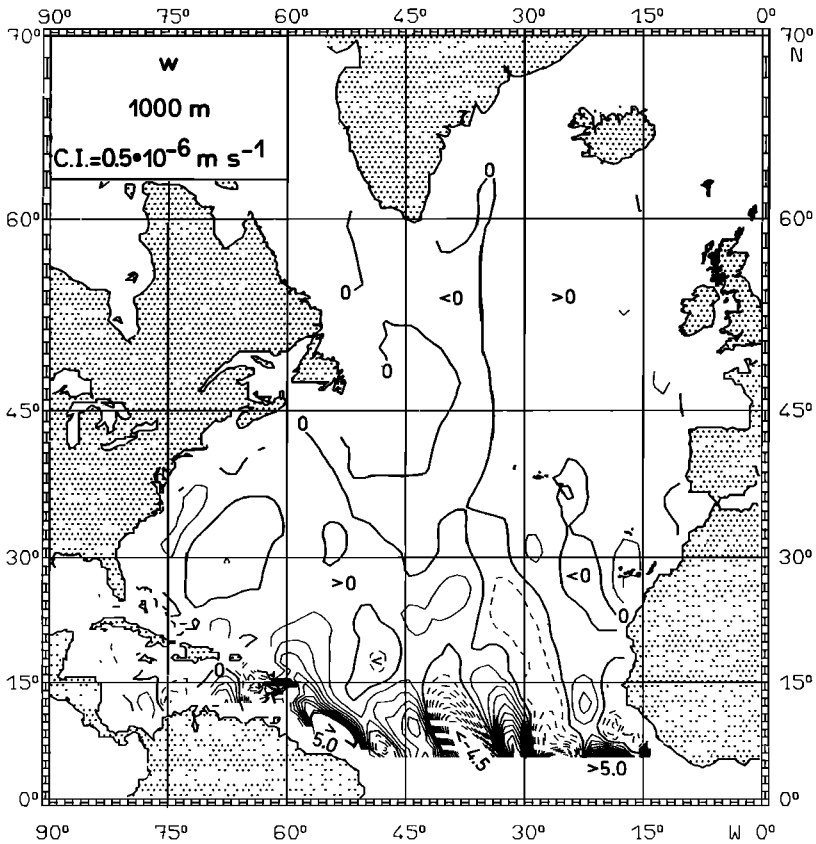

Fig. 7*b*

Fig. 7. Maps of "geostrophic" vertical velocity relative to 2000 m at (*a*) 100 m and (*b*) 1000 m according to equation (4). Contour interval is 2×10^{-6} m/s for Figure 7*a* and 5×10^{-7} m/s for Figure 7*b*.

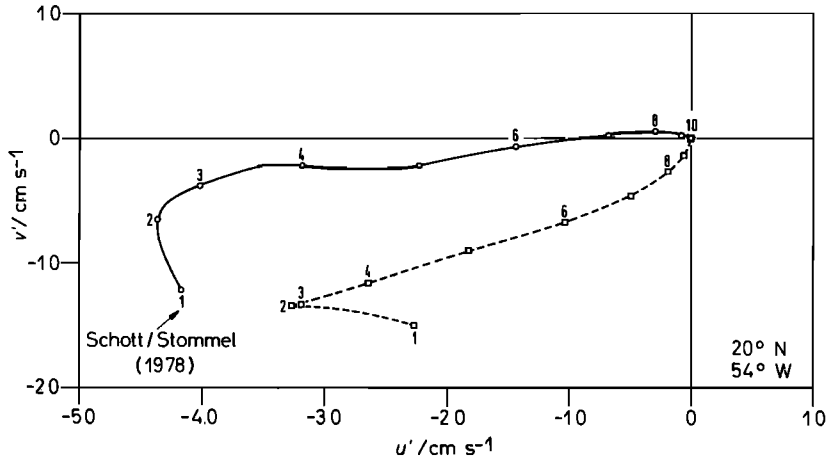

Fig. 8a

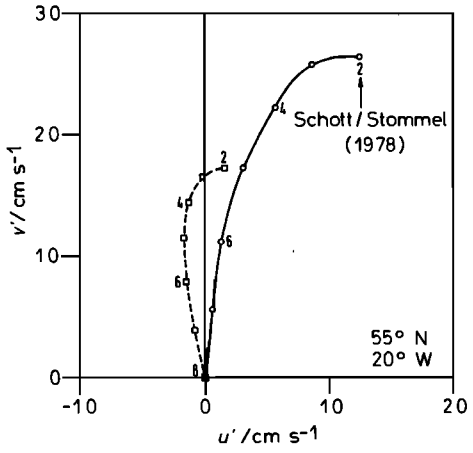

Fig. 8b

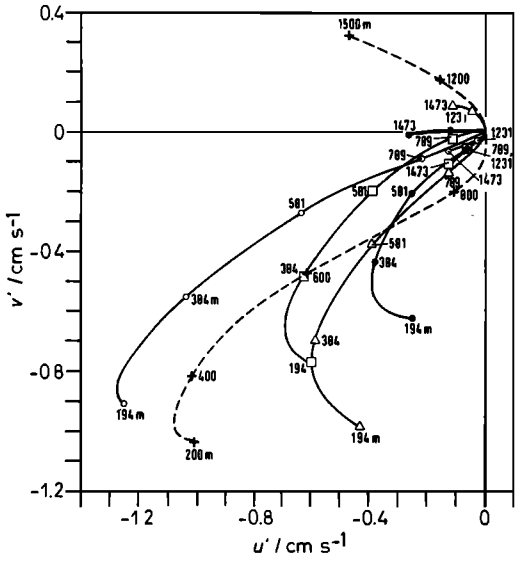

Fig. 8c

Fig. 8. Climatological velocity spirals compared to spirals obtained from historical sections at the same location. Figures 8*a* and 8*b* show the points A and C of *Schott and Stommel* [1978]. The β triangle results of *Armi and Stommel* [1983] at 27°N 32°W for different cruises are given in Figure 8*c*. The climatological spirals are dashed.

This latter variable, while being the perfect choice for models in density coordinates [e.g., *McDougall*, 1984], leads to cumbersome algebra in depth coordinates. We therefore have chosen to work with $\sigma(\theta, S)$ and $v(\theta, S)$ (based on the polynomial expansion given by *Veronis* [1972] with $\Delta\theta/\Delta S = 2 \times 10^3$ K) and will demonstrate in section 3 that this pair is more suitable for the estimation of diffusion coefficients than other combinations of temperature and salinity fields.

Maps of potential density σ and veronicity v at some levels are displayed in Figure 9. Comparison with maps of temperature θ and salinity S [*Levitus*, 1982] shows that v picks up many of the similarities between the θ and S fields, such as the fanning of the isolines in the surface layers, the subsurface maximum in the subtropics (visible in the 100-m maps), and the tongue of Mediterranean water (between 1000 m and 2000 m) as well as the maximum around 30°N in the western basin (between 300 m and 1000 m). Except for this latter feature these properties of θ and S seem to compensate in the potential density σ. By and large, this behavior can be understood from the definition of σ and v, in particular from the linearlized expressions (6). All four fields have a quite similar structure between 300 m and 500 m, described by a pronounced fanning north of 40°N and closed isolines between 20°N and 40°N. The similarity between σ and v is lost at deeper levels, in particular in the eastern basin where Mediterranean water prevails. Here the v distribution roughly coincides with the salinity on isopycnals as seen, for example, by comparison with the surface $\sigma = 27.4$ in the work by *Sarmiento et al.* [1982].

Corresponding features are revealed in the sections of σ and v showing the upper 2000 m (Figure 10). In the western and southern parts of the basin the isolines of σ and v tend to be parallel, i.e., v is almost constant on isopycnals, whereas in the eastern and northern basin below a few hundred meters, isolines tend to cross, i.e., v varies substantially on isopycnals.

In a sense, potential density σ (which in the upper ocean

resembles the in situ density ρ) combines the dynamically significant part of the temperature and salinity distributions, whereas veronicity v tends to behave more as a passive tracer, in particular where there is a close resemblance between σ and ρ. As such, veronicity should be useful as an indicator of mixing. It is, however, not clear how to interpret the data without detailed consideration of the tracer balance. *Veronis* [1972] made an attempt in this respect for two sections in the Atlantic. He interpreted regions where σ and v have parallel contours as regions of intense lateral mixing, and regions where the two sets of curves intersect as regions of relatively strong vertical mixing. The physical assumptions behind this interpretation are those inherent in concepts of water mass analysis [e.g., *Sverdrup et al.*, 1942], in particular the isentropic analysis [e.g., *Montgomery*, 1938; *Parr*, 1938]: the water masses are formed in some surface location and spread out along isopycnals subject to advection and mixing. If long-isopycnal mixing is dominant, tracers become uniform on isopycnals; i.e., isolines of σ and v would be parallel. If there is strong cross-isopycnal mixing, properties of overlying and underlying water are exchanged across the isopycnals, and isolines of σ and v would intersect. Of course, this interpretation is not imperative. For example, a constant v on isopycnals could also be caused by pure advection along isopycnals of a water mass which is formed with a tight correlation between σ and v. Moreover, it is not clear at all how to interpret parallel or crossing isolines if mixing is not dominating the advective terms. In the absence of any mixing the intersections of the surfaces $v = \text{const}$ with isopycnals are streamlines, and this would still be approximately so if mixing were only weak. Obviously, to study the relevance of mixing in this case requires more than the consideration of the crossing or noncrossing of isolines.

Assuming strong mixing processes, *Veronis* [1972] concluded from the parallel isolines of σ and v in the western basin that isopycnal mixing dominates here, whereas the crossing of the isolines in the eastern basin would indicate strong diapycnal mixing. As we show later, the results of the β spiral analysis partly contradict these interpretations: mixing is found to be relatively weak, and there is indication of isopycnal mixing at the rim of the Mediterranean water tongue and diapycnal mixing in the region of strong currents.

3. METHOD

The β spiral method is an inverse technique which is applied to the local gradients of the hydrographic data field to estimate the local absolute velocity profile. There are various formulations of this method [e.g., *Schott and Stommel*, 1978; *Behringer*, 1979; *Behringer and Stommel*, 1980; *Schott and Zantopp*, 1979, 1980; *Coats*, 1983; *Bigg*, 1985] which differ in the way mixing processes are treated (if not entirely neglected), the vertical velocity profile is obtained, and the actual inversion is handled. In this section we will give a survey of these problems and present the particular β spiral scheme which we have applied to the data discussed in the last section.

3.1. *Interior Dynamics*

The dynamics and thermodynamics which we use to describe the climatologically averaged state of the ocean follow the classical concepts of a geostrophic and hydrostatic momentum balance and an advective/diffusive balance of heat and salt. In contrast to other β spiral schemes, however, we allow for mixing terms in the vorticity balance. The balance equations are thus

Momentum

$$\mathbf{f} \times \mathbf{u} + \nabla p = 0$$
$$p_z + g\rho = 0 \tag{7}$$

Vorticity

$$f\nabla \cdot \mathbf{u} + \beta v = F \tag{8}$$

Mass

$$\nabla \cdot \mathbf{u} + w_z = 0 \tag{9}$$

Heat/salt

$$(\mathbf{u} \cdot \nabla + w\partial_z)\psi = G^{\psi} \tag{10}$$

where ρ and p are the perturbation density and pressure, respectively, and $\mathbf{u} = (u, v)$ and w are the velocities. Further, ψ is potential temperature θ or salinity S or a functional of these quantities such as potential density or veronicity. The terms F and G^{ψ} represent turbulent fluxes of (relative) vorticity and of the tracer ψ, respectively.

Strictly speaking, inclusion of a mixing term in the vorticity balance is inconsistent unless a corresponding term is included in the horizontal momentum balance. We will, however, assume that geostrophy always remains a good approximation, thus anticipating that vorticity mixing only contributes on scales of motion much smaller than the radius of the earth.

To introduce parameterizations for the mixing terms F and G^{ψ}, we conceptually divide the ocean into an upper part where turbulent transports associated with surface forcing such as deep convection and wind stirring are dominant, and the remaining interior layer where these transports do not contribute to the mixing. More specifically, we assume that for the large-scale flows considered here, the source terms F and G^{ψ} may be parameterized by diffusion coefficients below a depth $z = -D$, the maximum depth of the bottom of the seasonal thermocline. Figure 1 displays the March mean depth of the top of the thermocline according to the atlas of *Robinson et al.* [1979, Figure 42] which we identify with D in this investigation. The explicit forms of the terms F and G^{ψ} as well as the functional $\psi = \psi(\theta, S)$ will be specified in the next section.

3.2. *The Parameterization of Mixing*

In descriptive oceanography and water mass analysis it has long been recognized [e.g., *Montgomery*, 1938; *Reid*, 1981] that "spreading" of scalars (which somehow includes advection and mixing) should preferentially occur along surfaces of constant potential density, i.e., isopycnals. Nevertheless, dynamical modelers have used parameterizations of mixing in terms of horizontal and vertical coefficients. The concept of isopycnal and diapycnal mixing (i.e., mixing along isopycnals and across isopycnals, respectively) has remained at the stage of being proposed as a useful exercise [e.g., *Solomon*, 1971; *Redi*, 1982] (see, however, *McDougall* [1984]).

One reason for the lack of response, at least for analytical models, is the inconvenient nonlinear structure of isopycnal and diapycnal diffusion terms introduced by the dependence of the diffusion tensor on the isopycnal slopes. If, in the isopycnal coordinate system, diffusion along isopycnals is described by an isopycnal coefficient A_l and diffusion across isopycnals by a diapycnal coefficient A_c, the diffusion tensor K_{ij} with respect to horizontal and vertical directions is

$$K_{ij} = A_l\delta_{ij} + (A_c - A_l)\frac{(\partial_i\sigma)(\partial_j\sigma)}{|\partial\sigma|^2} \tag{11}$$

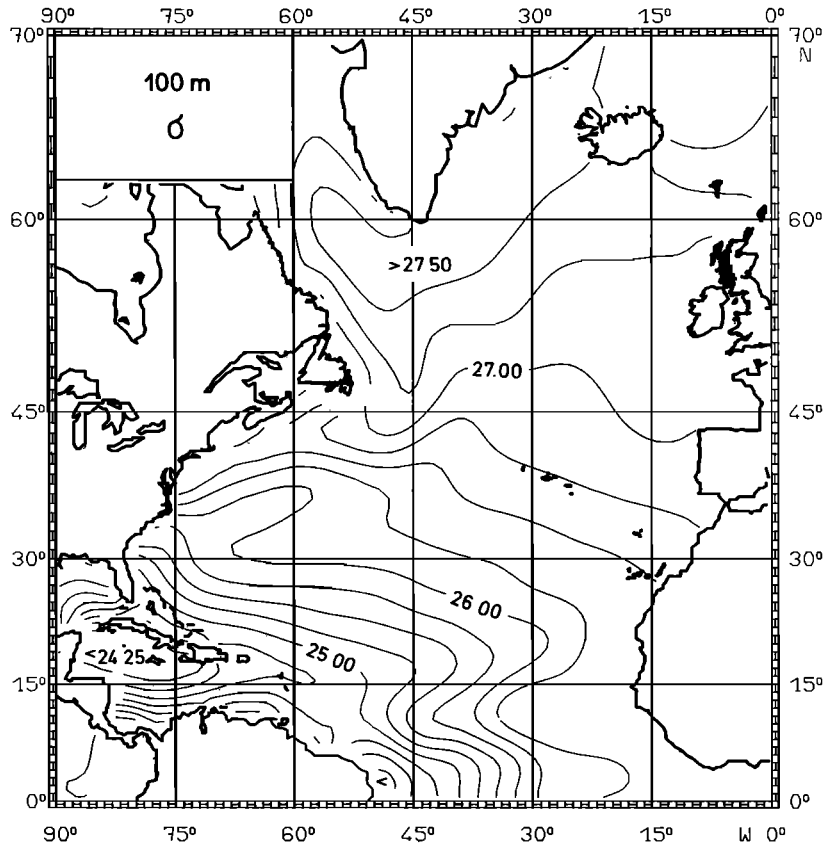

Fig. 9*a*

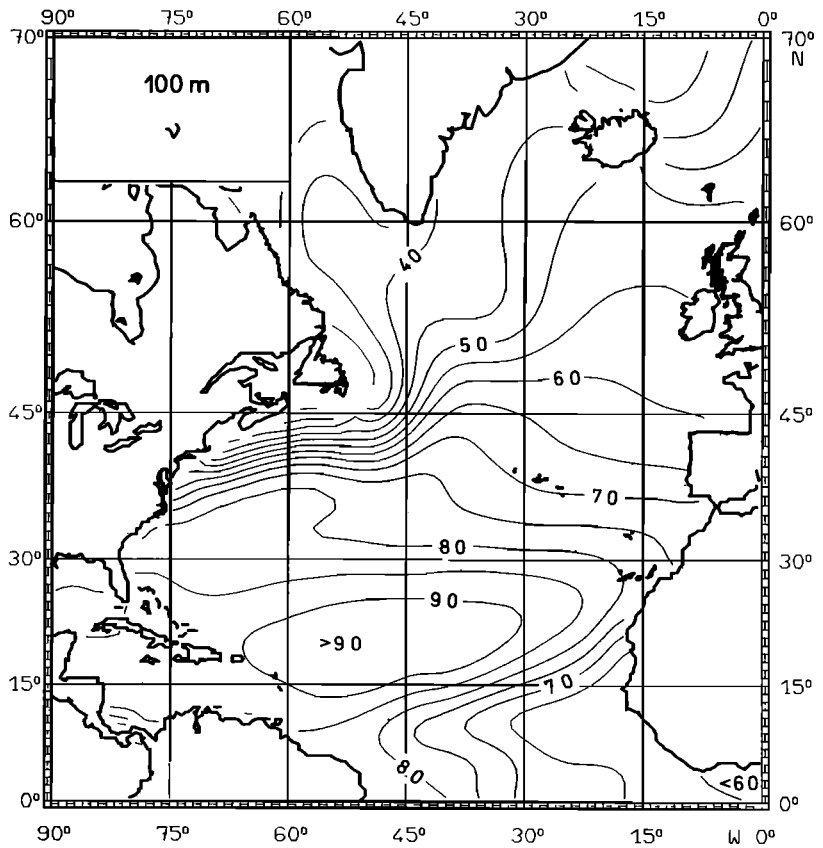

Fig. 9*b*

Fig. 9. Potential density σ and veronicity v at levels 100 m (Figures 9*a* and 9*b*), 500 m (Figures 9*c* and 9*d*), 1000 m (Figures 9*e* and 9*f*), and 1500 m (Figures 9*g* and 9*h*).

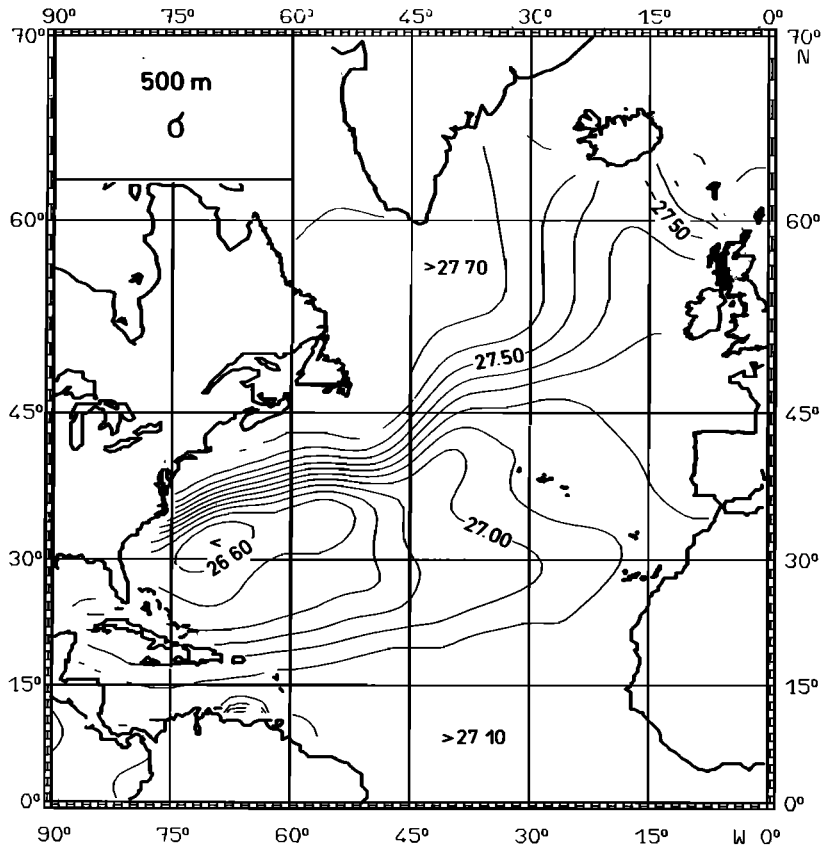

Fig. 9c

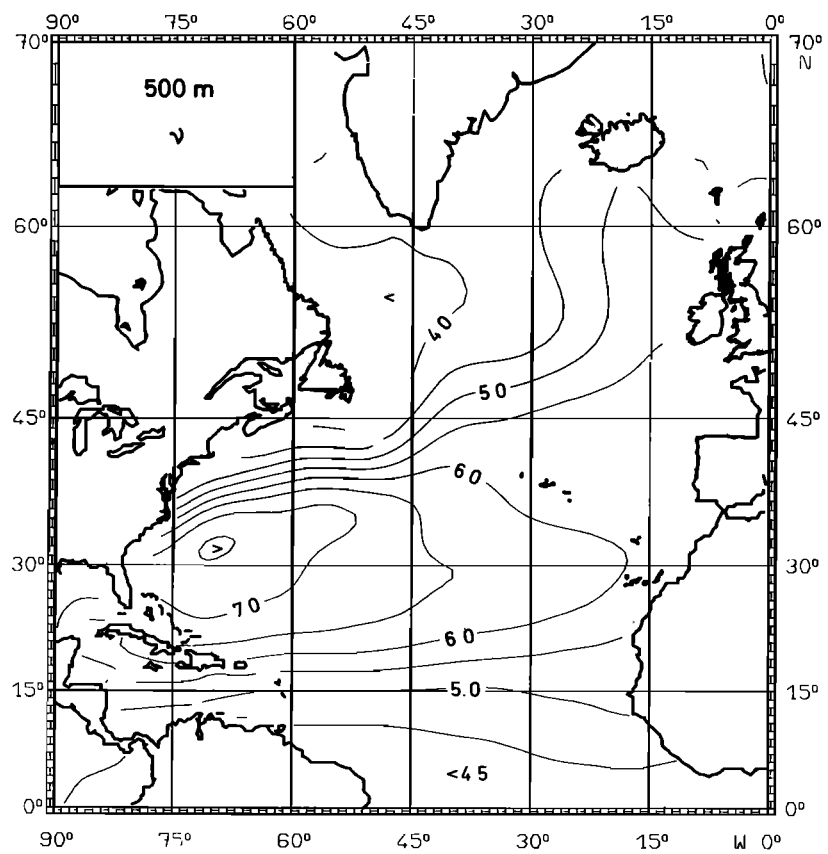

Fig. 9d

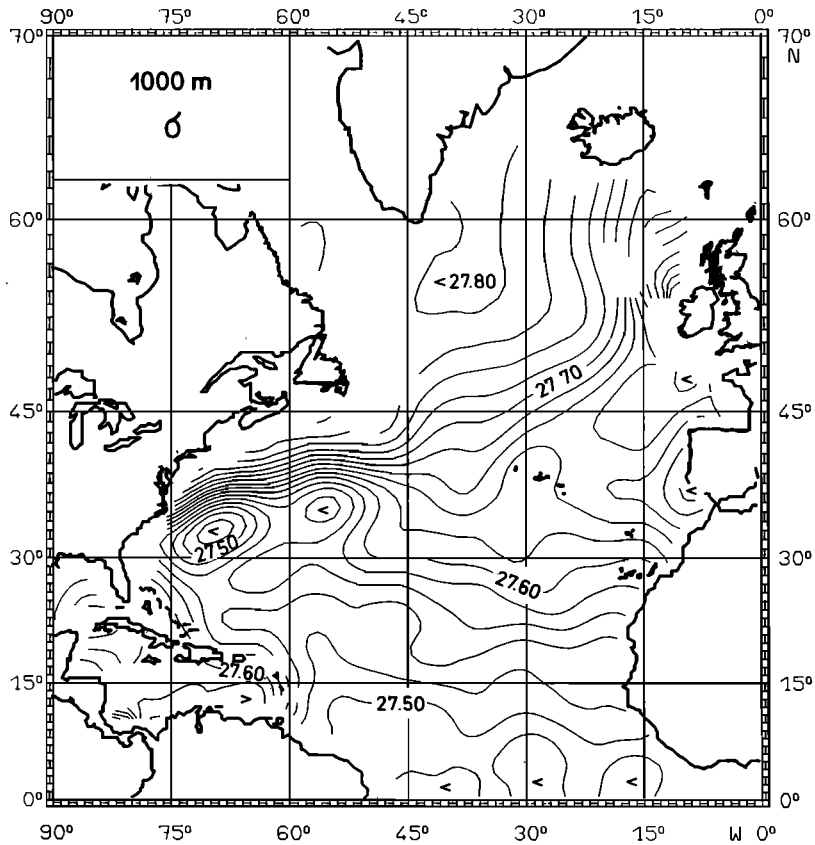

Fig. 9*e*

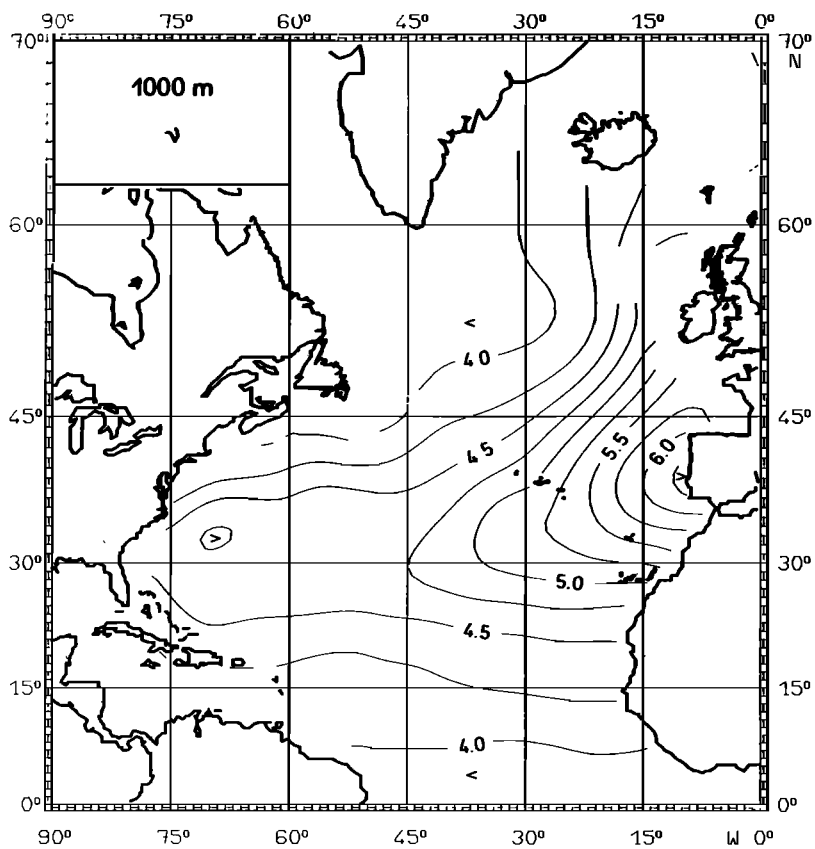

Fig. 9*f*

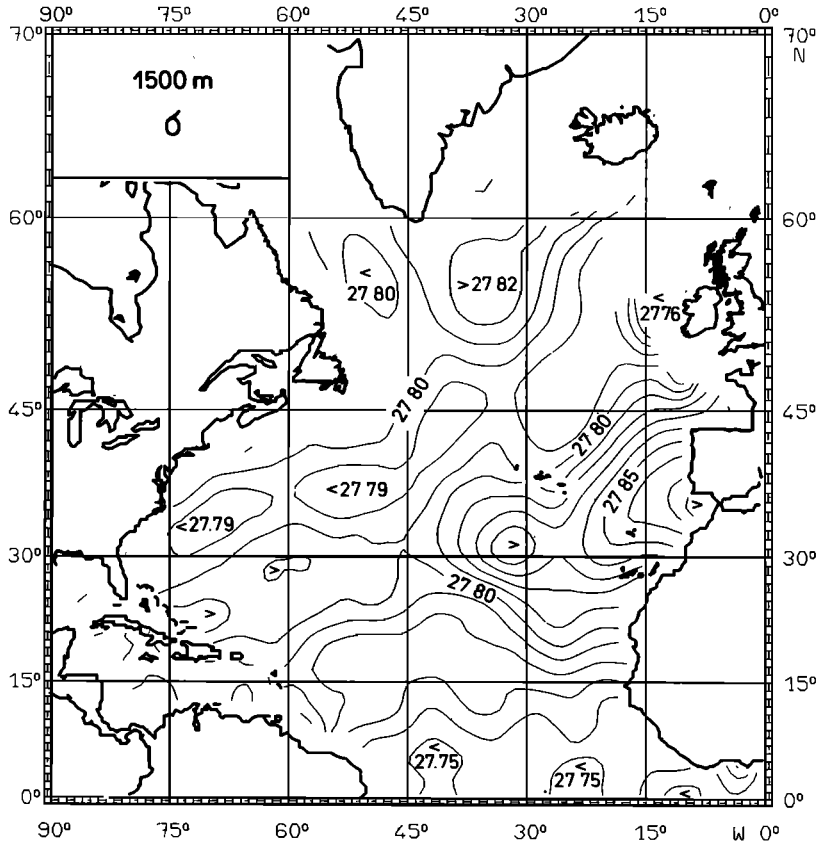

Fig. 9*g*

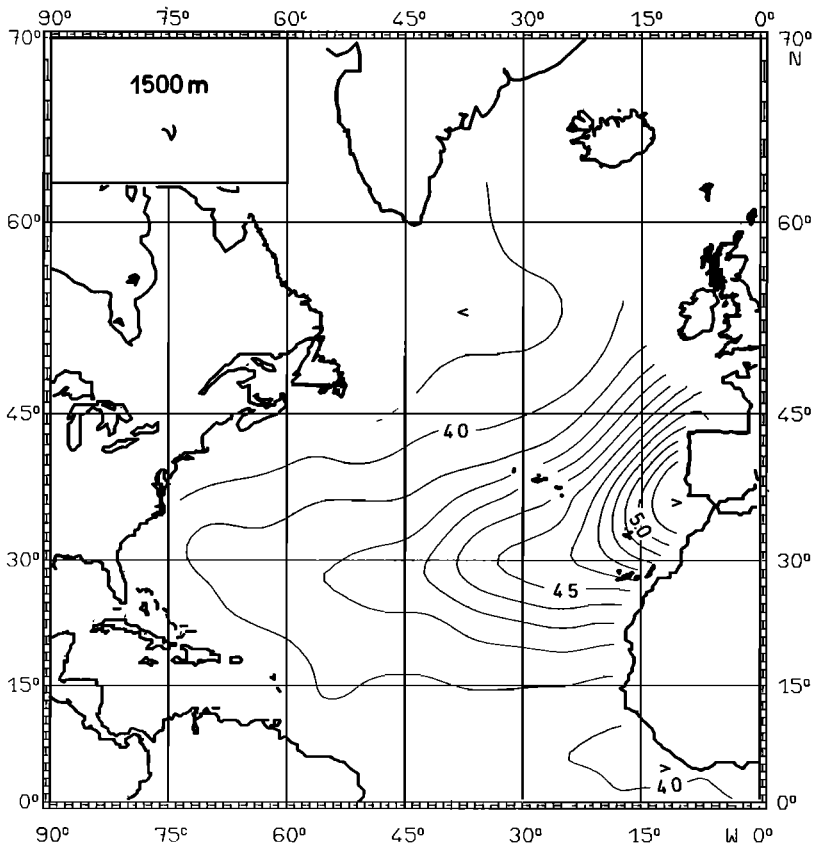

Fig. 9*h*

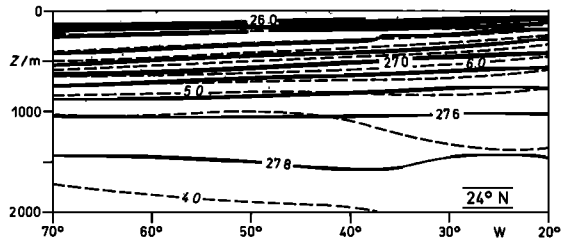

Fig. 10*a*

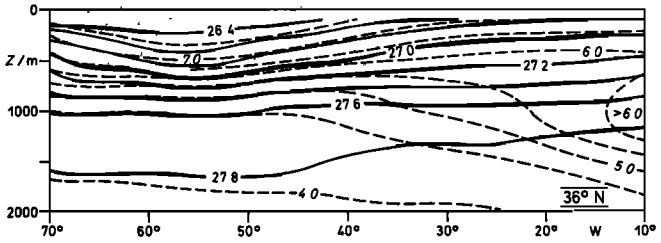

Fig. 10*b*

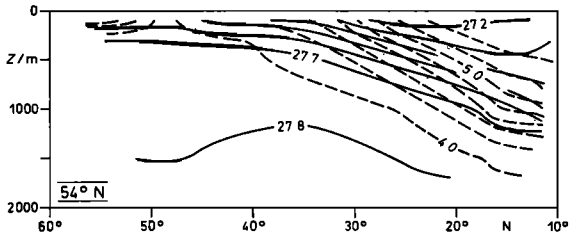

Fig. 10*c*

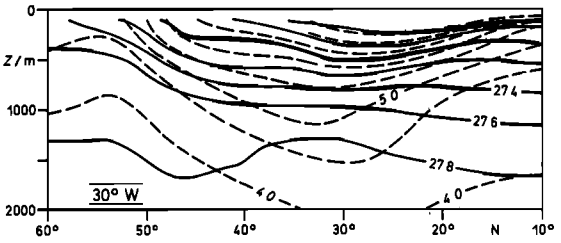

Fig. 10*d*

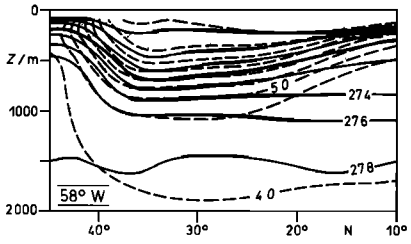

Fig. 10*e*

Fig. 10. Sections of potential density (solid lines) and veronicity (dashed lines) for the upper 2000 m: (*a*) 24°N, (*b*) 36°N, (*c*) 54°N, (*d*) 30°W, (*e*) 58°W.

and the mixing term G^{ψ} in the tracer balance becomes

$$G^{\psi} = \partial_i K_{ij} \partial_j \psi \tag{12}$$

Here we have used the notation x_1, x_2 for the horizontal coordinates and $x_3 = z$ for the vertical coordinate and ∂ is the three-dimensional gradient operator $\partial_j = \partial/\partial x_j$.

Notice that the formulation (11) ignores certain effects of double diffusion, cabbeling and compressibility as pointed out by *Kirwan* [1983].

With potential density as tracer, i.e., $\psi \equiv \sigma$, the diffusion term is thus simply

$$G^{\sigma} = \partial_i (A_c \partial_i \sigma) \approx \partial_3 A_c \partial_3 \sigma \tag{13}$$

From the β spiral scheme applied to σ as tracer thus only the diapycnal coefficient A_c can be determined. To obtain the isopycnal coefficient A_l, a tracer must be chosen that varies on isopycnals such as temperature or salinity or a functional of these fields which is different from σ. The isopycnal coefficient A_l enters the diffusion term in the form

$$\partial \cdot \left\{ A_l \left(\partial\psi - \frac{\partial\psi \cdot \partial\sigma}{|\partial\sigma|^2} \partial\sigma \right) \right\} = \partial \cdot \{ A_l |\partial\psi| \mathbf{n} \sin \phi \} \tag{14}$$

where ϕ is the angle between $\partial\sigma$ and $\partial\psi$ and $\mathbf{n}$ is the unit vector along the isopycnal. Apparently, if one wants to determine A_l from data, this term should be made as large as possible by appropriate choice of the tracer $\psi = \psi(\theta, S)$. The variable that maximizes the angle ϕ for given fields θ and S is obtained as follows. Linearizing the functional relationships for the purpose of demonstration,

$$\begin{aligned} \sigma &= -\alpha\theta + \beta S \\ \psi &= \gamma\theta + \delta S \end{aligned} \tag{15}$$

one finds

$$\sin \phi = \frac{\alpha\delta + \beta\gamma}{[\gamma^2(\partial\theta)^2 + \delta^2(\partial S)^2 + 2\gamma\delta\partial\theta \cdot \partial S]^{1/2}} \frac{\partial\theta \times \partial S}{|\partial\sigma|} \tag{16}$$

Neglecting the term $2\delta\gamma\partial\theta \cdot \partial S$ in the denominator, we find that sin ϕ becomes a maximum for

$$\beta\delta(\partial S)^2 = \alpha\gamma(\partial\theta)^2 \tag{17}$$

Introducing scales $\Delta\theta$, ΔS according to the average variability, i.e.,

$$\frac{\Delta\theta}{\Delta S} = \left[\frac{\langle(\partial\theta)^2\rangle}{\langle(\partial S)^2\rangle} \right]^{1/2} \approx \left[\frac{\langle(\partial_z\theta)^2\rangle}{\langle(\partial_z S)^2\rangle} \right]^{1/2} \tag{18}$$

where angle brackets denote some appropriate averaging, we find the variable which on average has the maximum gradient on isopycnals:

$$\psi = \nu(\theta, S) = [\beta(\Delta S)^2\theta + \alpha(\Delta\theta)^2 S]/(\Delta\theta\ \Delta S) \tag{19}$$

This is the veronicity introduced in section 2.3.

In a θ-S diagram where θ and S are scaled by $\Delta\theta$ and ΔS, respectively, the variables σ and ν defined by (16) are orthogonal straight lines. *Stommel* [1962] used these linearly independent variables in an analytical model of the oceanic θ-S curve. *Veronis* [1972] gave a polynomial representation of $\nu(\theta, S)$ now defined as the set of curves which everywhere is locally orthogonal to the curves $\sigma(\theta, S) = \text{const}$ in the (scaled) θ-S diagram. We will use these variables, potential density $\sigma(\theta, S)$ and veronicity $\nu(\theta, S)$, for the investigation of the role of mixing.

Mixing of vorticity will only be considered as due to vertical transport of horizontal momentum so that the mixing F in the vorticity equation is

$$F = [A(v_x - u_y)_z]_z \tag{20}$$

where A is the eddy coefficient. Horizontal eddy transport of vorticity will not be incorporated, since it causes the β spiral problem to be nonlocal (in the sense that reference velocities

and mixing parameters at each horizontal position can no longer be determined independently).

3.3. *Some Aspects of β Spiral Dynamics*

In the interior layer we attempt to infer the absolute velocity profile from a β spiral scheme. The aim of this method is the calculation of the absolute velocity from local gradients of measured ocean properties, such as temperature, salinity, or other tracers. There are various ways to devise a scheme for this purpose on the basis of the conservation equations (7)–(10). Because of noise in the observations the solutions for the absolute velocity differ depending on which equations are satisfied exactly and which are only approximately satisified in a least squares sense. To consider the scheme which we use in the remainder of this paper within the framework of previous β spiral methods, we give a brief survey of some of these schemes.

The β spiral schemes are not directly based on the momentum balance (7), since the determination of the pressure is a nonlocal problem. Also, the continuity constraint (9) relates the velocity at different horizontal positions. A local diagnostic problem that contains only vertical derivatives and relates only velocity and density is obtained by eliminating the pressure in (7) and the horizontal divergence between (8) and (9). This yields the thermal wind relations

$$u_z = (g/f)\rho_y \qquad v_z = -(g/f)\rho_x \tag{21}$$

and the local form of the vortex stretching equation

$$w_z = \frac{\beta}{f} v - F/f \tag{22}$$

One may replace this by a potential vorticity equation

$$(\mathbf{u}\cdot\nabla + w\,\partial_z)Q = \frac{F}{f} Q + fG_z + gJ_{xy}(\rho, \psi) \tag{23}$$

where $Q = f\psi_z$ is a potential vorticity and J_{xy} is the Jacobian operator with respect to x and y. Equation (23) is obtained by vertical differentiation of (10) and use of (21) and (22). Notice that while (23) is valid for any tracer governed by (10), we later use $Q = f\sigma_z$ as the potential vorticity (cf. equation (47) below).

With ρ and ψ given from observations the equations (10), (21), and (22) (or (23)) give four relations for the three velocity components. So obviously, a unique solution to the diagnostic problem does not exist. Indeed, as shown by *Olbers and Willebrand* [1984], one can generate a hierarchy of relations which expresses the three velocity components in terms of density with increasing order of derivatives involved. The lowest order is Needler's formula [*Needler*, 1985]. The u component is obtained by eliminating w between (10) and (23), which yields

$$uJ_{xz}(Q, \psi) + vJ_{yz}(Q, \psi) = \psi_z Q(G/\psi_z)_z + F\psi_z{}^2 + gJ_{xy}(\rho, \psi)\psi_z \tag{24}$$

Dividing by $J_{yz}(Q, \psi)$, taking the derivative with respect to z, and eliminating u_z and v_z by (21) then yields u in terms of the gradients of ρ and ψ up to third order. Representations for v and w are obtained correspondingly. Obviously, one can continue this procedure to express the velocity in terms of even higher gradients. However, unless ρ and ψ are not incidentally part of an exact solution of the entire dynamical problem, the resulting velocity profiles will not be compatible with all four equations (10), (21), and (22) of the β spiral dynamics, nor will the successive steps of the hierarchy yield identical results.

Closed expressions for the absolute velocity vector obtained from β spiral dynamics contain at least third-order derivatives of the ψ field. If ρ and ψ are taken from observations, they contain noise which generally will be enhanced by differentiation. The β spiral schemes do not use more than second-order gradients of the ψ field. Indeed, (24) is the β spiral equation of *Stommel and Schott* [1977], *Behringer* [1979], and others in its most general form. If the thermal wind relations (21) are integrated from some reference level $z = z_0$ in the form

$$u = u_0 + u_r = u_0 + \frac{g}{f}\int_{z_0}^{z} dz'\,\rho_y \qquad v = v_0 + v_r = v_0 - \frac{g}{f}\int_{z_0}^{z} dz'\,\rho_x \tag{25}$$

the unknown reference velocities u_0 and v_0 may be obtained by inserting (25) into (24) and considering the resulting equation at two different levels. This yields two equations for the two unknowns u_0 and v_0. In practice, because of noisy data a more stable solution is obtained by evaluating (24) at more than two levels and determining u_0 and v_0 from the resulting overdetermined set of equations by a least squares principle. The profiles of horizontal velocities then follow from (25), and the vertical component can be calculated from the ψ balance (10), i.e.,

$$w = \{G - \mathbf{u}\cdot\nabla\psi\}/\psi_z \tag{26}$$

The solution obtained in this scheme satisfies exactly the thermal wind relations (21) and the tracer balance (10), but the velocity profiles do not reproduce the linearized vorticity equation (22) as well as the potential vorticity balance (23). The philosophy behind this approach is thus to believe in the correctness of the thermal wind relations and the tracer balance but to allow inaccuracies in the linear vorticity balance to make the solution unique. This concept seems to agree with the fact that (22) is linearized and thus to some degree inaccurate: the omitted nonlinear terms in this equation are indeed of order $RoR/L < 1$ relative to those retained, where Ro is the Rossby number, R the radius of the earth, and L the horizontal length scale of the flow. The omitted terms in the thermal wind balance are of order Ro compared to those retained, i.e., much smaller ($L/R \approx 0.2$) than those in the vorticity equation.

However, inaccuracy of the equations is only one part of the disparity which may occur with a diagnostic use of the β spiral dynamics. The method uses observed density and tracer data which generally are inaccurate as well. Individual hydrographic sections contain noise from internal waves and synoptic scale eddies. In a climatological averaged field this noise will be reduced but not eliminated. Further, an objective analysis will have to interpolate into data-poor regions. We thus have to anticipate inaccuracies in the velocity estimates arising from the noise in ρ and ψ. In particular, the estimate of w from (26) will be biased because of the nonlinear form of this equation.

To be more specific, let ρ and ψ contain noise $\delta\rho$ and $\delta\psi$, respectively. For the highly averaged data set which we will use, the scales of the noise will be comparable with the scales of the flow itself. The thermal wind relations imply an error

$$\{\delta u, \delta v\} = O\left(\frac{gH}{f}\{\delta\rho_y, \delta\rho_x\}\right) \tag{27}$$

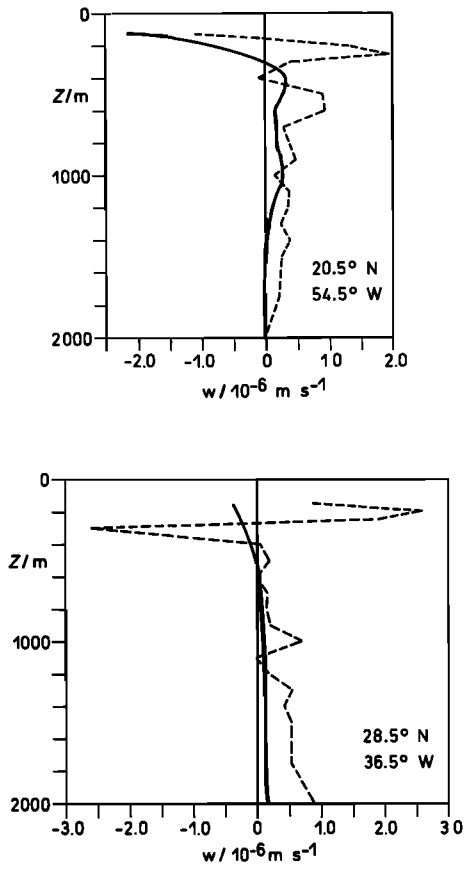

Fig. 11. Profiles of vertical velocity w. Solid lines represent w computed from the linear vorticity equation (22), and dashed lines w computed from the tracer balance equation (26).

for the horizontal velocities, where H is the vertical scale of the flow. From the tracer balance (26) the error in the vertical component becomes

$$(\delta w)_{TB} = O\left(\frac{gH}{f}\frac{H}{L}[\delta\rho_x{}^2 + \delta\rho_y{}^2]^{1/2}\right) \tag{28a}$$

The estimation of w from the vorticity balance (22) implies an error

$$(\delta w)_{VB} = \int \frac{\beta}{f}\,\delta v\,dz = O\left(\frac{gH}{f}\frac{H}{R}\,\delta\rho_x\right) \tag{28b}$$

so that

$$\frac{(\delta w)_{VB}}{(\delta w)_{TB}} = O\left(\frac{L}{R}\frac{\delta\rho_x}{[\delta\rho_x{}^2 + \delta\rho_y{}^2]^{1/2}}\right) \lesssim 0.2 \tag{29}$$

The error in the estimate of w from the vorticity balance is thus considerably lower than that from the tracer balance, especially when zonal gradients can be estimated more accurately than meridional gradients. Consideration of the bias due to nonlinearities in both equations supports this conclusion.

Apparently, though we tend to believe more in the dynamical accuracy of the tracer balance than that of the linearized vorticity balance, the data noise introduces a smaller error in the latter when estimating w. Thus we should calculate w from the vorticity balance rather than from the tracer balance. A hint toward this concept can be found in a comparison made by *Behringer* [1979, Figure 4]. Behringer calculated w from the tracer balance (26) and compared the result with the integral of the linear vorticity equation (22). While the first profile looks rather noisy, the result from the vorticity equation is very smooth. This feature is demonstrated in Figure 11, which compares the two profiles for w at two sites. As tracer we used potential density. It should be noted that particularly near surface and deep, estimates of w contain noise. Its origin is presumably different. Close to the surface, potential density is not conserved, so that w picks up all the inaccuracies which arise from neglecting the proper nonadiabatic terms in (26). The discrepancy in the deep values is most likely due to inaccuracies of the gradient estimates which directly affect w in (26) but appear to be smoothed in the vorticity balance by double integration. The β spiral scheme formulated in the next section is based on preceding error analysis. However, we would like to emphasize already here that the determination of w remains an unsatisfactory aspect of the method. As discussed in section 4.3, the vertical velocity cannot be estimated independently of other parameters.

The above considerations show that exact solutions of the four equations (10), (21), and (22) for the three unknown velocity components normally do not exist and that results such as Needler's formula [*Needler*, 1985] or β spiral solutions are obtained by ignoring the exact validity of one (or one combination) of these equations. The question arises concerning the validity of the equations (7)–(9) describing the complete dynamics. With u and v obtained from the integrated thermal wind relations (25) and w satisfying the vorticity equation (22), the continuity constraint requires that the reference velocities satisfy

$$(fu_0)_x + (fv_0)_y - F = 0 \tag{30}$$

If the friction had been retained in (7) the condition (30) would also guarantee the existence of a pressure field. In general, however, a local estimation of u_0 and v_0 will not satisfy (30), so that the velocity field obtained by combining such local β spiral results will neither be mass conserving nor be exactly geostrophically balanced.

3.4. *The β Spiral Scheme and Its Formal Solution*

We now introduce a β spiral scheme which takes account of the above considerations. In this scheme the vertical velocitiy will be obtained from the integrated vorticity equation

$$w = w_0 + \frac{1}{f}\int_{z_0}^{z} dz'\{\beta v - F\} \tag{31}$$

Using (20) and (25), this may be expressed entirely in terms of the reference velocities and the density field. Thus the mixing term contributes

$$-\frac{1}{f}\int_{z_0}^{z} dz'\,F = \frac{g}{f^2}\left[A\left(\nabla^2\rho - \frac{\beta}{f}\rho_y\right)\right]_{z_0}^{z} \tag{32}$$

Inserting (31) and the integrated thermal wind relations (24) into the tracer balance (10), we find

$$u_0\psi_x + v_0\left[\psi_y + \psi_z\frac{\beta}{f}(z - z_0)\right] + w_0\psi_z + M = b \tag{33}$$

where M collects the mixing terms

$$M = G - \frac{1}{f}\psi_z\int_{z_0}^{z} dz'\,F \tag{34}$$

which may be expressed in terms of the mixing coefficients A_c, A_l, and A and field gradients. Further, b is the baroclinic term

$$b = \frac{g}{f}\left\{J_{xy}\left(\psi, \int_{z_0}^{z} dz'\,\rho\right) - \psi_z \frac{\beta}{f}\int_{z_0}^{z} dz'(z'-z)\rho_x\right\} \qquad (35)$$

Equation (33) relates at each level z three unknown reference velocity components u_0, v_0, w_0 and the mixing parameters to the known gradients of the fields ρ and ψ. If we allow an imbalance $\varepsilon(z)$ on the right-hand side, we can construct a least squares solution. This will be described below. Notice at this point that in contrast to the scheme described in the previous section this scheme involves only first-order gradients of the data. This has been achieved by increasing the number of unknowns by one.

To formulate the least squares problem of constructing the reference velocities u_0, v_0, w_0 and the mixing coefficients A_c, A_l, and A from data, we assume that the fields ρ and ψ and their derivatives ρ_x, ρ_y, ψ_x, ψ_y, and ψ_z are given at several levels $z = z_j$, $j = 1, \cdots, N$. Then (33) may be written in the form

$$D_{jk}p_k - b_j = 0 \qquad j = 1, \cdots, N \qquad (36)$$

where D_{jk} and b_j are coefficients of the unknown parameters and baroclinic terms evaluated at the levels z_j, respectively, and p_k, $k = 1, \cdots, L$ are the unknown parameters u_0, v_0, w_0, A_c, A_l, and A or any subset of these. Physically meaningful are only those solutions of (36) which have positive diffusion coefficients, so we require that a condition

$$B_{kl}\,p_l \geq 0 \qquad k = 1, \cdots, L \qquad (37)$$

is satisfied where the matrix B_{kl} is defined appropriately.

Techniques for obtaining solutions to the overdetermined system (36) (in general we have $N > L$) subject to constraints of the form (37) can be found, for example, in the work by *Lawson and Hanson* [1974], also briefly described (for the underdetermined system) by *Wunsch and Minster* [1982]. A least squares solution to (36) is constructed by the method of singular value decomposition or, equivalently, by using the generalized Moore-Penrose inverse. In addition, we have applied a weighting of the equations (36) in the form

$$\mathbf{W}^{1/2}\mathbf{D}\mathbf{p} = \mathbf{W}^{1/2}\mathbf{b} \qquad (38)$$

by a positively definite symmetric matrix $\mathbf{W}^{1/2}$, the rationale of which will be discussed later. Furthermore, a resolution control is incorporated as described, for example, by *Wiggins* [1972] and *Wunsch* [1978].

To be more specific, consider the generalized inverse of $\mathbf{W}^{1/2}\mathbf{D}$ in the singular value decomposition

$$(\mathbf{W}^{1/2}\mathbf{D})_{GI}{}^{-1} = \sum_{k=1}^{L} \frac{1}{\lambda_k}\mathbf{V}_k\mathbf{U}_k{}^{+} \qquad (39)$$

where the $\lambda_k{}^2$ are the eigenvalues of $\mathbf{D}^{+}\mathbf{W}\mathbf{D}$ and the N-dimensional $\mathbf{U}_k$ and L-dimensional $\mathbf{V}_k$ are defined by the coupled eigenvector problems

$$\begin{aligned} \mathbf{D}^{+}\mathbf{W}^{1/2}\mathbf{U}_k &= \lambda_k\mathbf{V}_k \\ \mathbf{W}^{1/2}\mathbf{D}\mathbf{V}_k &= \lambda_k\mathbf{U}_k \end{aligned} \qquad k = 1, \cdots, L \qquad (40)$$

If $\mathbf{D}^{+}\mathbf{W}\mathbf{D}$ is singular, only contributions with nonzero λ_k are included in the sum (39). Then the rank of $(\mathbf{W}^{1/2}\mathbf{D})_{GI}$ is less than L, and the parameters become linearly dependent. In practice, even with appropriate scaling of the parameters the eigenvalues λ_k may span several decades and decay exponentially, so that it is very difficult to distinguish between very small eigenvalues and zero eigenvalues. The contributions from the low λ_k may lead to an unacceptably large amplification of the data noise in the parameter variance. In this case the resolution of the parameters from the data leads to the necessity to rely on the data noise, or, in other words, in the attempt to resolve more and more parameters, information will increasingly be drawn from the noise structure in the data. On the other hand, if we cut off more and more terms in (39), the parameters become more and more dependent; i.e., the resolution decreases. Apparently, there is a trade-off between resolution and variance of the parameters which is controlled by the range of the λ_k. Replacing (39) by the "tapered cutoff" version

$$(\mathbf{W}^{1/2}\mathbf{D})_{GI}{}^{-1} = \sum_{k=1}^{L} \frac{\lambda_k}{\lambda_k{}^2 + \lambda_c{}^2}\mathbf{V}_k\mathbf{U}_k{}^{+} \qquad (41)$$

we thus can control the variance of the parameters on account of the resolution by the value of λ_c. This will be seen below in the expression (45) of parameter covariance matrix computed from (41). The results of our β spiral fit described in the next section were obtained with $\lambda_c{}^2 = 10^{-3} \times \max(\lambda_k{}^2)$. Apart from the tapered cutoff modification the LSI/LDP algorithm of *Lawson and Hanson* [1974, p. 158] was used to find the least squares solution of (38) subject to the inequality constraints (37).

A rationale for considering the least squares solution of the overdetermined system can be given in terms of computational errors in the coefficients D_{jk} and b_j resulting from inaccurate data. Also, errors may arise from incorrect assumptions about the β spiral dynamics. In the presence of such inconsistencies the best solution for the reference velocities and mixing parameters is considered to be the one minimizing some positive definite norm of the residuals $\varepsilon_j = D_{jk}p_k - b_j$, such as

$$\varepsilon^2 = \sum_{i,j=1}^{N} \varepsilon_i W_{ij}\varepsilon_j \qquad (42)$$

with a weighting matrix W_{ij}. The geometrical and statistical aspects of such an approach have been outlined, for example, by *Olbers et al.* [1976] and *Müller et al.* [1978]. It is useful to interprete W_{ij} as a metric in an N-dimensional space and the least squares problem as the minimizing of the square distance ε^2 of the vector N-dimensional $\mathbf{b} = (b_j)$ to the model vector $(D_{jk}p_k)$ which lies on the L-dimensional hyperplane spanned by the L vectors (D_{jk}), $k = 1, \cdots, L$.

The choice of the metric represents a subjective element in the analysis which formally sets all linear schemes based on the same β spiral dynamics equivalent. This is discussed in detail in Appendix B for the schemes employed by *Stommel and Schott* [1977], *Behringer* [1979] and *Behringer and Stommel* [1980]. The pure formality of such an equivalence, however, should be emphasized, since the performance of different weighting with respect to the ability to extract the information contained in the data may be quite different.

If the maximum likelihood principle is to be applied, the metric must be chosen as the inverse of the covariance matrix $\langle\varepsilon_i\varepsilon_j\rangle$ of the residuals (angle brackets denote ensemble averages). A simpler diagonal metric has been investigated by *Müller et al.* [1978]. The metric $W_{ij} = \delta_{ij}w_{(j)}$ with

$$w_j = \frac{1}{\langle\varepsilon_j\rangle^2}\left(\sum_k \frac{\langle\varepsilon_j\varepsilon_k\rangle}{\langle\varepsilon_j\rangle^2\langle\varepsilon_k\rangle^2}\right)^{-1} \qquad (43)$$

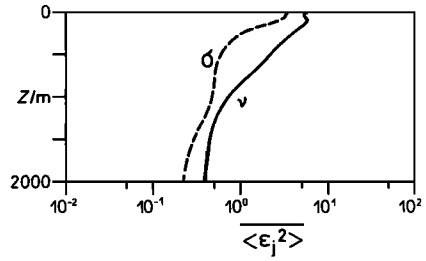

Fig. 12. Profiles of the basin average of the variances $\langle \varepsilon_j^2 \rangle$ (relative units). The weighting $w_{(j)}$ is the inverse of $\langle \varepsilon_j^2 \rangle$.

weights the residuals with their rms standard deviation and with an integral measure of their correlation with the residuals at the other levels. Thus strongly correlated data are weighted less than uncorrelated data. The metric (43) can be shown to be the closest approximation (in a least squares sense) of a diagonal metric to the maximum likelihood metric. The evaluation of (43) still meets practical difficulties, as the correlation structure of the data is rather poorly known. However, if one assumes that the vertical correlation scale l_j at level j is large compared to the distance from neighboring levels in the data set, a coarse approximation to the sum of correlations would be the number levels within the correlation scale, or $l_j/\Delta h_j$, where Δh_j is the vertical separation of the levels. Then (43) becomes

$$w_{(j)} = \frac{\Delta h_j}{l_j \langle \varepsilon_j^2 \rangle} \tag{44}$$

For each 10° square the variance $\langle \varepsilon_j^2 \rangle$ at each level z_j has been estimated by a Monte Carlo simulation by generating random ensembles for the density and tracer fields, respectively, with the prescribed horizontal correlation behavior of the data gradients discussed in Appendix A. A mean variance profile was obtained by averaging over all 10° squares. This mean variance profile was finally used to construct the weighting (44) shown in Figure 12. Notice that the variances $\langle \varepsilon_j^2 \rangle$ strongly decrease from the surface with increasing depth. This structure follows the pattern of natural variability in the data, which is large in the upper ocean and decreases with depth.

The effect of nonuniform correlation length l_i was investigated extensively with l_i decreasing or increasing with depth, but finally l_i was taken constant, since the range of levels utilized for the fitting procedure was divided again for reasons discussed in the next section.

Parameter estimation is only one aspect of a statistical least squares procedure. Estimating the parameter variances and correlations and, more important, testing the model validity are the second step of this method [e.g., *Müller et al.*, 1978]. If we ignore the fact that the matrix **D**, relating the vector **b** of baroclinic terms to the parameter vector **p**, itself is a random quantity, one obtains the parameter covariances from

$$\langle \delta \mathbf{p}\, \delta \mathbf{p}^+ \rangle = \frac{\langle \varepsilon^2 \rangle}{N - L} (\mathbf{D}^+ \mathbf{W} \mathbf{D})_{GI}^{-1}$$

$$= \frac{\langle \varepsilon^2 \rangle}{N - L} \sum_{k=1}^{L} \frac{\lambda_k^2}{(\lambda_k^2 + \lambda_c^2)^2} \mathbf{V}_k \mathbf{V}_k^+ \tag{45}$$

This relation holds exactly if the weight matrix **W** is taken as the inverse of $\langle \delta \mathbf{b}\, \delta \mathbf{b}^+ \rangle$ according to the maximum likelihood principle. For the diagonal weights (44) this formula is still approximately correct if the number of levels N is replaced by the number of uncorrelated levels. To account for errors in **D**, we will assume that (45) underestimates the variances by a factor of 2 but that the correlation structure of the parameters is not influenced.

Model validity can be investigated by performing, for example, a confidence test on the quantity ε^2 [cf. *Müller et al.*, 1978]. Again, the information was not available to obtain the distribution parameters of ε^2, and we had to abandon this approach. Instead we will have to check the validity of our results by comparing a priori knowledge of the North Atlantic circulation with the resulting pattern of the velocity field and of the mixing parameters.

3.5. *Modeling Strategy*

The results obtained by applying the above described β spiral scheme to the North Atlantic part of *Levitus'* [1982] atlas will be presented in section 4. The calculations were performed as follows.

Temperature and salinity were used to compute in situ density and the tracer variables potential density $\sigma(\theta, S)$ (referred to surface pressure) and veronicity $\nu(\theta, S)$. The horizontal gradients were estimated by central differences over 2°. This narrow spacing turned out to be necessary close to the coasts, where the isolines of the tracer frequently crowd. Away from the coasts, because of the smoothness of the data analysis the estimations of the gradients are relatively stable with respect to the spacing over which the differences were taken. This, however, is not true in the deep part of the water column, in particular in the vicinity of topographic features such as the Mid-Atlantic Ridge. Here the horizontal gradients were unstable with respect to variation of the spacing and assumed in some places unrealistically high values. As a consequence of this behavior the results of the β spiral fit (i.e., the reference velocities) critically depended on the vertical extent of the data profile if this dropped below 2000 m. The limited accuracy of the estimated field gradients has already been discussed in section 2.1. For this reason we discarded data from below 2000 m from the least squares fit (although velocity profiles shown below extend to deeper levels). The upper limit of the profile length was chosen as the maximum depth D of the top of the thermocline as shown in Figure 2.1. In higher latitudes, where D takes values of 900 m, about 10 levels remain for the least squares fit; in lower latitudes, with D of the order of 200 m, the number of levels is about 15–20. The vertical spacing of the levels in the interval from D to 2000 m is $\Delta h = 100$ m for $D \geq 300$ m; for shallower $D \geq 150$ m the spacing is $\Delta h = 50$ m.

The model outlined in the preceding section contains six parameters: the three reference velocities u_0, v_0, and w_0 and the diffusivities A_c, A_l, and A. So far, we have assumed these mixing parameters to be constant with depth, but at least for the diapycnal diffusivity A_c (see, for example, *Gargett* [1984]) a depth dependence seems to be well established. But also the other two diffusivities are expected to vary with depth. The vorticity mixing described by the coefficient A should be more effective in the upper part of the analyzed depth interval where the pool of constant potential vorticity is located [*Rhines and Young*, 1982]. Also, the isopycnal coefficient A_l should be different for water masses in the Mediterranean tongue or outside.

In principle, a depth-varying coefficient could be handled by introducing more parameters describing the profile. However, we decided instead to break up the depth interval into two subsets, $-D \geq z \geq -800$ m and -800 m $\geq z \geq -2000$ m,

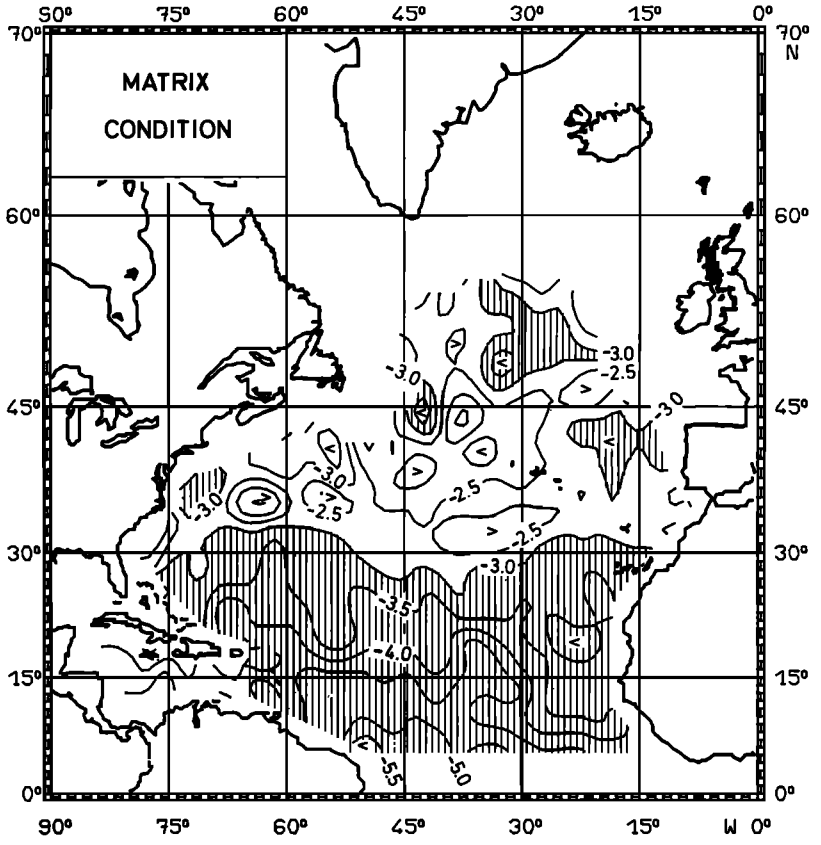

Fig. 13*a*

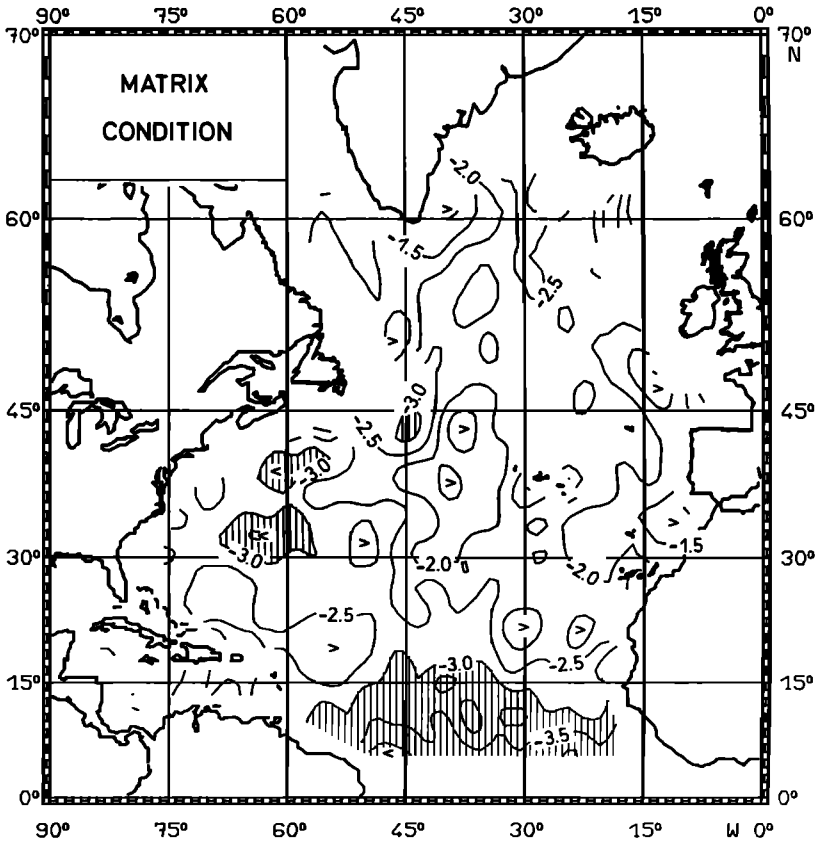

Fig. 13*b*

Fig. 13. Condition index of matrix $\mathbf{D}^{+}\mathbf{WD}$ for a model with no diffusion. The depth range is (*a*) *D*–800 m and (*b*) 800–2000 m. Shaded areas show condition index below 10^{-3}.

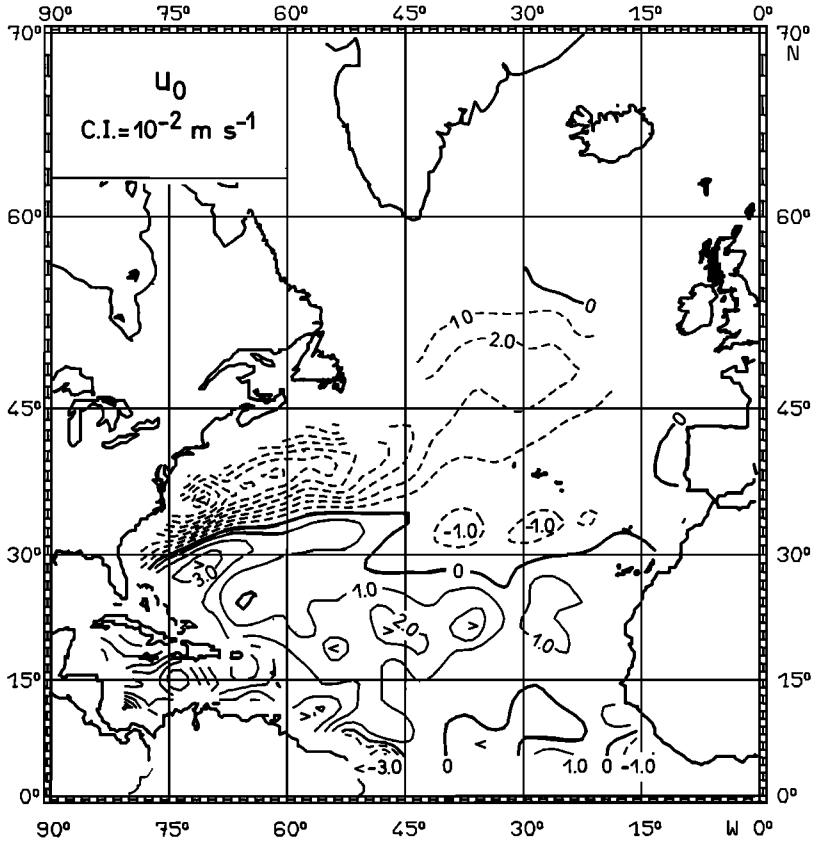

Fig. 14*a*

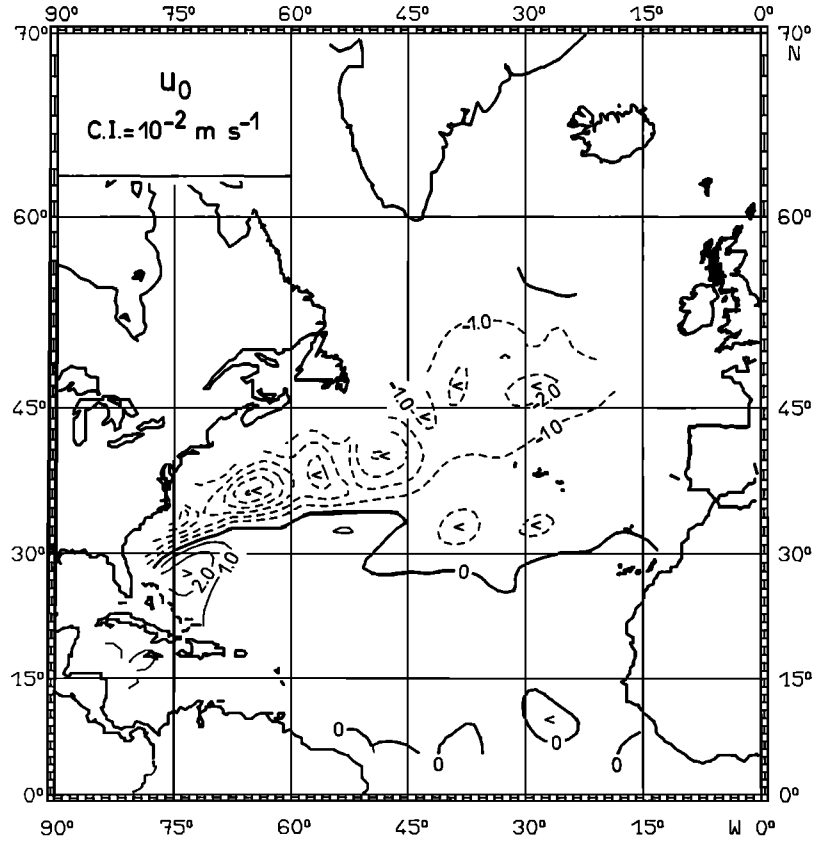

Fig. 14*b*

Fig. 14. Zonal reference velocity u_0 computed from the depth range D–800 m (units are centimeters per second): (*a*) no truncation and (*b*) with truncation $\lambda_c^2/\lambda_{max}^2 = 10^{-3}$ (cf. equation (41)).

with about the same number of levels over most of the area and to fit constant diffusivities to these subsets. The reason for this strategy can be taken from Figure 13, showing the condition of the matrix $\mathbf{D}^+\mathbf{WD}$ computed for the depth ranges given above for a model with no diffusion at all. The matrix condition is here defined as the ratio of the smallest eigenvalue to the largest eigenvalue, i.e., min $\{\lambda_k^2\}$/max $\{\lambda_k^2\}$. In contrast to the lower subset the determination of the reference velocities appears as an ill-conditioned problem in the upper set of levels (Figure 13*a*), as the condition index is below 10^{-3} over most of the domain. Inclusion of the mixing terms does not change this situation.

As we have explained in the previous section, the inverse of the condition index reflects the variances of the estimated parameters: if the condition index is low and not kept under control by a suitable cutoff value λ_c^2 as indicated in (45), the parameters tend to collect data noise, and the estimates become useless. If we switch on the variance control, however, by choosing λ_c^2 appropriately, the parameter estimates become dependent, and we are able to determine only two (or even one) linear combinations of the three reference velocities. An example for this singular behavior that is typical for most of the low-index area in Figure 13*a* can readily be given. Suppose that the gradient of the ψ field does not turn rapidly enough with depth, e.g, if ψ_x is very much smaller than ψ_y. In this case it is impossible to get a reliable estimate of u_0 from (33). In the framework of the least squares solution this is reflected in the singularity of $\mathbf{D}^+\mathbf{WD}$: one of the eigenvalues will be much less than the others. If one nevertheless attempts to resolve u_0, all parameters will be spoiled by data noise. If the cutoff is used, u_0 is essentially constrained to its initial value, and the remaining parameters are resolved unless their variances become larger for other reasons. This basic type of singular behavior occurs, of course, for other orientations of the ψ gradient. This is immediately evident if (33) is written in the form

$$\mathbf{u}_0 \cdot \boldsymbol{\mu} \frac{\partial \psi}{\partial \mu} - v_0 \frac{\beta}{f}(z - z_0)\psi_z + M = b \qquad (46)$$

where $\boldsymbol{\mu}$ is the direction normal to the $\psi =$ const surfaces. Since the second term in (46) is $O(L/R)$ compared to the first, the equation essentially constrains only the normal velocity component $\mathbf{u}_0 \cdot \boldsymbol{\mu}$, and if $\boldsymbol{\mu}$ does not turn with depth, the determination of the three reference velocities becomes a singular problem.

The situation described above is clearly elucidated in Figure 14, showing the u_0 field obtained from the upper subset corresponding to the condition index in Figure 13*a*. In the result shown in Figure 14*a* the matrix was not truncated. Figure 14*b* gives the result for truncation with $\lambda_c^2 = 10^{-3}$ max (λ_k^2), which essentially affects the solution in the shaded domain of Figure 13*a*. South of 30°N the isopycnals have predominant zonal orientation. Consequently, the resolution of u_0 makes the determination of the reference velocities ill conditioned, leading to the unrealistic large zonal velocities in Figure 14*a*. In the truncated case (Figure 14*b*) these are clearly reduced to values closer to the initial value $u_0 = 0$ at $z_0 = -2000$ m. Notice, however, that unless this initial guess of u_0 (or, equivalently, the depth of the reference level z_0) has been chosen in a meaningful way, it is not evident at all that the truncated solution is better than the untruncated one. Thus without a priori knowledge about the parameters which are not sufficiently constrained by the model the truncation method does not give by itself meaningful results.

Other major differences between the untruncated and the truncated cases occur along the path of the Gulf Stream and its extension, where Figure 13*a* also indicates a poor condition of the matrix. Again there is no substantial turning of the gradient of potential density (see Figures 9*c* and 9*e*). The untruncated solution (Figure 14*a*) shows a broad westward flow of unrealistic large velocity at the reference level of 2000 m. In this solution the level of no motion in the Gulf Stream region would be well above 1000 m depth. The truncation breaks up this structure in several blobs with lower velocity values, and the level of no motion drops significantly below the 1000-m level. There are other features in both of these solutions which do not agree with traditional concepts of the circulation; for example, the vertical velocities do not decay with depth but get unrealistic large values in the deep ocean (of the order of 10^{-3} cm s^{-1} at the 2000-m level). We should emphasize again that this deficiency cannot be overcome by inclusion of the mixing terms.

Apart from the case discussed above in which one component of the ψ gradient becomes small, there may be more severe configurations leading to singularity of the matrix $\mathbf{D}^+\mathbf{WD}$. A prominent candidate is the pool of homogeneous potential vorticity [*Rhines and Young*, 1982]. Maps of potential vorticity $f\sigma_z$ on isopycnals have been computed by *McDowell et al.* [1982] and *Holland et al.* [1984] (their Figure 4 is based on the *Levitus* [1982] data set). The maps show that $f\sigma_z$ is almost uniform on isopycnals below the mixed layer down to a depth of about 600 m in the subtropical gyre. In the form (24) of the β spiral equation used by *Schott and Stommel* [1978] it is most obvious that the determination of the reference velocities degenerates to a singular problem: both coefficients $J_{xz}(f\sigma_z, \sigma)$ and $J_{yz}(f\sigma_z, \sigma)$ vanish. Of course, our approach based upon (33) also becomes singular, as can be shown by a detailed analysis of the resulting $\mathbf{D}^+\mathbf{WD}$. It is indeed a well-known property of the thermocline equations (7)–(10) that for $f\sigma_z$ being constant on σ, solutions can only be given up to an arbitrary barotropic flow. This statement, first proved by *Needler* [1972], is reflected here in the singularity of $\mathbf{D}^+\mathbf{WD}$. Notice furthermore that additionally the baroclinic term b given by (35) becomes very small in the pool of homogeneous potential vorticity: with σ being almost identical to ρ one gets $b = O(L/R)$ compared to the values outside the pool.

The difference in the performance of the β spiral technique in response to shallow and deeper hydrographic data emerged already in previous attempts to obtain current profiles at single locations [*Schott and Stommel*, 1978; *Behringer*, 1979; *Schott and Zantopp*, 1980; *Behringer and Stommel*, 1980; *Lindstrom et al.*, 1980]. We attribute the problem to these singularities. There is little doubt that the data of the upper subset are unable to resolve the model parameters in a physically meaningful way; i.e., though formally being overdetermined, the model equations (36) do not sufficiently constrain the reference velocities. This does not imply that the assumed dynamical balance, i.e., the β spiral model, is wrong in the upper range of levels.

From these considerations we are led to the strategy of determining the reference velocities exclusively from the deeper levels. The upper subset is only used for estimating a possible depth dependence of the mixing coefficients. To be more specific, the final results presented in section 4 were obtained by the following steps:

1. The balance of potential density σ in the deeper subset

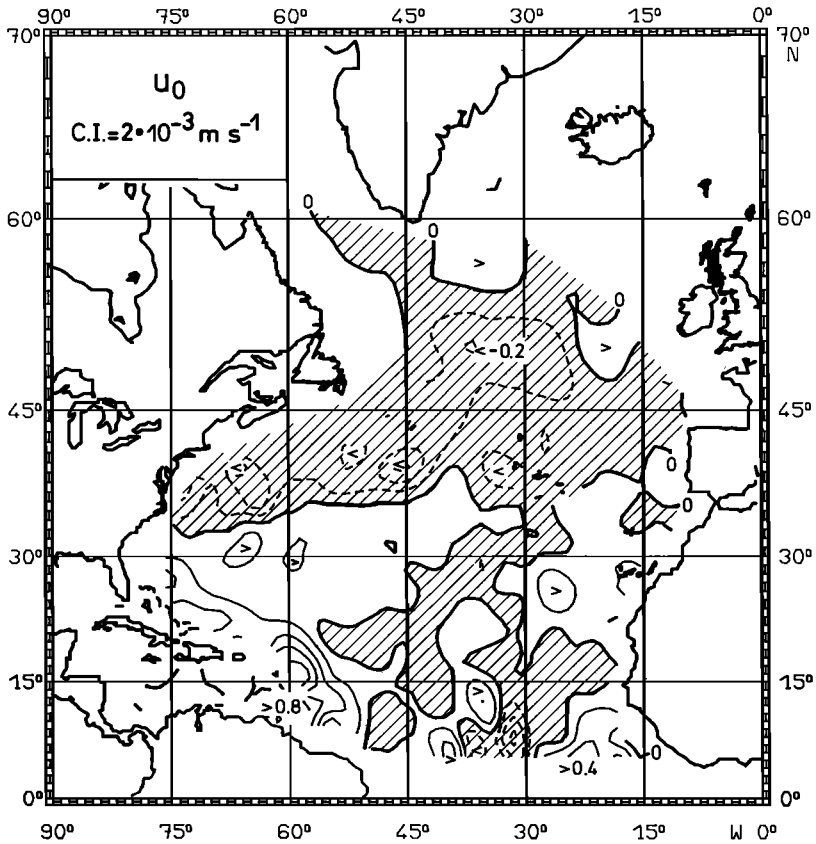

Fig. 15*a*

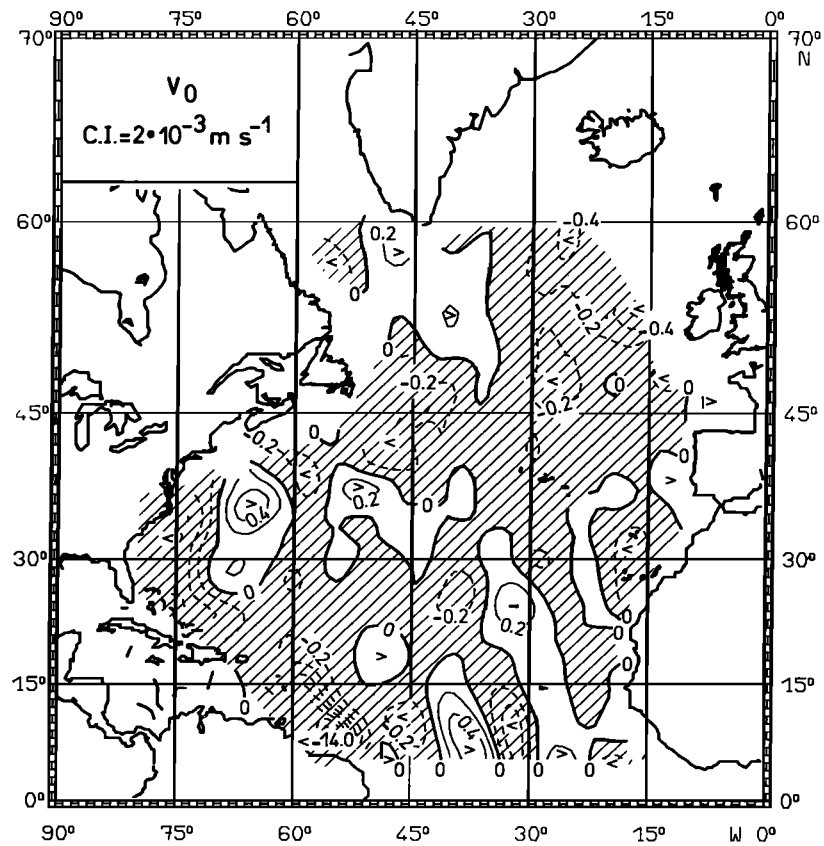

Fig. 15*b*

Fig. 15. Reference velocity (*a*) u_0, (*b*) v_0, and (*c*) w_0. Units are 10^{-2} m/s for Figures 15*a* and 15*b* and 10^{-6} m/s for Figure 15*c*. Negative values are shaded.

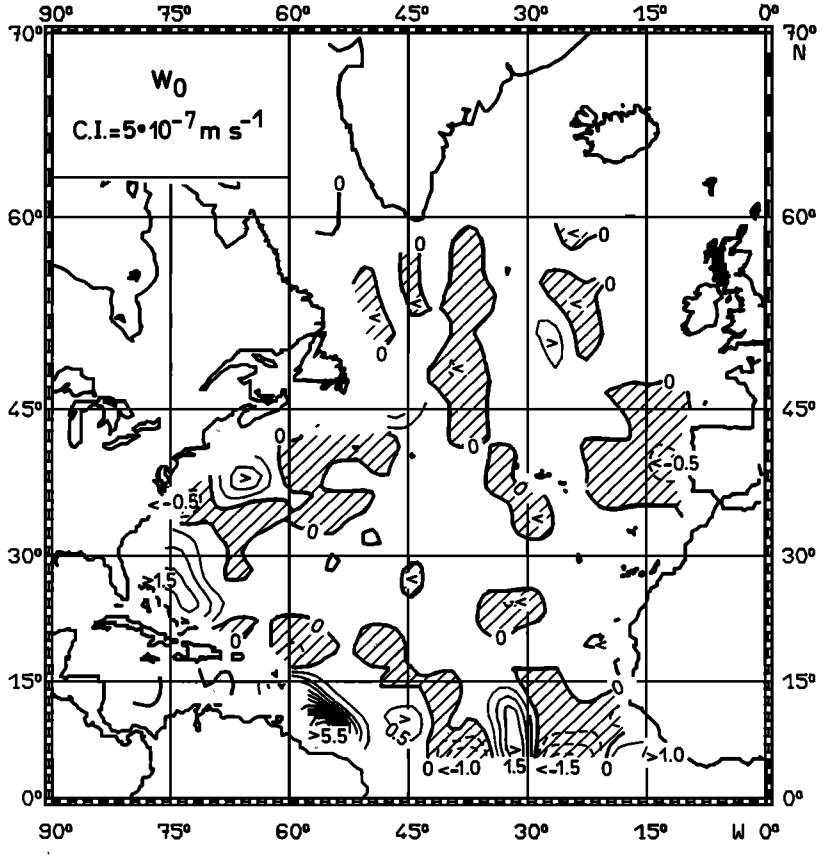

Fig. 15c

of levels was used to determine the reference velocities u_0, v_0, and w_0 and the deep values of the diapycnal diffusivity A_c and the vorticity diffusion coefficient A.

2. The balance of veronicity v in the deeper subset of levels was used to determine the deep value of the isopycnal diffusivity A_l.

3. The upper subset of data was used to determine upper values of the diffusivities, again A_c and A from the σ balance and A_l from the v balance.

This strategy arises as the most effective separation of the entire estimation problem into subdivisions. There are, of course, other strategies, e.g. combining the σ and v data in the corresponding subsets or even estimating all parameters in one run. After many trials, however, it turned out that the above scheme over all yielded the lowest parameter variances.

4. The Circulation Parameters

In this section we will present the resulting circulation parameters of the North Atlantic obtained by the methods outlined in the preceding sections. We rather tend to refer to these parameters as properties of the *Levitus* [1982] data set, since it is by no means obvious to what extent they represent properties of the actual circulation of the North Atlantic, even if we restrict our view to the long-term time-averaged flow. The sparsity of the original data base contributes to this uncertainty, but there are also some methodological aspects of our β spiral approach which oppose a simple interpretation of the individual parameter estimates in terms of a large-scale flow field. Indeed, once the reference velocities and the mixing parameters are determined, we may obtain velocity profiles from (24) and (31). The individual stations may then be combined, but the result is not strictly a physical flow pattern, since such an elementary constraint as continuity is not satisfied. A further inconsistency is the spatial variability of the resulting diffusion coefficients, which has not been considered in the equations. We will, however, ignore these inherent inconsistencies in the following discussion.

4.1. *Reference and Absolute Velocities*

The reference velocities u_0, v_0, and w_0 are presented in Figure 15. We recall that these velocities refer to the depth of 2000 m. It should be noted how small these velocities are: u_0 and v_0 do not exceed a few millimeters per second, and w_0 is of the order of 10^{-5} cm/s. These values are at least an order of magnitude smaller than the corresponding velocities near the surface (cf. Figures 6*a* and 7*a*). Standard deviations of the reference velocities are shown in Figure 16. They are generally large in regions of increased oceanic variability (measured by the $\langle \varepsilon^2 \rangle$ contribution in (45)) and low values of the matrix condition. Notice that the u_0 error reflects the low matrix condition south of 30°N, while the other two components appear to be unaffected. We have explained in section 3.4 how this feature arises through the relatively uniform orientation of the density gradients.

The reference velocities are generally larger than the corresponding standard deviations, though in many places, in particular for u_0 and w_0, the excess is relatively small. If the reference velocities (or one component) cannot be distinguished from zero, the data noise is too large to distinguish the true reference level from the initially chosen level of 2000 m. The β spiral method is in principle independent of the initially chosen reference level; i.e., the resulting absolute velocity profile does not depend on this choice (except for possible effects of truncation). Thus taking, for example, the surface

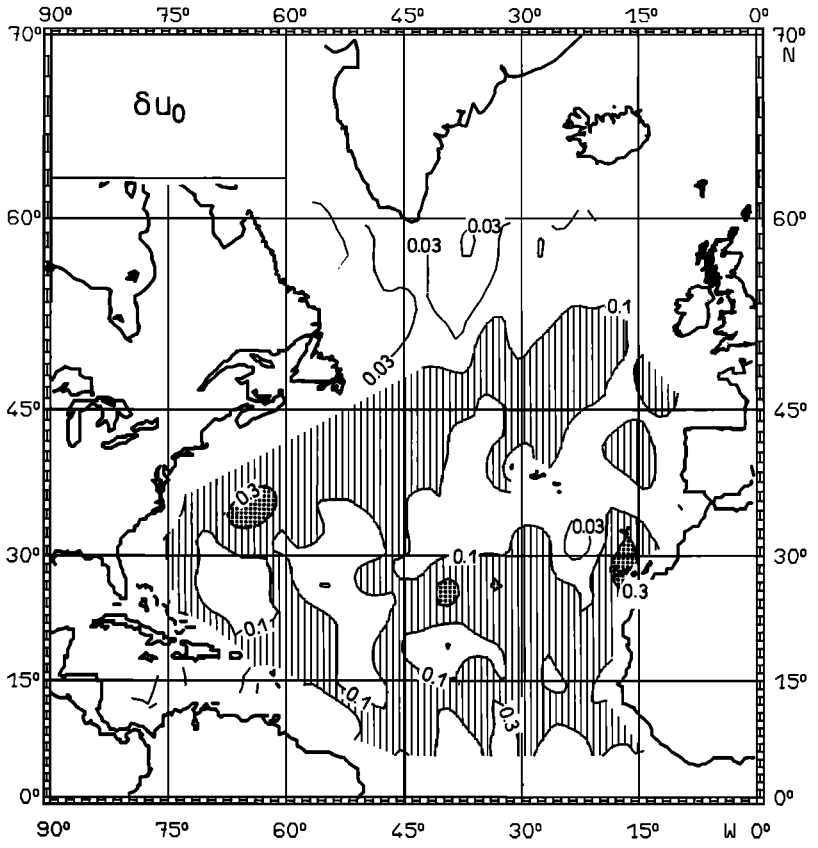

Fig. 16*a*

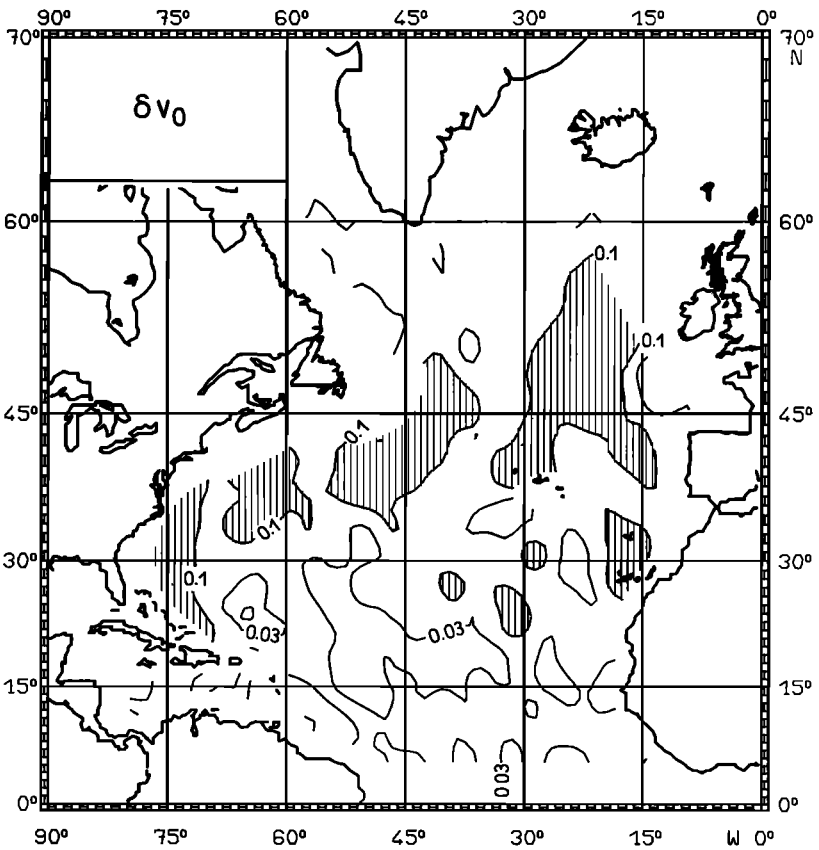

Fig. 16*b*

Fig. 16. Standard deviation of the reference velocity component (*a*) u_0, (*b*) v_0, and (*c*) w_0. Shaded areas show where the standard deviation exceeds 0.3 cm/s (Figures 16*a* and 16*b*) or 0.3×10^{-4} cm/s (Figure 16*c*).

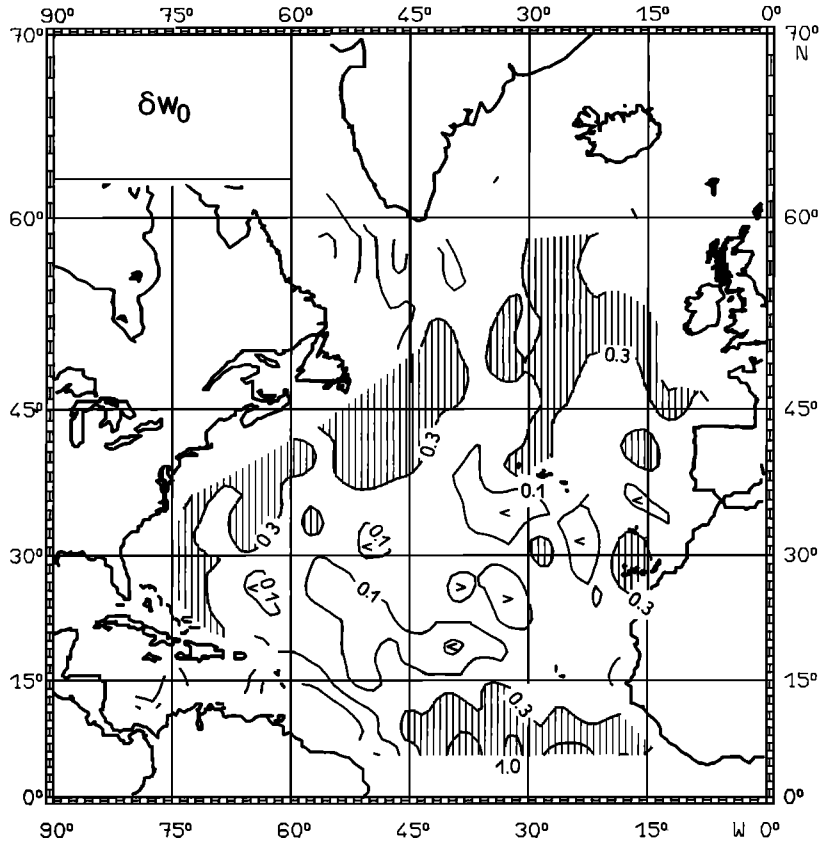

Fig. 16c

as initial level z_0, the reference velocities would certainly exceed their standard deviations, but the absolute profiles would be identical. Expressed in other words, the standard deviations apply not only to the reference velocities but also to the absolute velocities at each level.

Because of the smallness of the reference velocities the pattern of the absolute velocities in levels above roughly 1000 m is hardly distinguishable from the geostrophic velocities relative to 2000 m shown in Figure 6. To supplement these vector plots, we present maps of the absolute velocity vectors for the depths 2000 m, 1500 m, and 500 m in Figure 17. Whereas the 500-m level shows a smooth flow pattern, we are faced with a relatively noisy field at the deeper levels, especially when approaching the equatorial region (notice the difference in the vector scale). However, at all levels there is clear indication of the basic current systems. We will discuss these in some detail.

The dominant feature on the 2000-m map (Figure 17*a*) is the flow structure along the western boundary, originating from the Norwegian Sea overflow. After passing the region of the Gibbs fracture zone at about 50°N, 30°W the current splits. The northern branch takes a counterclockwise course around the southern Labrador Sea and then flows around Newfoundland to join there with the southern branch. These waters form the southeastward flowing deep boundary current which extends all along the western boundary and carries water into the South Atlantic. The velocities of this flow are about 0.5 cm/s, and the width is 300–400 km. The observational evidence of this entire flow system has recently been summarized by *Warren* [1981] and *Reid* [1981]. The latter description made reference to *Defant*'s [1941] calculation of the geostrophic circulation on the basis of the Meteor data. Defant's map of the absolute flow at 2000 m (reproduced by *Reid* [1981]) is indeed strikingly similar to our result. Besides the agreement of the pattern of the deep western countercurrent, both maps show similar current structures in the eastern basin. Both maps also agree on the north-southward alternating current structure between 20°N and 30°N east of the Mid-Atlantic Ridge and the low-velocity regions south of the Azores. In the western basin, away from the boundary current, the flow fields by and large disagree. Our result yields a narrow northeastward recirculation at about 30°N, 70°W and east of this a basically southeastward flow.

At the 1500-m level (Figure 17*b*) there is a strong boundary current south of 35°N off the North American coast. The rest of the flow appears rather patchy, with regions of stronger currents interrupted by almost motionless water. At 1000 m depth the current direction in the Gulf Stream–North Atlantic current region is essentially reversed (cf. Figure 6*b*), so that the level of no motion in agreement with the classical conceptions lies here between 1500 m and 1000 m.

Figure 17*c* displays the circulation in the main thermocline, which closely conforms with the wind-driven circulation gyres of the Sverdrup regime. The map is dominated by a broad Gulf Stream leaving the North American coast at about 35°N and turning almost eastward to a branching point at 45°W. The extremely large width of this current (about 800 km) as well as of the other currents in the surface layers is most likely caused by the time averaging of highly variable current meanders and the surrounding eddy field. Notice that the deep western boundary current in Figure 17*a* is much narrower, though it is presumably broader than the instantaneous Gulf Stream. The northern branch of the Gulf Stream extends into a broad, fan-shaped North Atlantic current system which fills the entire North Atlantic north of 40°N and east of 40°W. It is

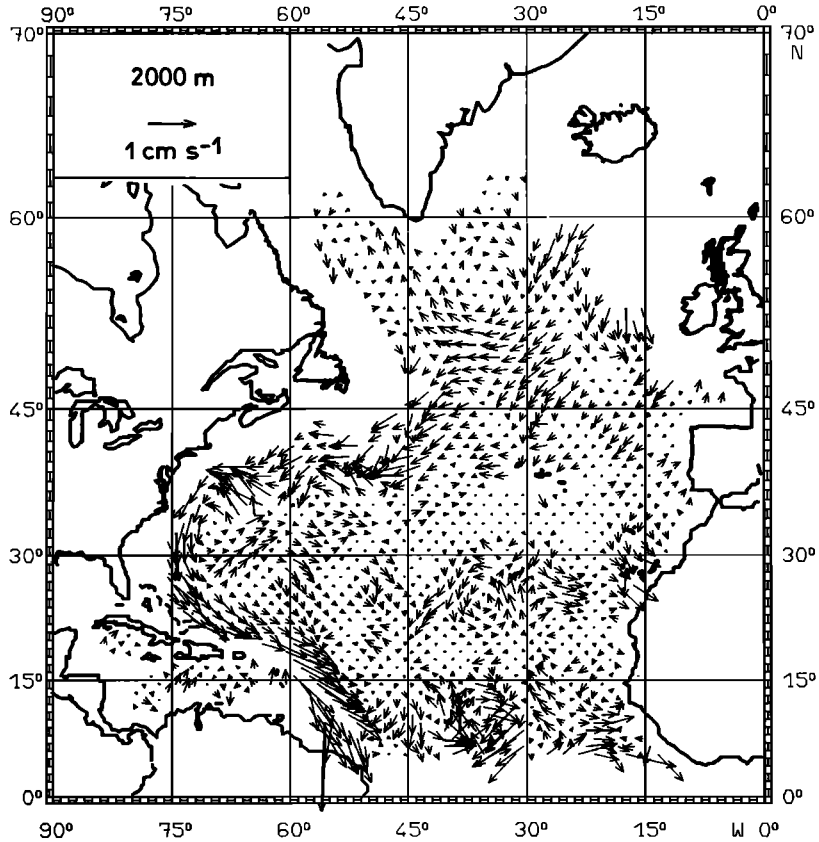

Fig. 17*a*

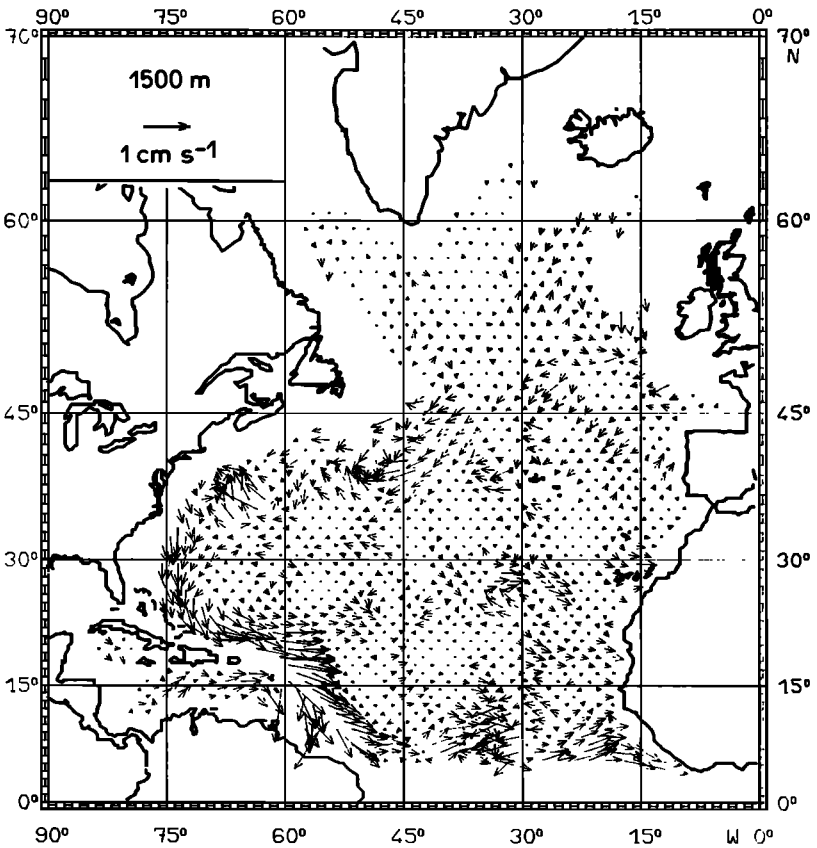

Fig. 17*b*

Fig. 17. Absolute horizontal velocity at (*a*) 2000 m depth, (*b*) 1500 m depth, and (*c*) 500 m depth.

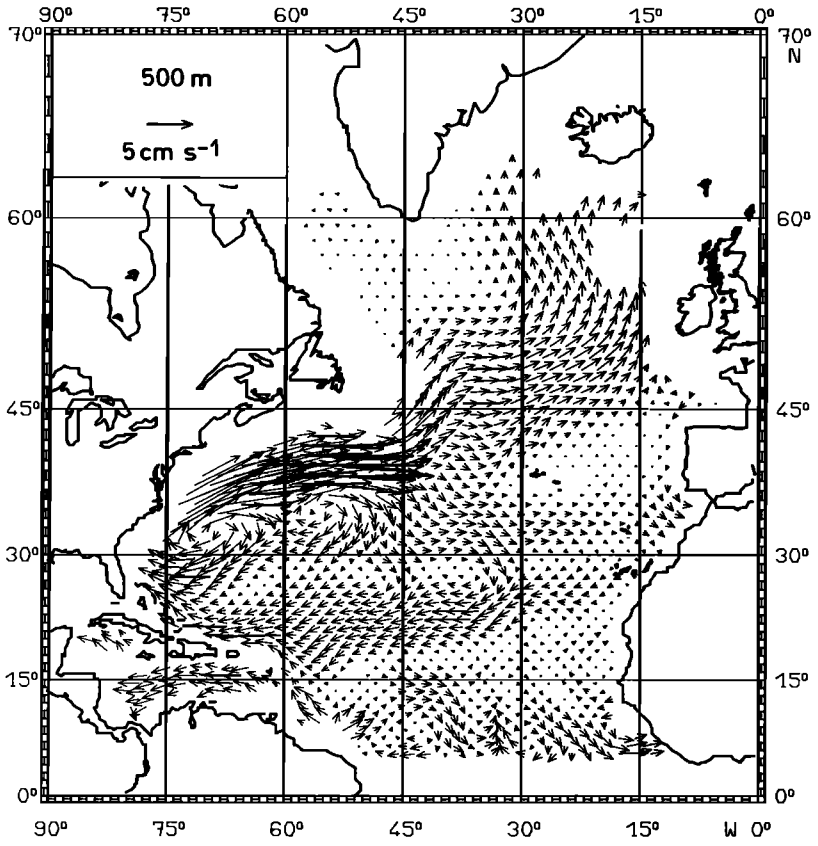

Fig. 17c

separated from the southern branch by a pool of stagnant water around the Azores.

The southern branch of the Gulf Stream splits again into a broad eastward flow between 30°N and 35°N toward Gibraltar and into the branch which partly forms the large recirculation cell of the subtropical gyre. This gyre shrinks in its north-south extension with increasing depth (see also Figure 6*a* for the 100-m depth flow). Notice that our solution also exhibits the tight recirculation cell on the western side of the subtropical gyre which was revealed in many earlier studies [e.g., *Jacobsen*, 1929; *Stommel et al.*, 1978; *Reid*, 1978]. Finally, we want to point out the existence of the northern cyclonic gyre, which is much weaker than the subtropical gyre but clearly visible down to 500 m depth.

The circulation pattern described above by and large confirms the classical concepts of the circulation in the North Atlantic. In general, the currents are too weak and broad, but the overall structure agrees favorably with the traditional results. The baroclinic structure of the flow can be directly inferred from the velocity distribution along some sections, which is displayed in Figure 18. The figures present the velocity component normal to these sections so that the results can be compared with geostrophic calculations based on a level of no motion or with results of Wunsch's inverse method [*Wunsch*, 1978; *Wunsch and Grant*, 1982]. For this reason we chose sections with actual hydrographic stations (except for the section 30°W).

In some of the sections, e.g., 24°N, 53°N, 59°N, and 57°W, there is indication of almost horizontal levels of no motion. In many respects they look similar to Defant's choice of the reference surface [*Defant*, 1941], decreasing from south to north as evident in the 57°W section and to some degree also in the 30°W section.

Apart from the 30°W section, which covers the Mediterranean outflow, the overall structure of the velocities is rather simple and stands in strong contrast to the inverse solutions obtained by *Wunsch and Grant* [1982]. These solutions yield a banded type of structure for the velocity field with strong barotropic components. In many places the current direction alternates on horizontal scales of 1000 km or less coherently from top to bottom, where our solution yields a broad current of uniform direction reversing at one depth. This difference may partly be due to a different data base (Wunsch and Grant use instantaneous hydrographic sections), but presumably, methodological aspects will also contribute. In this respect *Luyten and Stommel* [1982] have pointed out that inverse solutions might have a dominating control by topography, which in the β spiral method could only enter implicitly through the structure of the hydrographic fields.

4.2. *Mixing Coefficients*

Our model allows investigation of the relevance of diapycnal and isopycnal diffusion as well as vertical diffusion of vorticity. We obtain estimates for each of the corresponding diffusion coefficients A_c, A_l, and A which should characterize the importance of the mixing processes in the deeper layer ($-2000 \leq z \leq 800$ m) and the upper layer ($-800 \leq z \leq$ depth of mixed layer). Maps of the coefficients A_c, A_l, and A for these two layers are presented in Figures 19, 20, and 22. We will discuss these results with respect to balances of potential density σ, veronicity v (or equivalent passive tracers which vary on isopycnals), and vorticity. In addition, we will consider the

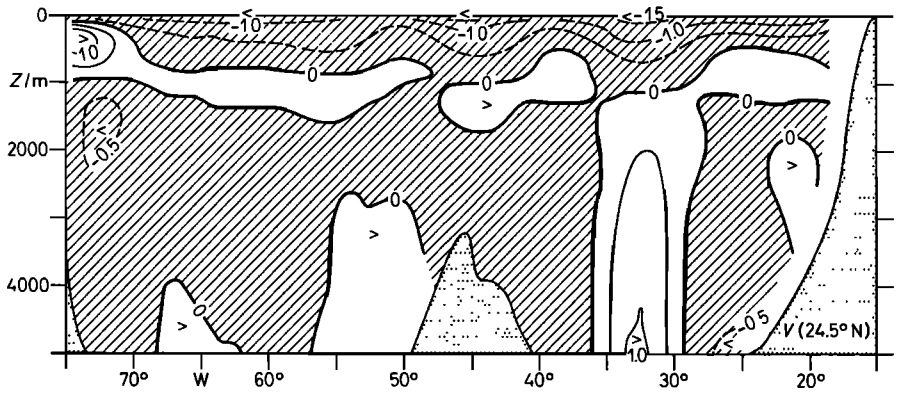

Fig. 18*a*

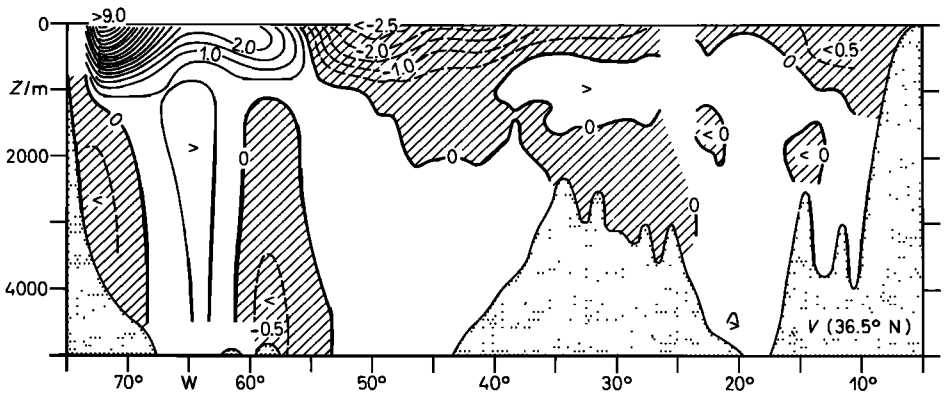

Fig. 18*b*

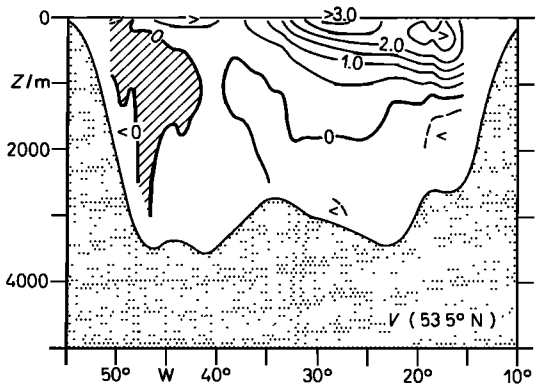

Fig. 18*c*

Fig. 18. Absolute velocity along (*a*) 24°N, (*b*) 36°N, (*c*) 53°N, (*d*) 59°N, (*e*) 30°W, and (*f*) 57°W showing the velocity component normal to these sections. Units are 10^{-2} m/s.

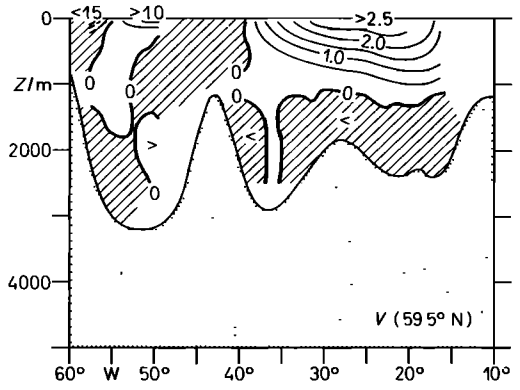

Fig. 18*d*

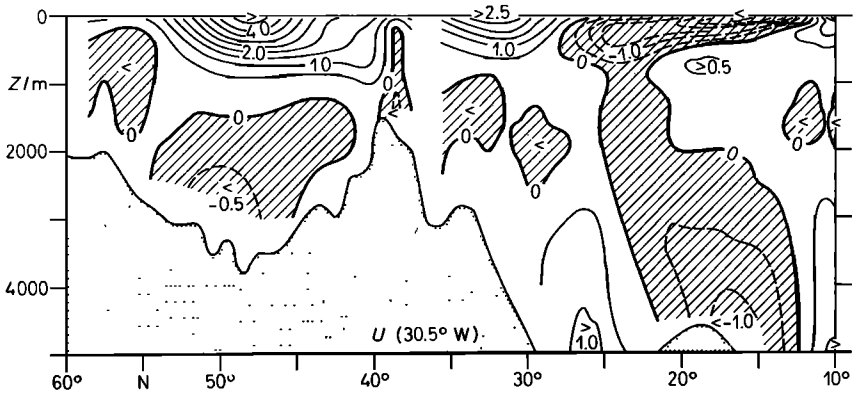

Fig. 18*e*

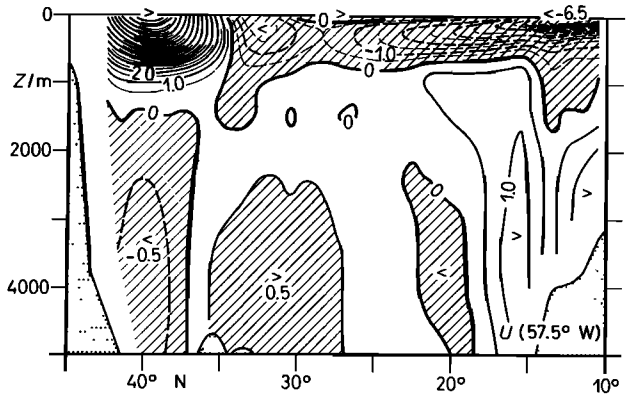

Fig. 18*f*

Fig. 18. (continued)

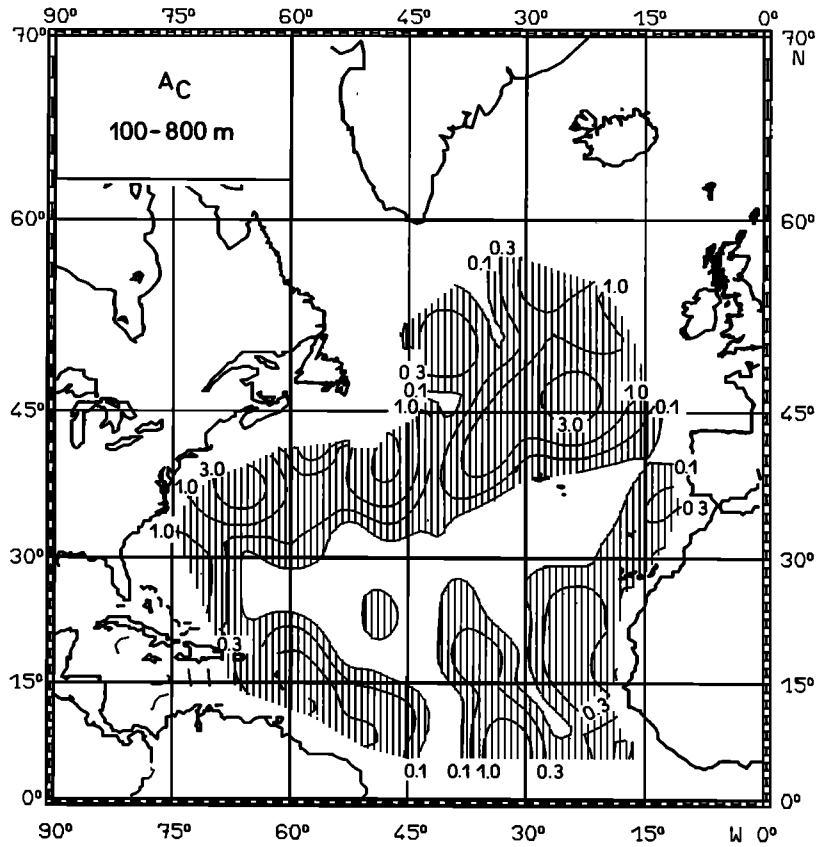

Fig. 19*a*

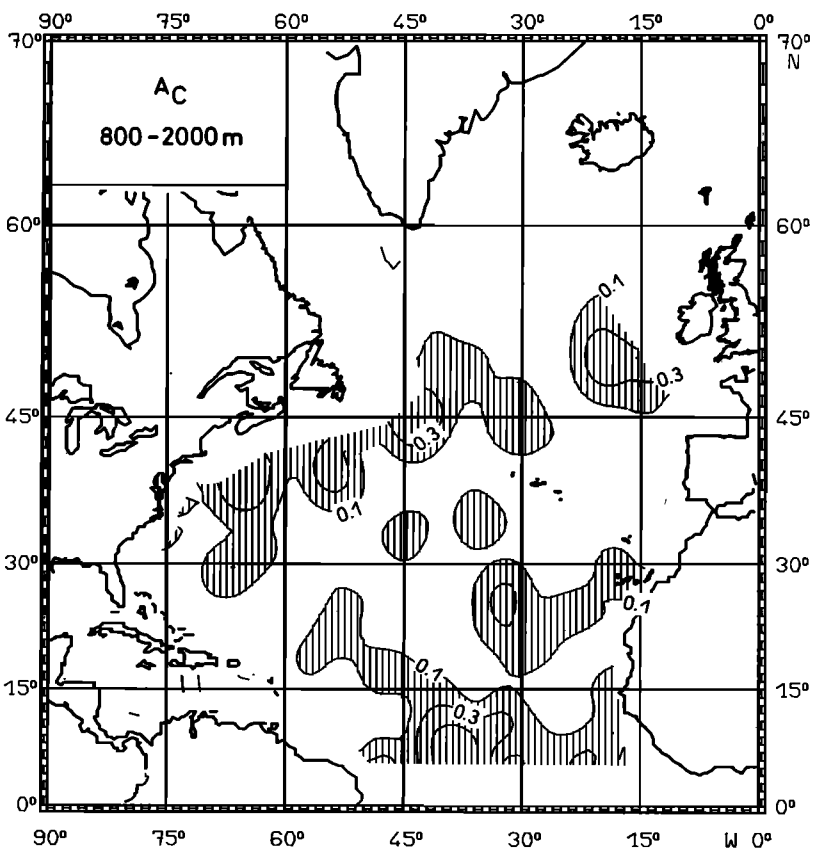

Fig. 19*b*

Fig. 19. Diapycnal diffusion coefficient A_c for (*a*) upper and (*b*) lower depth range (units are 10^{-4} m^2/s).

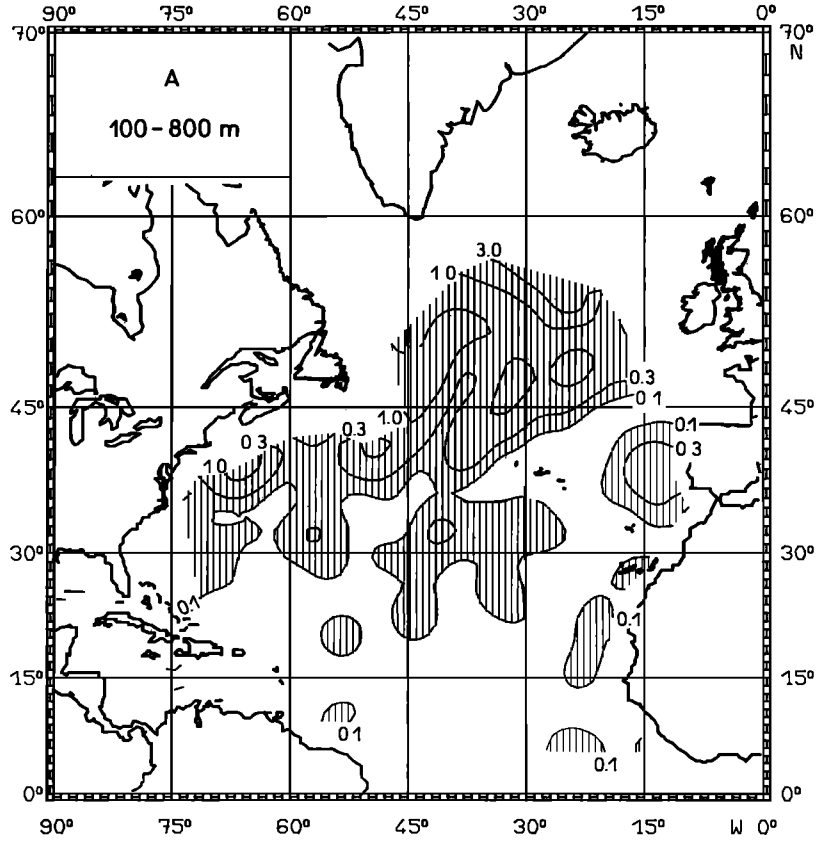

Fig. 20*a*

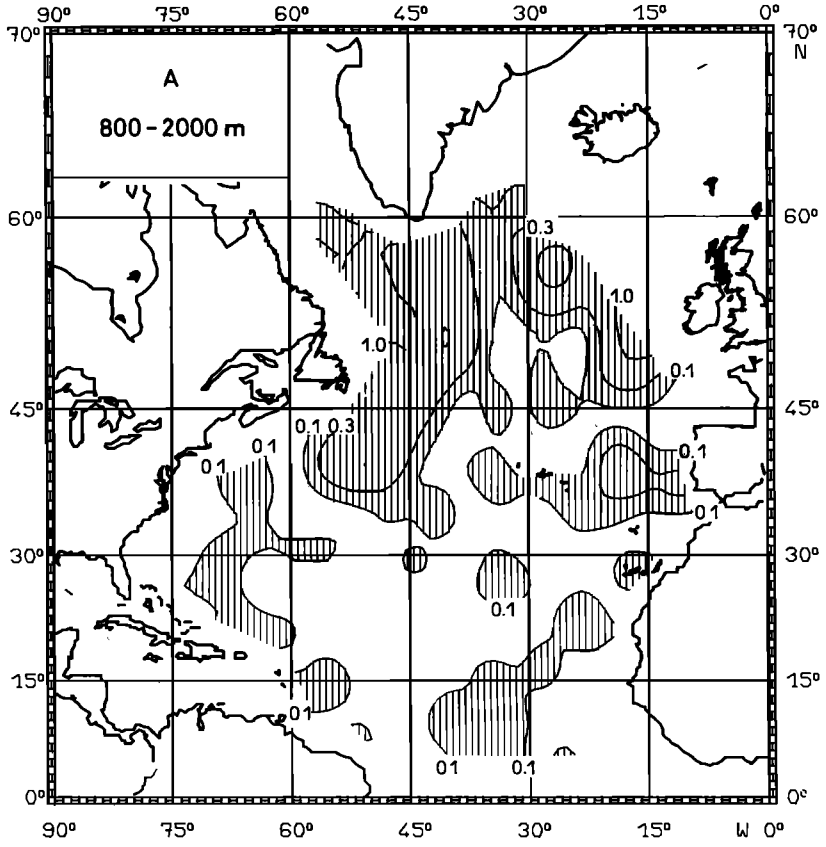

Fig. 20*b*

Fig. 20. Vorticity mixing coefficient A for (*a*) upper and (*b*) lower depth range (units are m^2/s).

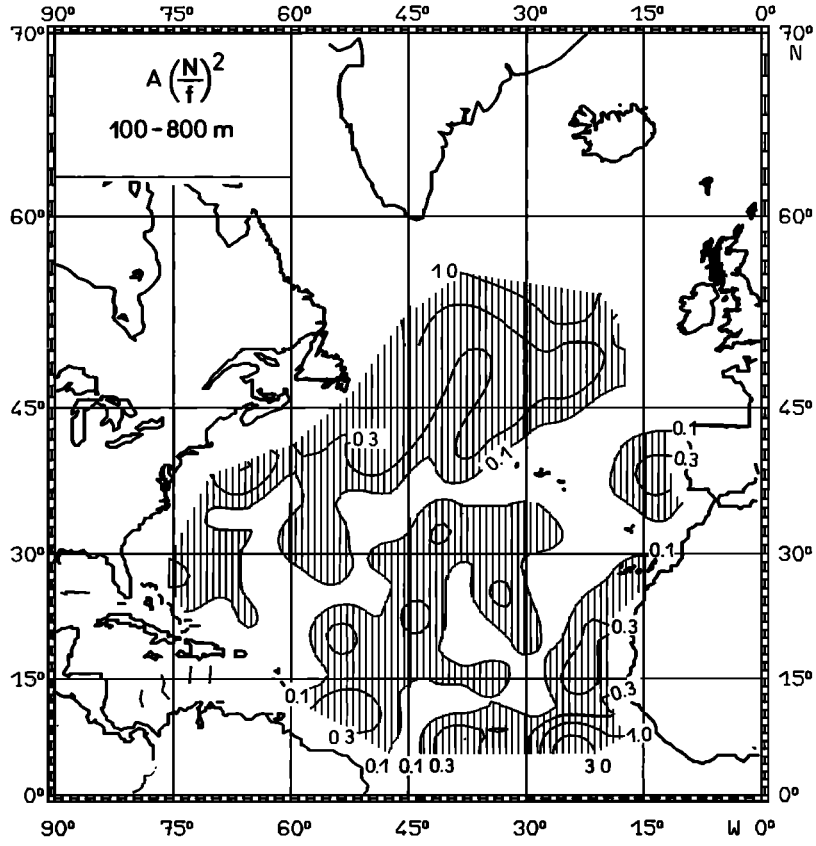

Fig. 21*a*

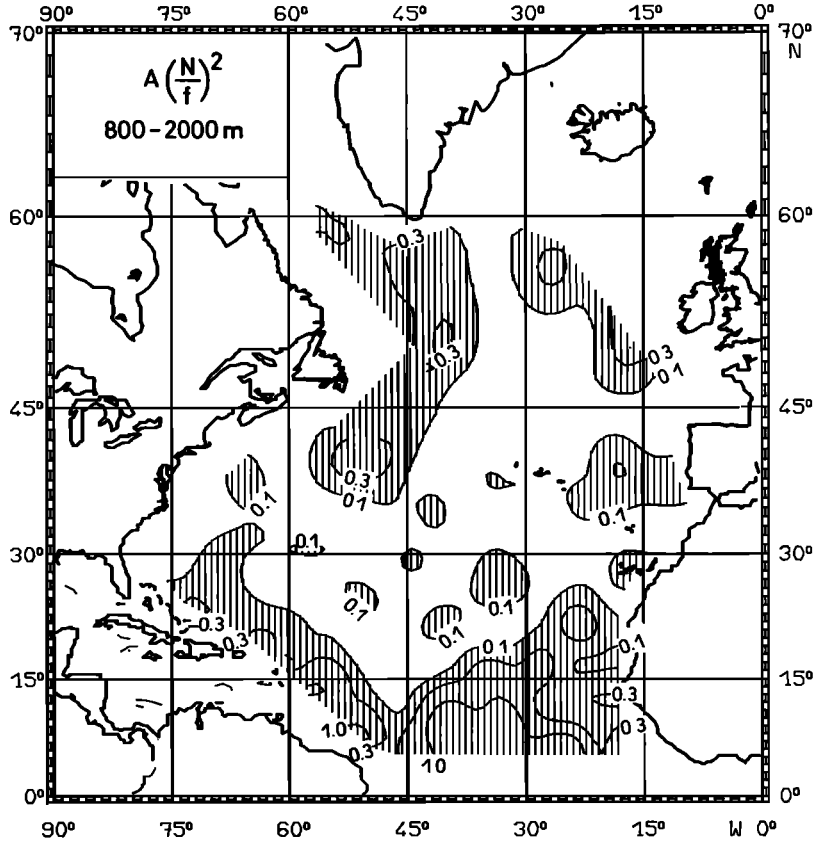

Fig. 21*b*

Fig. 21. Lateral mixing coefficient $A(N/f)^2$ of potential vorticity for (*a*) upper and (*b*) lower depth range (units are 10^4 m^2/s).

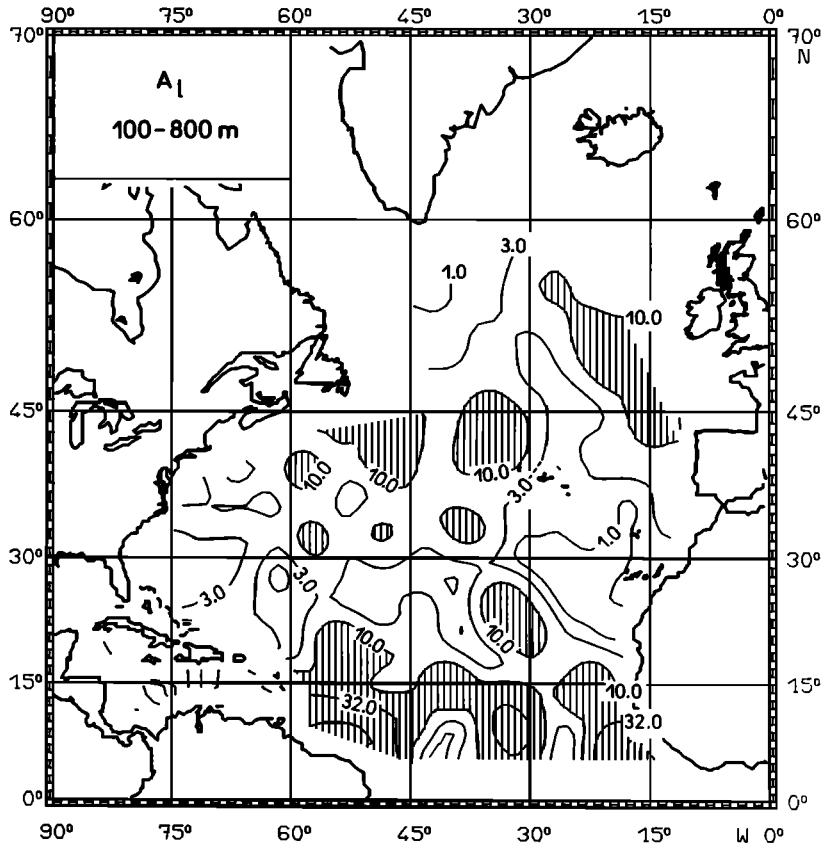

Fig. 22*a*

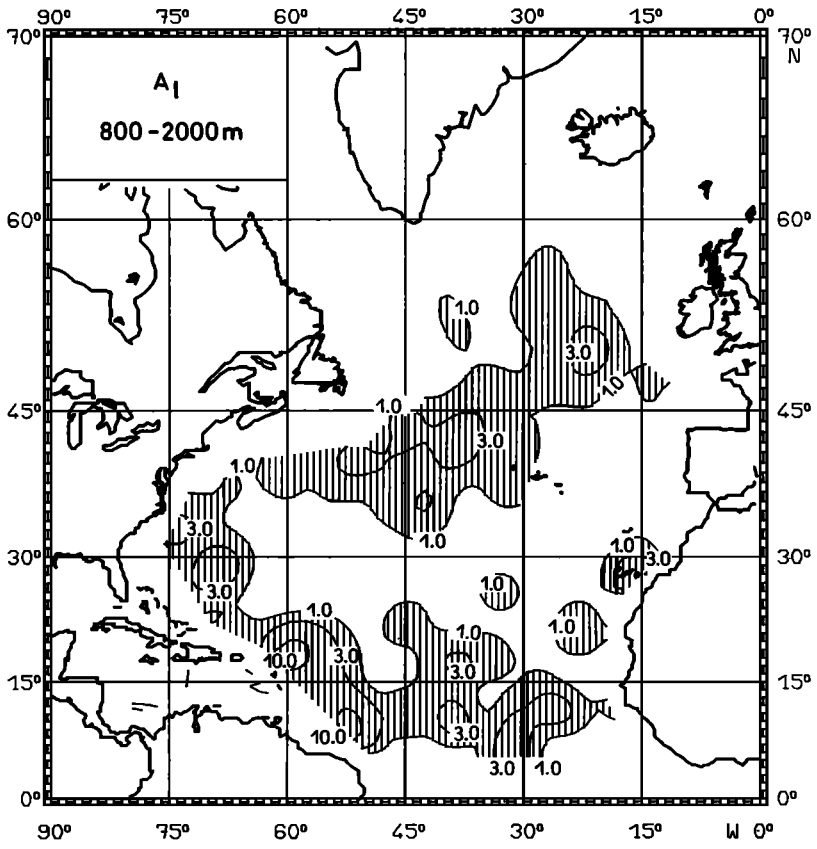

Fig. 22*b*

Fig. 22. Isopycnal diffusion coefficient A_I for (*a*) upper and (*b*) lower depth range (units are 10^2 m^2/s).

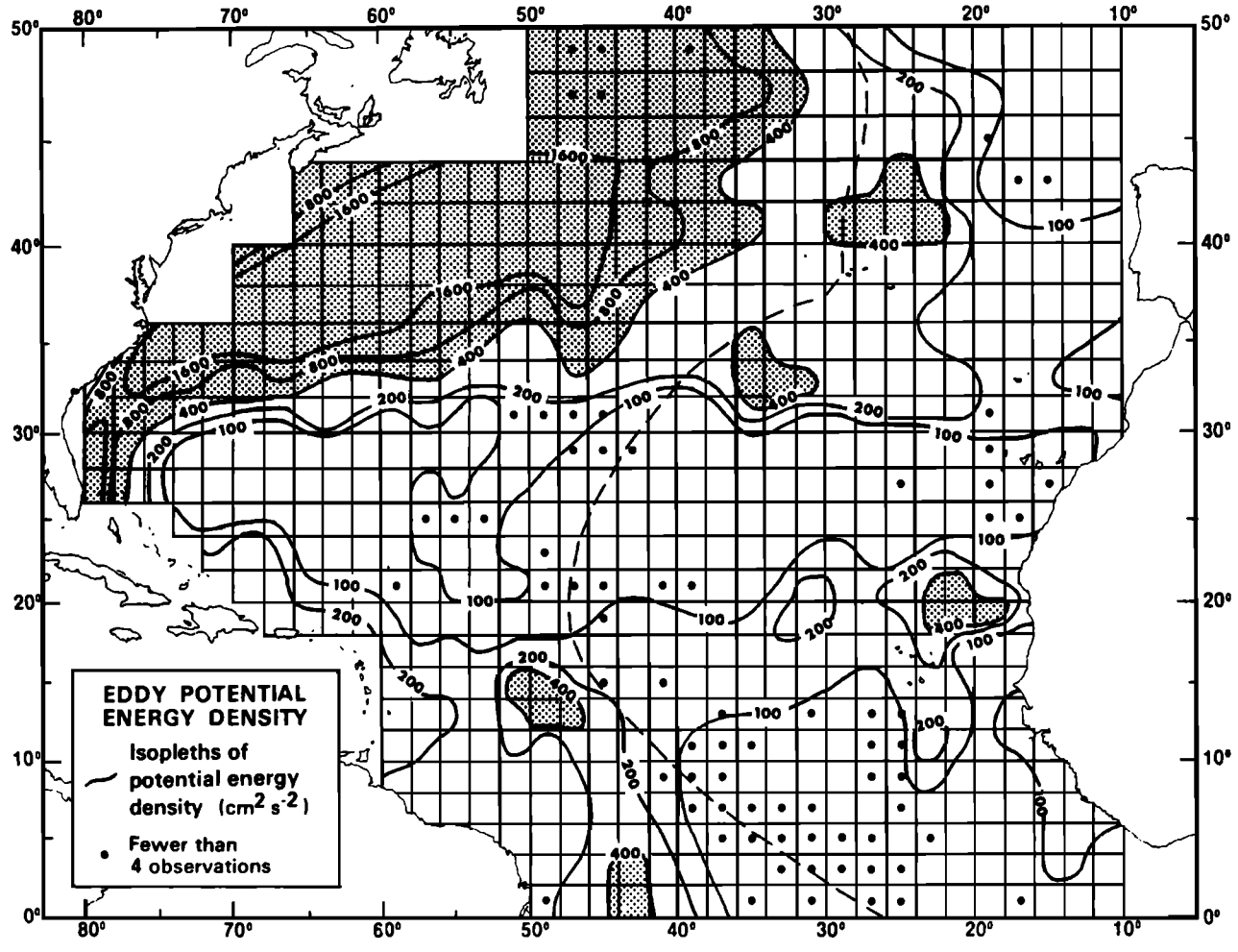

Fig. 23. North Atlantic eddy potential energy as compiled by *Dantzler* [1977].

balance of potential vorticity $Q = f\sigma_z$, which is affected by diapycnal diffusion and vorticity diffusion (cf. (23)). We have pointed out the particular role of this tracer within the framework of the β spiral technique. Moreover, Q has an important dynamically active role in shaping the oceanic circulation, which has been exploited in recent theories of the wind-driven gyres in the subtropical oceans [*Rhines and Young*, 1982; *Luyten et al.*, 1983]. In both theories, mixing of potential vorticity is assumed to be weak. This assumption can principally be tested by our model. Notice that the source term in (23) can approximately be cast into a diffusive form for Q if the differences between σ and ρ are ignored and if A is taken to be constant and terms of order L/R are neglected, where L is the horizontal scale of the density field and R is the earth radius. Then, assuming for simplicity A_c to be constant

$$\mathbf{u} \cdot \nabla Q + wQ_z = A\left(\frac{N}{f}\right)^2 \nabla^2 Q + A_c Q_{zz} \qquad (47)$$

where N is the stability frequency. Hence lateral diffusion of potential vorticity is described by the coefficient AN^2/f^2, and diapycnal diffusion by A_c. The quasi-geostrophic analog of (47) has been considered by *Rhines and Young* [1982]. Maps for AN^2/f^2 are shown in Figure 21.

The most obvious feature of the maps in Figures 19–22 is the marked correspondence between large values of the diffusivities and the regions of stronger currents. All three diffusivities assume their largest values in the region of the Gulf Stream and the North Atlantic current and, with the exception of the vorticity mixing coefficient A in the upper layer, a significant increase of the coefficients also occurs approaching the North Equatorial current system. In between, in the low-velocity regime within the subtropical gyre, the diffusivities are generally smaller by at least an order of magnitude. This overall structure seems to be connected with the increased oceanic variability in the regions of strong currents. Figure 23 reproduces the maps of eddy potential energy density from *Dantzler* [1977]. Eddy kinetic energy [*e.g., Wyrtki et al.*, 1976] shows a similar pattern. A close correspondence between the eddy activity displayed in these maps and the overall pattern of the mixing coefficients is apparent in both layers. In the case of vorticity mixing and isopycnal diffusion a loose connection to the eddy field can readily be drawn (see, for example, *Holland et al.* [1983] and *Haidvogel et al.* [1983]). Though parameterization efforts of eddy effects on the mean circulation and eddy-induced dispersion are still in their infancy, it appears sensible that the coefficients of a simple diffusive form for the eddy-induced transports would depend on the eddy activity as measured by eddy energy (see, for example *Armi* [1979] and *Armi and Haidvogel* [1982]) or the eddy-induced rate of strain [*Garrett*, 1983].

A similar imbedding of the resulting structure of the diapycnal diffusivity within a generally accepted concept of the associated mixing processes is less obvious. According to recent theoretical work [e.g., *Olbers*, 1983; *Holloway* 1983] as well as

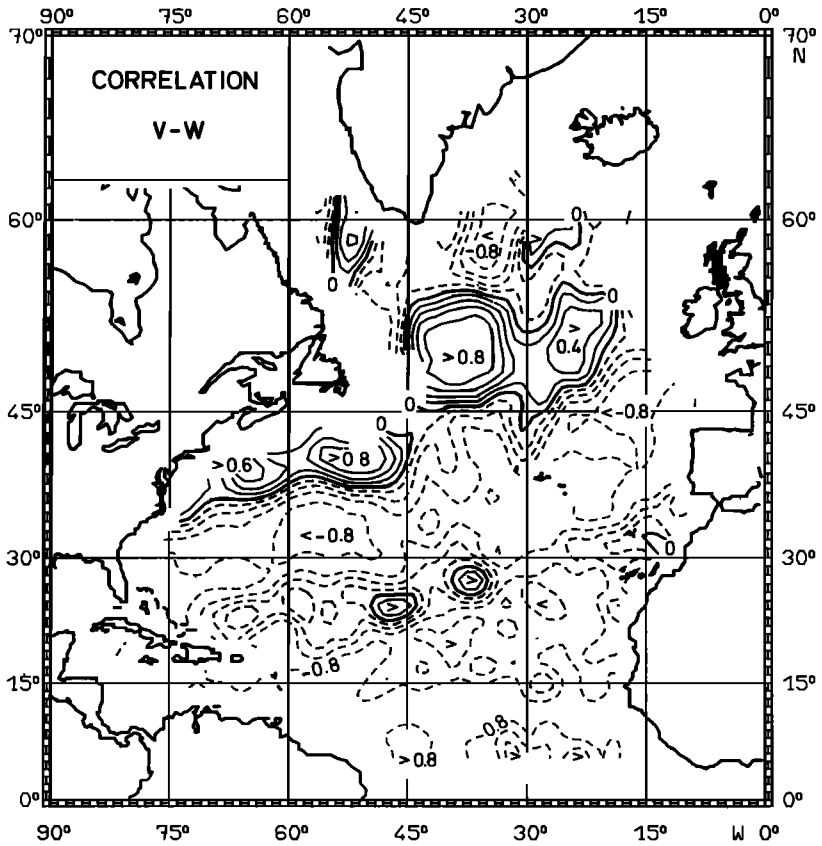

Fig. 24. Correlation between meridional reference velocity v_0 and vertical reference velocity w_0.

observational evidence [*Woods*, 1968; *Eriksen*, 1978], diapycnal mixing should mainly be caused by breaking internal waves, so that the coefficient A_c should correlate with the energy level of the internal wave field. The internal wave energy, however, is observed to be rather uniform [*Garrett and Munk*, 1975; *Wunsch and Webb*, 1979] and could hardly be responsible for the strong drop of A_c shown, for example, in Figure 19*a* at the boundary of the North Atlantic current. There are, of course, other candidates for diapycnal mixing, such as double diffusion [e.g., *Turner*, 1981], the significance of which, however, is even less known than that of wave breaking.

The question thus arises to what extent we can at all expect to relate the resulting diffusion coefficients to mixing processes caused by small-scale oceanic variability in the sense used in large-scale oceanographic problems, i.e. mixing due to mesoscale eddies, internal waves, and small-scale turbulence. Much of the diffusive structure in our data may entirely be the consequence of the climatological averaging. The averaging of a seasonally shifting current system such as the Gulf Stream or the North Equatorial current would not only cause a broadening of the currents but also induce an artifical mixing in the data which has no direct connection to the local mean eddy or internal wave field but nevertheless would contribute to the diffusion coefficients determined from those data. This question about real or artificial mixing cannot be answered from the averaged data alone but requires a more synoptic data set of the large-scale oceanic mass field, which does not exist. We should thus emphasize that our mixing coefficients are likely to be biased toward larger values than those associated with subgrid scale oceanic processes. The value of the resulting diapycnal diffusivity A_c (Figure 19) is generally too small to be of major importance in the corresponding balances. In both layers within the subtropical gyre, A_c is less than 10^{-5} m^2/s, and in the region of stronger currents it increases to about 5×10^{-5} m^2/s in the deep layer. Still, the diapycnal diffusion terms in the balances of potential density, veronicity, or potential vorticity are generally small compared with the advective terms, with Peclet numbers typically $O(10)$. In the upper layer, A_c becomes as large as 5×10^{-4} m^2/s in some places in the strong current regime. With such high values of A_c the diapycnal terms contribute significantly to the balances of σ, v, and Q.

It is not obvious how to compare these resulting A_c with estimates obtained by other methods. There is a vast body of literature on different estimation methods for the vertical diffusivity in the ocean interior, with a wide range of results, which either refer to single points or large water bodies (see, for example, *Garrett* [1979] and *Gargett* [1984]). Estimates from microstructure observations [e.g., *Gregg*, 1977] generally yield values which are two orders of magnitude less than *Munk*'s [1966] abyssal recipe of 10^{-4} m^2/s, whereas box models of chemical tracers seem to confirm these larger values [e.g., *Broecker and Peng*, 1982; *Li et al.*, 1984]. Our values with their possible bias and their large regional variations cover the entire range of estimates.

The vorticity diffusion coefficient (Figure 20) becomes as large as a few 10^{-1} m^2/s with the path of the Gulf Stream and the North Atlantic current in both layers. Away from these regions, A is typically several 10^{-2} m^2/s. These values are considerably larger than the coefficients for vertical momentum transfer in numerical models; for example, *Cox and Bryan* [1984] use 10^{-3} m^2/s. However, a value of 10^{-1} m^2/s does not affect the geostrophic balance (Av_{zz}/fu is typically 10^{-2})

and also yields only a minor correction in the vorticity balance ($Av_{xzz}/\beta v$ is typically 10^{-1}).

The lateral diffusion coefficient AN^2/f^2 of potential vorticity in Figure 21 has been obtained for the upper layer with N at 500 m and for the lower layer with N at 1200 m. Because of the f dependence, AN^2/f^2 increases toward the equator, so that the contours mediate the shape of a bowl with high values (about 5×10^3 m^2/s in both layers) around the rim and low values (below 10^3 m^2/s) within the subtropical gyre. In the upper layer a ridge of high AN^2/f^2 appears separating the bowl. There is some similarity of this pattern with the pool of homogeneous potential vorticity shown by *Holland et al.* [1984] (their Figure 4 is based on the same data set): apparently, mixing can only work and coefficients can only be determined to be different from zero where there are gradients. We find that both mixing processes of potential vorticity (lateral mixing arising from vertical diffusion of momentum and vertical mixing arising from diapycnal diffusion of potential density) are irrelevant within the gyre; however, along the rim, $(AN^2/f^2)\nabla^2 Q/(wQ_z)$ may become of order unity.

While we found the pattern of the coefficients worthy of some discussion, we have so far ignored one of the basic tools of our method, which is the determination of parameter variances. It turned out that even with our rather conservative estimates of the standard deviations, most individual values of A_c and A are statistically not different from zero. Typical values for the standard deviation in the deeper layer are around 3×10^{-5} m^2/s for A_c and 0.1–0.3 m^2/s for A, with a less pronounced horizontal structure.

Thus from this statistical point of view we have to conclude that the local balance of potential density and potential vorticity in this data set is consistent with an advective regime. This result appears to hold even more strongly for the actual oceanic state because the coefficients we have determined are likely to be biased toward larger values in our climatologically averaged data set.

The situation is similar for the case of isopycnal diffusion. For the upper layer, values for the isopycnal diffusivity A_I (Figure 22*a*) are a few 10^3 m^2/s in the regions of stronger eddy activity and about an order of magnitude less in the calm zone between 15°N and 40°N. However, most of these are statistically not different from zero. In the deeper layer (Figure 22*b*) we find A_I to be a few 10^2 m^2/s in the region of strong eddy activity, and only a few of these values exceed their rms standard deviations. Notice that though less in magnitude, the deep values of A_I have a more coherent pattern than the larger, upper values. We believe that this pattern is associated with the Mediterranean water tongue, which is located within the deeper layer of our analysis (see, for example, Figures 9*f* and 9*h*). It appears that the spreading of this water mass requires some lateral diffusion along its rim, which is supported by the results of *Needler and Heath* [1975], who modeled the Mediterranean outflow with a constant velocity and constant isopycnal diffusivity. They found best agreement with the data by choosing A_I in the range (1.5–3) $\times 10^3$ m^2/s for an advection speed of (2–4) $\times 10^{-3}$ m/s. Similar results were found by *Richardson and Mooney* [1975]. We may further compare our estimates with the lateral diffusion coefficient of 5×10^2 m^2/s obtained from the salinity balance for the β triangle data [*Armi and Stommel*, 1983]. Our values in this region (center at 27°N, 32°W) are about (1–2) $\times 10^2$ m^2/s but are statistically not significant.

4.3. *Parameter Correlations*

We have so far left aside a large part of the statistical information offered by the method about the parameters and hence the model we have chosen. The parameter covariance matrix (45) yields, besides the variances, the correlation between the different parameters. In most applications of least squares estimations the off-diagonal elements of the covariance matrix are simply ignored; in some cases the correlations can be utilized for a deeper insight into the problem. If we were free to choose the model structure and parameterization, we would prefer one with less correlated parameters over another with highly correlated parameters, since the latter indicates a certain amount of redundancy in the choice of the parameterization. Highly correlated parameters generally describe the same features in the data. In this respect the parameter correlations can be used as a tool for model building. Our model, however, originates from the physical conservation equations and the given hydrographic structure so that we are not faced with model building (as an exception the mixing terms allow some freedom) but rather with the estimation of parameters which have a well-defined physical meaning. In this situation, high parameter correlation can only be taken as a warning not to overrate the resulting parameters. Examples will be given below.

Most of the parameter correlations turned out to be reasonably small with a variable sign. A noteworthy exception is the correlation between w_0 and the diapycnal diffusivity A_c. This correlation is positive almost everywhere and large (say, above 0.7) over large regions. This behavior can readily be understood from the model equation (33), the diapycnal mixing term (13), and the structure of the density profile. The parameters w_0 and A_c enter (33) in the form $w_0\sigma_z - A_c\sigma_{zz}$, which is roughly approximated by $(w_0 - A_c/d)\sigma_z$, since σ increases more or less exponentially (with scale d) with depth. Hence the model depends effectively only on the linear combination $w_0 - A_c/d$, making an independent estimation of w_0 and A_c impossible. Only if the stratification deviates significantly from an exponential form would we have a chance to obtain uncorrelated estimates for w_0 and A_c.

An even more dramatic example of this behavior concerns the reference velocities v_0 and w_0. The correlation of these parameters is displayed in Figure 24 and shows by far the largest overall correlation value of the entire analysis. Again this result can readily be understood from the model structure. Neglecting the β term in (33) (it is of order L/R compared to the other terms), we notice that v_0 and w_0 appear as the sum $-v_0\, dz/dy + w_0$, where dz/dy is the north-south slope of the isopycnals. Now this does not change much with depth, so that the model essentially constrains v_0 and w_0 only in the combination $-sv_0 + w_0$, where s is a mean slope. Over most of the subtropical gyre, $s > 0$, and thus v_0 and w_0 are positively correlated. In the Gulf Stream–North Atlantic current system, s and the correlation reverse sign. Obviously, the β spiral method is unable to determine uncorrelated values for the reference velocities v_0 and w_0. The remaining correlations of the reference velocities are significant only in restricted areas; for example, u_0 and v_0 have consistently high correlation (above 0.8) only in the area between the Azores and Spain.

When dealing with the problems of the matrix condition in sections 3.4 and 3.5 we have already demonstrated that the least squares technique (and this applies to any other inverse modeling technique as well) is in fact a very delicate tool which should not be used as a black box generating parameters. The analysis of the parameter correlations enforces this view in a unique way. We like to emphasize, however, that these tools only reflect on a formal level the physical facts which can be revealed by a detailed study of the model equations.

5. DISCUSSION

The basic idea of diagnostic inverse modeling of the ocean circulation is to combine dynamical arguments with the information contained in data sets of oceanic fields or data of forcing functions. The objectives include the determination of circulation parameters (especially the three-dimensional absolute velocity field) and the testing of dynamical concepts (especially the role of mixing in the budgets of heat, salt, and potential vorticity). The β spiral approach presented in this paper can contribute to both these objectives, with some limitations, however, which partly are inherent in the model formulation and partly arise through insufficient knowledge about the data used in our particular application. In this section we shall discuss the pros and cons of our method and summarize our main results.

At the beginning we should point out again that the present β spiral model is not able to embrace the current knowledge of ocean circulation. There are other methods in development (see, for example, *Wunsch* [1984]) which can make use of a more general kind of data having a relation to the circulation and which can consider any statement about circulation properties that can be cast into a mathematical constraint. The β spiral method, in the present as well as in previous formulations, is designed to study local tracer balances in conjunction with the geostrophic shear of the horizontal velocity and the planetary vorticity constraint. There is no attempt to incorporate any knowledge obtained from the forcing functions of the large-scale oceanic motion or to use directly the knowledge about large-scale connections acquired by investigation of sources and sinks of water masses. The kind of statements obtained from such studies can, however, be useful when trying to validate the results from the β spiral model. This, in fact, was one of the aims of the present study.

Within the framework of the β spiral method one can use any conservative tracer which is advected by the currents. In practice, the requirements on data quality and observational density reduce the choice to standard hydrographic data, i.e., essentially temperature and salinity. But even with these data the possible range of applications of the β spiral method is restricted to crossing points of hydrographic sections, since density as well as tracer gradients are needed in two different directions. The main work went along these lines since the set-up of the method by *Stommel and Schott* [1977]. The use of nonsynoptic hydrographic sections for diagnostic inverse modeling has frequently been questioned [e.g., *Wunsch and Grant*, 1982] because in general they do not give an instantaneous view of the oceanic mass field. The resulting model circulation cannot be expected to represent an instantaneous state or even a possible state of the real oceanic circulation. The situation may even be rated worse when considering the climatological average of essentially all available hydrographic data as produced by *Levitus* [1982] which was used in our analysis. It is certainly true that because of data sampling problems both in space and time, the atlas of *Levitus* [1982] is by no means a real climatological average. However, one can argue that a mean in some restricted sense may be physically more meaningful than a composite of two nonsynoptic sections. In any case, in view of the present severe data restriction for studying ocean circulation both paths can equally be justified.

We have chosen the North Atlantic part of the Levitus atlas, since here the density of original observations is significantly larger than in other areas. Moreover, the North Atlantic is the area of most other inverse modeling activities (presumably for the same reason), which enables comparison. There are various computations of absolute β spiral profiles [e.g., *Schott and Stommel* 1978] (for further references, see section 3), and patterns of absolute circulation have been obtained by *Wunsch and Grant* [1982] on the basis of Wunsch's inverse method and a selection of individual hydrographic sections. A noteworthy early step toward the circulation in the Atlantic is *Defant*'s [1941] attempt to compute maps of absolute geostrophic velocities. We should further mention the diagnostic circulation models of *Holland and Hirschman* [1972] and *Mellor et al.* [1982] as well as *Worthington*'s [1976] circulation scheme. The results differ significantly in many details, even in such important questions as the vertical structure of the Gulf Stream: Worthington's scheme requires the Gulf Stream to reach the bottom, whereas most other work reveals an intermediate level of no motion. Disagreement also exists with respect to the recirculation pattern as well as the extension of the Gulf Stream into the North Atlantic current. In contrast to *Worthington*'s [1976] scheme some of *Wunsch and Grant*'s [1982] results seem to support the broad, basin-wide recirculation and splitting of the Gulf Stream envisioned in the classical description of the wind-driven circulation (see, for example, *Reid* [1981] for a review). Another aspect of the models by *Wunsch and Grant* [1982] is that the circulation frequently breaks down into a cellular structures of smaller scale. This is the outstanding feature mediated in their sections of horizontal velocities: in vast regions the ocean seems to move almost barotropically in alternating columns with horizontal scales of the order of a thousand kilometers. As suggested by *Luyten and Stommel* [1982], this behavior of the inverse solution may partly be due to a heavy weighting of deeper layers, thus emphasizing topographically induced details, and partly it may arise from small-scale transient irregularities in the data.

The circulation associated with the climatological average not only differs in detail from the pictures gained from individual hydrographic sections, but the overall patterns already have a drastically different appearance. The smoothing technique definitely takes away more than the instantaneous eddy transients in the original data. Features which may be rated as long-term mean signal in individual sections appear in the climatological average in a rather blurred shape with considerably reduced gradients. This particularly concerns strong currents which appear in each section as sharp fronts but may have a seasonal or lower-frequency oscillation. The circulation gained from these data is a rather simple broad-brush picture dominated by broad currents and basin-wide circulation cells. The main results are contained in Figures 17 and 18, which reveal less complex flow patterns than those obtained by *Wunsch and Grant* [1982]. The upper layers are dominated by a broad Gulf Stream which splits at about 40°N and 40°W in a North Atlantic current and the subtropical gyre recirculation which includes the Azores current and the North Equatorial current as well as a tight recirculation cell in the western region. In the lower layers the outstanding feature is the deep western boundary current fed by overflow water from the Norwegian Sea which penetrates through the Gibbs fracture zone and partly circulates around the Labrador Sea. The vertical sections also clearly demonstrate the broad horizontal circulation which shows one or two current reversals and some indications of almost horizontal levels of no motion. The overall appearance of this circulation bears strong resemblance to the classical flow pattern deduced by *Wüst* [1935] and *Defant* [1941].

The actual β spiral method used in this work extends previous formulations in some aspects. At first, we have put a stronger emphasis on the determination of the vertical velocity, which in any inverse model appears to be most susceptible

to data noise. It is extremely important which constraints of the β spiral are used to estimate the vertical velocity (or, expressed in terms of the inverse theory framework, how to choose the weighting of the constraints). A detailed analysis revealed that estimations from the vorticity constraint contain less noise than estimations from the tracer balance. The rationale for this result is virtually the same as the difference in scaling obtained for the mean vertical velocity when constrasting the mass or tracer balance with the vorticity balance of planetary scale flow. The resulting profiles of vertical velocity are smoothly decaying with one or two inversions, one of which is predominantly in the upper 1000 m of the water column.

The determination of the reference velocities from the climatological data posed essentially the same problem of earlier calculations with section data: the results were very dependent on which part of the water column the data were taken from. Two reasons could be identified. The first is a technical aspect and is associated with the poor quality of gradient estimation for very deep layers, generally below 2000 m depth. The second reason is of a physical nature, and it is associated with the pool of homogeneous potential vorticity located in the upper part of the ocean within the regime of the wind-driven circulation. If potential vorticity is constant on isopycnals, the β spiral dynamics no longer constrains the velocities (the velocity vector can have any direction along isopycnals), and accordingly, the β spiral procedure breaks down. Consequently, the part of the water column with homogeneous potential vorticity had to be abandoned in the least squares fitting procedure, and reference velocities were essentially determined from an intermediate layer which is below the bowl of the wind-driven gyre and above 2000 m depth.

We should emphasize here again that the velocity field resulting from local β spiral estimation does not conserve mass and does not satisfy any meaningful boundary conditions. Moreover, the determination of the vertical velocity remains unsatisfactory (as in other diagnostic calculations). This deficiency is the price paid for the simplicity of the method, which determines the velocity from local properties (the gradients of density and tracer) independently of the velocity structure of adjoining points. Obviously, continuity is a nonlocal property, and consideration of this constraint as well as boundary conditions cannot be achieved in a local analysis. One can think of various ways to overcome this limitation of the β spiral method. Work in this direction is under way and will be reported elsewhere.

A second point of advance is a rational way of including mixing parameters in the estimation scheme. A first step in this direction was pursued by *Schott and Zantopp* [1980]. The determination of diffusion coefficients for heat and salt is one of the central problems of oceanographic research, and the methods developed range from the study of small-scale turbulence to balances of chemical tracers over ocean basins. The estimates for the diffusion coefficients span a corresponding range: for example, microstructure measurements indicate vertical mixing coefficients below 10^{-6} m^2/s, (see, for example, *Gargett* [1984]), whereas large-scale balances of chemical tracers yield values larger than *Munk*'s [1966] abyssal recipe value of 10^{-4} m^2/s [*Broecker and Peng*, 1982; *Li et al.*, 1984]. The role of vorticity mixing and mixing of potential vorticity has received new attention with the introduction of the theories of *Rhines and Young* [1982] as well as of *Luyten et al.* [1983], which attempt to explain the vertical structure of the wind-driven circulation on the basis of the potential vorticity balance. The theories are based upon low or vanishing potential vorticity mixing, respectively. All relevant diffusion coefficients can principally be determined within the β spiral framework: the coefficients describing diapycnal and isopycnal mixing of heat and salt as well as the coefficient describing vertical diffusion of vorticity, or equivalently, horizontal diffusion of potential vorticity. Results may become rather noisy, since second-order derivatives of the data are involved (the reference velocities are obtained from first-order derivatives in our scheme). Moreover, with an increasing number of parameters to be resolved their variance will generally also increase. For this reason we pursued an elaborate strategy in which the mixing parameters are determined in separate steps which specifically adapted tracer combinations.

Some definite statements about the resulting diffusion coefficients can be made. Within the subtropical gyre and, more generally, outside the regimes of stronger currents the diapycnal and isopycnal diffusivities (as well as their standard deviations) are considerably smaller than the classical values, e.g., those used in numerical models of the ocean circulation. The diapycnal diffusivity in the subtropical gyre is less than 10^{-5} m^2/s, and the isopycnal is about 10^2 m^2/s. Toward the surrounding strong current region these values increase roughly by an order of magnitude. The pattern thus resembles maps of eddy activity. We have to conclude that mixing of heat and salt in the ocean is a relatively weak process that seems to be overemphasized in numerical models. This conclusion becomes even more stringent when realizing that our values are likely to be overestimated because of the climatological averaging of the hydrographic data.

Vertical diffusivities of vorticity are of the order of 10^{-1} m^2/s in the regimes of strong currents and an order of magnitude smaller in quiet regions. If associated with the vertical transfer of horizontal momentum, diffusivities of the order of 10^{-1} m^2/s appear rather large. However, as pointed out by P. Rhines (personal communication, 1985), these large values do not succeed in carrying all the momentum downward because the momentum transfer is almost balanced by adjustment of the density field: when the horizontal momentum profile of a broad current begins to deepen, the readjustment of the density field is accompanied by horizontal geostrophic circulation, which nearly compensates the acceleration induced by the momentum transfer.

The corresponding diffusivities of potential vorticity are $(N/f)^2$ times those of vorticity. They thus range between 10 m^2/s and 10^3 m^2/s. These values agree favorably with the range of estimates (from Lagrangian diffusivities of fluid particles, which should equal the diffusivity of potential vorticity) discussed by *Rhines and Holland* [1979].

Finally, a further goal we had envisioned with the present project was the incorporation of the statistical framework that has become a standard tool in inverse modeling. The aim is to compute parameter covariances and to test for model validity. The computational expense in general is relatively small compared to the least squares fitting procedure. The crucial ingredient, however, is the covariance structure of the data functionals which enter the model constraints. In our case this involves the spatial correlation of the geostrophic heat and salt transports, which are fourth-order statistics of the original measurements. Accurate estimates of those quantities were beyond reach. We had to restrict the statistical aspects to a Monte Carlo simulation of transport variances and could perform with these quantities an approximate maximum likelihood weighting of the equations. Rough estimates of parame-

ter variances and correlations were obtained, but no rigorous statistical test of model validity could be performed.

Overall, the results of our analysis seem to conform to the present knowledge about the dynamical concepts of large-scale oceanic flow and the shape of the circulation in the North Atlantic. This latter statement is based on rather subjective measures which, as *Wunsch and Grant* [1982] pointed out, are essentially untestable. With regard to the consistency of the β spiral dynamics (essentially the utilization of the linearized vorticity balance) we found no severe contradiction within the analyzed domain. This result is a consequence of the smooth behavior of the analyzed climatological state. It gives confidence to the use of large-scale geostrophic circulation models (without explicit inclusion of eddies) for investigating climatological aspects of ocean circulation.

APPENDIX A: STATISTICAL ACCURACY OF THE ANALYZED FIELDS

Input to the construction of the temperature and salinity maps of the Levitus atlas [*Levitus*, 1982] are the 1°-square mean values $\phi_s^{\text{obs}} = \phi^{\text{obs}}(\mathbf{x}_s)$ of the observed data at all those 1° squares $\mathbf{x}_s = (x_s, y_s)$ that contain observations. The analyzed field $\phi_i = \phi(\mathbf{x}_i)$ at $\mathbf{x}_i$ is calculated in an iterative way as

$$\phi_i^{(n)} = \phi_i^{(n-1)} + \sum_s w_{is}^{(n)} [\phi_s^{\text{obs}} - \phi_s^{(n-1)}] \tag{A1}$$

where $\phi_i^{(n)}$ denotes the analysis after the nth iteration. The weights of the nth iteration

$$w_{is}^{(n)} = \text{const} \times \Delta F \exp\left\{-\frac{4(\mathbf{x}_i - \mathbf{x}_s)^2}{R_n^2}\right\} \tag{A2}$$

depend on the distance between the observational and the analyzed point. A scaling factor ΔF has been introduced which is the average area per observation. The constant in (A2) is chosen so that $\sum_s w_{is}^{(n)} = 1$. The influence radius R_n is varied at each iteration step. Formally, $w_{is}^{(n)} = 0$ for those $\mathbf{x}_s$ where no data exist, so that the sum in (A1) can be extended over all s. In practice, the sum is restricted to observations within the radius of influence, i.e., $|\mathbf{x}_i - \mathbf{x}_s| \le R_n$.

The solution to (A1) in vector notation is given by

$$\boldsymbol{\phi}^{(n)} = \mathbf{A}^{(n)} \boldsymbol{\phi}^{\text{obs}} + \mathbf{B}^{(n)} \boldsymbol{\phi}^{(0)} \tag{A3}$$

with

$$\mathbf{A}^{(n)} = \mathbf{I} - \mathbf{B}^{(n)}$$
$$\mathbf{B}^{(n)} = \prod_{m=1}^{n} (\mathbf{I} - \mathbf{W}^{(n)}) \tag{A4}$$

where $\mathbf{W}^{(n)} = (w_{is}^{(n)})$ and $\mathbf{I}$ is the $M \times M$ unit matrix. The vector $\boldsymbol{\phi}^{(0)}$ contains the first-guess estimate of the analyzed field, which was taken as the zonal average over the respective basins. Actually, four iterations were carried out with the values $R_1 = 1541$ km, $R_2 = 1211$ km, $R_3 = 881$ km, and $R_4 = 771$ km.

In order to compute the horizontal correlation function of the analyzed field (which is needed for estimating the accuracy of horizontal gradients) one would have to perform Monte Carlo simulations with (A3) based on the actual distribution of data points. One limiting case, however, can be deduced directly by assuming that all grid points contain data. The response of the analysis scheme (A3) to a sine wave can then be computed analytically by writing (A3) in a continuous representation. The response function for this case has been given by *Levitus* [1982]. It has a somewhat different shape than (A2). Based on the wavelength whose amplitude is reduced by 0.5, an equivalent influence $R_e \approx 600$ km is found. At first, it seems surprising that this value is smaller than either of the values for R_n given above. However, from (A4) it is seen that if all grid points contain data, and hence $W^{(n)}$ is regular with all eigenvalues between 0 and 1, then for large n we have $\mathbf{B}^{(n)} \to 0$ and $\mathbf{A}(n) \to \mathbf{I}$; i.e., $\boldsymbol{\phi}^{(n)} \to \boldsymbol{\phi}^{\text{obs}}$ regardless of the values of R_n. Hence the effective influence radius would become smaller with each iteration even if the R_n were kept fixed, and the relative importance of the first guess is reduced with each step.

On the other hand, the situation is different if $\mathbf{W}^{(n)}$ is singular (corresonding to grid points without observations). Here the influence of the first-guess field (more precisely, that part of the first-guess field which lies in the null space of $\mathbf{W}^{(n)}$) is not reduced. As the first guess has a large horizontal scale, the effective influence radius must be somewhat larger than 600 km. The actual value depends on the data density and therefore also on position, in particular on the depth.

The concept of an "effective" influence radius is equivalent to approximating the matrix $\mathbf{A}^{(n)} = (a_{is})$ in (A3) by

$$a_{is} = \text{const}\ h(\mathbf{x}_i - \mathbf{x}_s)\ \Delta F \tag{A5}$$

with $h(\mathbf{r}) = \exp(-4r^2/R_e^2)$, the constant again being determined by $\sum_s a_{is} = 1$. In order to proceed with the calculation of the covariance, we assume that the observations at different 1° squares are uncorrelated and that the statistical errors in the first-guess field can be neglected. This seems justified as long as the main source of variability is connected with quasi-geostrophic eddies with horizontal scales of $O(100$ km). Furthermore, we assume that the statistics of the observations are homogeneous within the effective radius of influence. With those assumptions the covariance of the estimate (A4) is given by

$$C_\phi(\mathbf{x}, \mathbf{x}') = \langle \phi(\mathbf{x})\phi(\mathbf{x}') \rangle = \sigma_\phi^2 \frac{\sum_s h(\mathbf{x} - \mathbf{x}_s)h(\mathbf{x}' - \mathbf{x}_s)(\Delta F)^2}{\left[\sum_s h(\mathbf{x} - \mathbf{x}_s)\Delta F\right]^2} \tag{A6}$$

where σ_ϕ^2 is the variance of the observations. The expression (A6) can be evaluated if the locations $\mathbf{x}_s$ of those 1° squares that contain data are known. Provided that a sufficient number of the points lie within the radius of influence and are distributed sufficiently uniformly, the sums in (A6) can be approximated by integrals over the continuous variable $\mathbf{s} = \mathbf{x} - \mathbf{x}_s$, yielding

$$C_\phi(\mathbf{x}, \mathbf{x}') = C_\phi(\mathbf{x} - \mathbf{x}') = \sigma_\phi^2\ \Delta F \frac{\int d^2\mathbf{s}\ h(\mathbf{s})h(\mathbf{s} + \mathbf{x}' - \mathbf{x})}{[\int d^2\mathbf{s}\ h(\mathbf{s})]^2} \tag{A7}$$

The integrations are restricted to those $\mathbf{s}$ for which the argument of the weight function h has a modulus $\le R_e$. With an error of 2%, however, we may extend the integration over all values of $\mathbf{s}$ and obtain

$$C_\phi(\mathbf{r}) = 2\sigma_\phi^2 \frac{\Delta F}{\pi R_e^2} \exp(-2r^2/R_e^2) \tag{A8}$$

with $\mathbf{r} = \mathbf{x}' - \mathbf{x}$. Introducing the number of independent observations within the radius of influence,

$$M = \pi R_e^2 / \Delta F \tag{A9}$$

we obtain for the variance of the analyzed field

$$\hat{\sigma}_\phi{}^2 = \frac{2}{M}\sigma_\phi{}^2 \tag{A10}$$

Horizontal derivatives of $\phi(\mathbf{x})$ will be estimated as finite differences over a separation Δ, e.g.,

$$\frac{\partial\phi}{\partial x} = \phi_x = \frac{\phi(x+\Delta, y) - \phi(x, y)}{\Delta} \tag{A11}$$

The variance of this estimate is given by

$$\sigma_{\phi_x}{}^2 = \frac{2}{\Delta^2}\{C_\phi(\mathbf{0}) - C_\phi(\Delta, 0)\} \tag{A12}$$

and with (A8) and (A9) we finally obtain for $\Delta \ll R_e$

$$\sigma_{\phi_x}{}^2 = \left(\frac{2}{R_e}\right)^2 \hat{\sigma}_\phi{}^2 = \frac{8}{MR_e{}^2}\sigma_\phi{}^2 \tag{A13}$$

The estimation of the statistical accuracy of the analyzed fields and their gradients thus requires knowledge of the influence radius as well as number and variance of independent observations. The quantities σ_ϕ and M strictly refer to the 1°-square mean values. In their analysis, *Levitus and Oort* [1977] provide the variance and number of all NODC data within 10° squares that have passed certain quality controls (in the atlas of *Levitus* [1982] this information is given for 5° squares). Other statistical information is not available. Taking the number and variance of all data in the 10° squares presumably leads to an underestimation of the variance, as not all individual observations will be truly independent.

As pointed out above, the effective influence radius probably is somewhat larger than 600 km For all results presented above, the value $R_e = 1000$ km was chosen. It is emphasized again that (A8)–(A13) apply only to the purely statistical errors in the analyzed fields. If the data density within one influence radius is low, the error connected with the first-guess field is likely to dominate. That error, however, is of a nonstatistical nature and hence cannot be estimated by statistical considerations.

Appendix B: Relation Between Different Least Squares Schemes of the β Spiral Dynamics

The choice of the weighting matrix $\mathbf{W}$ in (42), if not derived from statistical considerations such as, for example, the maximum likelihood principle, is to some degree a subjective component in the analysis. Essentially, the differences between the present approach and those by *Stommel and Schott* [1977], *Behringer* [1979], and *Behringer and Stommel* [1980] result from different choices for that matrix.

The scheme of *Stommel and Schott* [1977] is obtained from (36) by eliminating $p_3 = w_0$ by dividing by D_{j3} and successively subtracting the equation at level $j+1$ from that at level j (this is the equivalent of vertical differentiation). Then

$$\sum_{k\neq 3} D_{jk}'p_k - B_j' = \varepsilon_j' \qquad j = 1, \cdots, N-1 \tag{B1}$$

where $(D_{jk}', B_j', \varepsilon_j') = \Gamma_{ji}(D_{ik}, B_i, \varepsilon_i)$ with $\Gamma_{ji} = (\delta_{ji} - \delta_{j+1,i})/(z_j - z_{j+1})$. Determining the p_k from the least squares principle

$$(\varepsilon')^2 = \boldsymbol{\varepsilon}'\mathbf{W}'\boldsymbol{\varepsilon}' = \sum_{i,j=1}^{N-1} \varepsilon_i'W_{ij}'\varepsilon_j' \tag{B2}$$

thus is equivalent to choosing $\mathbf{W} = \boldsymbol{\Gamma}^+\mathbf{W}'\boldsymbol{\Gamma}$ as weighting for the system (36). Notice that this $\mathbf{W}$ possesses a rank $N-1$ so that information on one of the equations (36) is lost which then is used with vanishing residual to determine the profile of the vertical velocity.

Behringer [1979] proposed three numerical schemes based on equation (24) with vanishing diffusion. The linear scheme

$$\begin{aligned} &v_0 - u_0\tan\phi_j - d_j = \varepsilon_j' \\ &d_j = v_j' - u_j'\tan\phi_j \end{aligned} \qquad j = 1, \cdots, M = N-1 \tag{B3}$$

is equivalent to (B1). Minimizing the sum of squared residuals ε_j' without any weighting yielded unsatisfactory results, since in this form a bias must occur to data from shallow depths where the currents $v_0 + v_j'$ and $u_0 + u_j'$ are larger. Two nonlinear schemes

$$\begin{aligned} &\frac{v_0 + v_j'}{u_0 + u_j'} - \tan\phi_j = \varepsilon_j''' \\ &\tan^{-1}\left(\frac{v_0 + v_j'}{u_0 + u_j'}\right) - \phi_j = \varepsilon_j'''' \end{aligned} \tag{B4}$$

with a more uniform magnitude of the equations yielded (also unweighted) better results but prohibited an exact analytical solution of the least squares problem.

Behringer and Stommel [1980] consider another linear scheme of estimating u_0 and v_0 as the weighted sums

$$\begin{aligned} u_0 &= \sum_{i=1}^{M-1}\sum_{j=i+1}^{M} p_{ij}U_{ij} \\ v_0 &= \sum_{i=1}^{M-1}\sum_{j=i+1}^{M} q_{ij}V_{ij} \end{aligned} \tag{B5}$$

of the solution U_{ij} and V_{ij} of the pairs i and j of (B3), neglecting the residuals. The weights p_{ij} and q_{ij} are taken as inverses of the variances of U_{ij} and V_{ij}, normalized to unity, i.e.,

$$p_{ij} = \left[\sigma_{U_{ij}}{}^2 \sum_{kl} \sigma_{U_{kl}}{}^{-2}\right]^{-1} \tag{B6}$$

and similarly for q_{ij}.

Notice that (B5) are highly redundant estimators, since the actual data information contained in $2M$ values d_j and $\tan\phi_j$ is blown up to the $M(M-1)$ values U_{ij} and V_{ij}. Again it can easily be shown that the estimation scheme is equivalent to linear schemes discussed above with a specific choice of weighting.

Acknowledgments. We thank Sydney Levitus for providing an early version of his analysis and George Veronis for careful reading of the manuscript and helpful suggestions. The assistance of S. Trier and A. Schurbohm in the preparation of the manuscript is gratefully acknowledged. This is a contribution of SFB 133 "Warmwassersphäre des Atlantik," which is supported by the Deutsche Forschungsgemeinschaft.

References

Armi, L., Effects of variations in eddy diffusivity on property distributions in the oceans, *J. Mar. Res.*, *37*, 515–530, 1979.

Armi, L., and D. B. Haidvogel, Effects of variable and anisotropic diffusivities in a steady-state diffusion model, *J. Phys. Oceanogr.*, *12*, 785–794, 1982.

Armi, L., and H. Stommel, Four views of a portion of the North Atlantic subtropical gyre, *J. Phys. Oceanogr.*, *13*, 828–858, 1983.

Behringer, D. W., On computing the absolute geostrophic velocity spiral, *J. Mar. Res.*, *37*, 459–470, 1979.

Behringer, D. W., and H. Stommel, The beta spiral in the North Atlantic subtropical gyre, *Deep Sea Res.*, *27A*, 225–238, 1980.

Bigg, G. R., The beta spiral method, *Deep Sea Res.*, *32*, 465–484, 1985.
Broecker, W. S., and T.-H. Peng, *Tracers in the Sea*, Lamont-Doherty Geophysical Observatory of Columbia University, Palisades, N. Y., 1982.
Bryden, H. L., Geostrophic vorticity balance in midocean, *J. Geophys. Res.*, *85*, 2825–2828, 1980.
Coats, D. A., The absolute flow field in the South Pacific Ocean, *Deep Sea Res.*, *30*, 1033–1057, 1983.
Cox, M. D., and K. Bryan, A numerical model of the ventilated thermocline, *J. Phys. Oceanogr.*, *14*, 674–687, 1984.
Dantzler, H. L., Potential energy maxima in the tropical and subtropical North Atlantic, *J. Phys. Oceanogr.*, *7*, 512–519, 1977.
Defant, A., Quantitative Untersuchungen zu Statik und Dynamik des Atlantischen Ozeans: Die absolute Topographie des physikalischen Meeresniveaus und der Druckflächen sowie die Wasserbewegungen in Raum des Atlantischen Ozeans, *Wiss. Ergeb. Dtsch. Atl. Exped. Meteor 1925–27*, 6, Part 2, 1, 191–260, 1941.
Dietrich, G., Atlas of the hydrography of the northern North Atlantic Ocean based on the Polar Front Survey of the IGY winter and summer 1958, 140 pp., Cons. Int. Pour l'Explor. Mer, Serv. Hydrog., Charlottenlund Slot, Denmark, 1969.
Emery, W. J., and J. S. Dewar, Mean temperature-salinity, salinity-depth and temperature-depth curves for the North Atlantic and the North Pacific, *Prog. Oceanogr.*, *11*, 219–305, 1982.
Eriksen, C. C., Measurements and models of the fine structure, internal gravity waves, and wave breaking in the deep ocean, *J. Geophys. Res.*, *83*, 2989–3009, 1978.
Fuglister, F. C., Atlantic Ocean atlas of temperature and salinity profiles and data from the International Geophysical Year of 1957–1958, *Woods Hole Oceanogr. Inst. Atlas Ser.*, *1*, 209 pp., 1960.
Fuglister, F. C., Gulf Stream '60, *Prog. Oceanogr.*, *1*, 265–373, 1963.
Gargett, A. E., Vertical eddy diffusivity in the ocean interior, *J. Mar. Res.*, *42*, 359–393, 1984.
Garrett, C., Mixing in the ocean interior, *Dyn. Atmos. Oceans*, *3*, 239–264, 1979.
Garrett, C., On the initial streakiness of a dispersing tracer in two- and three-dimensional turbulence, *Dyn. Atmos. Oceans*, *7*, 265–277, 1983.
Garrett, C., and W. H. Munk, Space-time scales of internal waves: A progress report, *J. Geophys. Res.*, *80*, 291–297, 1975.
Gregg, M. C., Variations of small-scale mixing in the main thermocline, *J. Phys. Oceanogr.*, *7*, 436–452, 1977.
Haidvogel, D. B., A. R. Robinson, and C. G. M. Rooth, Eddy-induced dispersion on mixing, in *Eddies in Marine Science*, edited by A. R. Robinson, pp. 481–491, Springer-Verlag, New York, 1983.
Helland-Hansen, B., and F. Nansen, The Norwegian Sea: Its physical oceanography based upon the Norwegian researches 1900–1904, *Rep. Norw. Fish. Mar. Invest.*, *2*, 1–390, and suppl., 1909.
Holland, W. R., and A. D. Hirschman, A numerical calculation of the circulation in the North Atlantic Ocean, *J. Phys. Oceanogr.*, *2*, 336–354, 1972.
Holland, W. R., D. E. Harrison, and A. J. Semtner, Jr., Eddy-resolving numerical models of large-scale ocean circulation, in *Eddies in Marine Sciences*, edited by A. R. Robinson, pp. 379–403, Springer-Verlag, New York, 1983.
Holland, W. R., T. Keffer, and P. B. Rhines, Dynamics of the oceanic general circulation: The potential vorticity field, *Nature*, *308*, 698–705, 1984.
Holloway, G., A conjecture relating oceanic interval waves and small-scale processes, *Atmos. Oceans*, *21*, 107–122, 1983.
Jacobsen, J. P., Contribution of the hydrography of the North Atlantic: The 'Dana' Expedition 1921–22, in *The Danish 'Dana'-Expedition 1920–22 in the North Atlantic and Gulf of Panama*, *Oceanogr. Rep. 1*(3), 98 pp., 'Dana' Committee, Copenhagen, 1929.
Kirwan, A. D., On "Oceanic isopycnal mixing by coordinate rotation," *J. Phys. Oceanogr.*, *13*, 1318–1319, 1983.
Lawson, C. L., and R. J. Hanson, *Solving Least Squares Problems*, 340 pp., Prentice-Hall, Englewood Cliffs, N. J., 1974.
Leetma, A., and F. Bunker, Updated charts of the mean annual wind stress, convergences in the Ekman layers, and Sverdrup transports in the North Atlantic, *J. Mar. Res.*, *36*, 311–322, 1978.
Levitus, S., Climatological atlas of the world ocean, *NOAA Tech. Pap.*, *3*, 173 pp., 1982.
Levitus, S., and A. H. Oort, Global analysis of oceanographic data, *Bull. Am. Meteorol. Soc.*, *58*, 1270–1284, 1977.
Li, Y.-H., T.-H. Peng, W. S. Broecker, and H. G. Oštlund, The average vertical mixing coefficient for the oceanic thermocline, *Tellus*, *36B*, 212–217, 1984.
Lindstrom, E. J., D. W. Behringer, B. A. Taft, and C. Ebbesmeyer, Absolute geostrophic velocity determination from historical hydrographic data in the western North Atlantic, *J. Phys. Oceanogr.*, *10*, 999–1009, 1980.
Luyten, J. R., and H. Stommel, Recirculation revisited, *J. Mar. Res.*, *40*, suppl., 407–426, 1982.
Luyten, J. R., J. Pedlosky, and H. Stommel, The ventilated thermocline, *J. Phys. Oceanogr.*, *13*, 292–309, 1983.
Mamayev, O. I., T-S curves and the vertical stability of ocean waves (in Russian), *Dokl. Akad. Nauk, SSSR*, *146*, 347–349, 1962.
McDougall, T. J., The relative roles of diapycnal and isopycal mixing on subsurface water mass conversion, *J. Phys. Oceanogr.*, *14*, 1577–1589, 1984.
McDowell, S., P. Rhines, and T. Keffer, North Atlantic potential vorticity and its relation to the general circulation, *J. Phys. Oceanogr.*, *12*, 1417–1436, 1982.
Mellor, G. L., C. R. Mechoso, and E. Keto, A diagnostic calculation of the Atlantic Ocean, *Deep Sea Res.*, *29*, 1171–1192, 1982.
Montgomery, R. B., Circulation in upper layers of southern North Atlantic deducted with use of isentropic analysis, *Pap. Phys. Oceanogr. Meteorol.*, *6*(2), 55 pp., 1938.
Müller, P., D. Olbers, and J. Willebrand, The IWEX spectrum, *J. Geophys. Res.*, *83*, 479–500, 1978.
Munk, W. H., Abyssal recipes, *Deep Sea Res.*, *13*, 707–730, 1966.
Munk, W., Internal waves and Small-scale processes, in *Evolution in Physical Oceanography*, edited by B. Warren and C. Wunsch, pp. 264–291, MIT Press, Cambridge, Mass., 1981.
Needler, G. T., Thermocline models with arbitrary barotropic flow, *Deep Sea Res.*, *18*, 895–903, 1972.
Needler, G. T., The absolute velocity as a function of conserved measurable quantities, *Prog. Oceanogr.*, *14*, 421–429, 1985.
Needler, G. T., and R. A. Heath, Diffusion coefficients calculated from the Mediterranean salinity anomaly in the North Atlantic Ocean, *J. Phys. Oceanogr.*, *5*, 173–182, 1975.
Olbers, D. J., Models of the oceanic internal wave fields, *Rev. Geophys.*, *21*, 1567–1606, 1983.
Olbers, D. J., and J. Willebrand, The level of no motion in an ideal fluid, *J. Phys. Oceanogr.*, *14*, 203–212, 1984.
Olbers, D. J., P. Müller, and J. Willebrand, Inverse technique analysis of large data set, *Phys. Earth Planet. Inter.*, *12*, 248–252, 1976.
Parr, A. E., On the validity of the dynamic topographic method for the determination of ocean current trajectories, *J. Mar. Res.*, *1*, 119–132, 1938.
Proudman, J., *Dynamical Oceanography*, 409 pp., Methuen, London, 1953.
Redi, M. H., Oceanic isopycnal mixing by coordinate rotation, *J. Phys. Oceanogr.*, *12*, 1154–1158, 1982.
Reid, J. L., On the Middepth circulation and salinity field in the North Atlantic Ocean, *J. Geophys. Res.*, *83*, 5063–5067, 1978.
Reid, J. L., On the mid-depth circulation of the world ocean, in *Evolution in Physical Oceanography*, edited by B. Warren and C. Wunsch, pp. 70–111, MIT Press, Cambridge, Mass., 1981.
Rhines, P. B., and W. R. Holland, A theoretical discussion of eddy-induced circulation, *Dyn. Atmos. Oceans*, *3*, 285–325, 1979.
Rhines, P. B., and W. R. Young, Homogenization of potential vorticity in planetary gyres, *J. Fluid Mech.*, *122*, 347–367, 1982.
Richardson, P. L., and K. Mooney, The Mediterranean outflow—A simple advection-diffusion model, *J. Phys. Oceanogr*, *5*, 476–482, 1975.
Robinson, M. K., R. A. Bauer, and E. H. Schroeder, Atlas of North Atlantic–Indian Ocean monthly mean temperature and mean salinities of the surface layer, *Ref. Publ. 18*, U.S. Naval Oceanogr. Office, Washington, D. C., 1979.
Sarmiento, J. L., C. G. H. Rooth, and W. Roether, The North Atlantic tritium distribution in 1972, *J. Geophys. Res.*, *87*, 8047–8056, 1982.
Schott, F., and H. Stommel, Beta spirals and absolute velocities in different oceans, *Deep Sea Res.*, *25*, 961–1010, 1978.
Schott, F., and R. Zantopp, Calculation of absolute velocities from different parameters in the western North Atlantic, *J. Geophys. Res.*, *84*, 6990–6994, 1979.
Schott, F., and R. Zantopp, On the effect of vertical mixing on the determination of the absolute currents by the beta spiral method, *Deep Sea Res.*, *27A*, 173–180, 1980.
Solomon, H., On the representation of isentropic mixing in ocean circulation models, *J. Phys. Oceanography.*, *1*, 233–234, 1971.
Stommel, H., On the cause of the temperature-salinity curve in the ocean, *Proc. Nat. Acad. Sci. U.S.A.*, *48*, 764–766, 1962.
Stommel, H., and F. Schott, The beta spiral and the determination of

the absolute velocity field from hydrographic station data, *Deep Sea Res.*, *24*, 325–329, 1977.

Stommel, H., P. Niiler, and D. Anati, Dynamic topography and recirculation of the North Atlantic, *J. Mar. Res.*, *36*, 449–468, 1978.

Sverdrup, H. U., M. W. Johnson, and R. H. Fleming, *The Oceans: Their Physics, Chemistry, and General Biology*, 1087 pp., Prentice-Hall, Englewood Cliffs, N. J., 1942.

Turner, J. S., Small-scale mixing processes, in *Evolution of Physical Oceanography*, edited by B. Warren and C. Wunsch, pp. 236–263, MIT Press, Cambridge, Mass., 1981.

Veronis, G., On properties of seawater defined by temperature, salinity, and pressure, *J. Mar. Res.*, *30*, 227–255, 1972.

Warren, B. A., Deep circulation of the world ocean, in *Evolution of Physical Oceanography*, edited by B. Warren and C. Wunsch, pp. 6–41, MIT Press, Cambridge, Mass., 1981.

Wiggins, R. A., The general linear inverse problem: Implication of surface waves and free oscillations on earth structure, *Rev. Geophys.*, *10*, 251–285, 1972.

Woods, J. D., Wave-induced shear instability in the summer thermocline, *J. Fluid Mech.*, *32*, 791–800, 1968.

Worthington, L. V., *On the North Atlantic Circulation, Oceanogr. Stud.*, vol. 6, 110 pp., Johns Hopkins University Press, Baltimore, Md., 1976.

Wunsch, C., Determining the general circulation of the oceans: A preliminary discussion, *Science*, *196*, 871–875, 1977.

Wunsch, C., The general circulation of the North Atlantic west of 50°W determined from inverse methods, *Rev. Geophys.*, *16*, 583–620, 1978.

Wunsch, C., An eclectic Atlantic Ocean circulation model, I, The meridional flux of heat, *J. Phys. Oceanogr.*, *14*, 1712–1733, 1984.

Wunsch, C., and B. Grant, Towards the general circulation of the North Atlantic Ocean, *Prog. Oceanogr.*, *11*, 1–59, 1982.

Wunsch, C., and J.-F. Minster, Methods for box models and ocean circulation tracers: Mathematical programming and nonlinear inverse theory, *J. Geophys. Res.*, *87*, 5647–5662, 1982.

Wunsch, C., and S. Webb, The climatology of deep ocean internal waves, *J. Phys. Oceanogr.*, *9*, 235–243, 1979.

Wüst, G., Schichtung und Zirkulation des Atlantischen Ozeans: Das Bodenwasser und die Stratosphäre, *Wiss. Ergeb. Dtsch. Atl. Exped. Meteor 1925–1927*, *6*, 288 pp., 1935.

Wyrtki, K., L. Magaard, and J. Hager, Eddy energy in the oceans, *J. Geophys. Res.*, *81*, 2641–2646, 1976.

D. J. Olbers, Max-Planck-Institut für Meteorologie, 2000 Hamburg, Federal Republic of Germany.

M. Wenzel and J. Willebrand, Institut für Meereskunde an der Universität Kiel, 2300 Kiel, Federal Republic of Germany.

(Received April 5, 1985;
accepted July 8, 1985.)